

Designing Nanoscale Materials
Lecture Series by 2004 Debye Institute
Professor

Christopher B. Murray

IBM Research

Ornstein Laboratory 166

Office phone 253 2227

cbmurray@alum.mit.edu

Debye Lecture 6

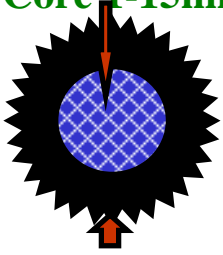
Nanostructured Magnetic Materials for Information Technology

C. B. Murray

Magnetic Nanocrystals and Nanocrystal Superlattices

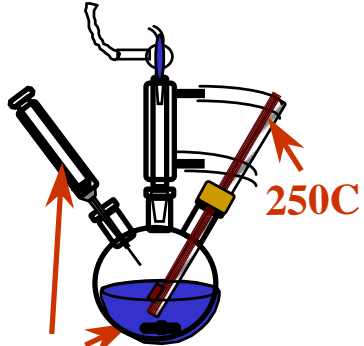
C.B. Murray, S. Sun, F. X. Redl, K. S. Cho and W. Gaschler.
IBM T. J. Watson Research Center; Yorktown Heights, NY

**Inorganic
Core 1-15nm**



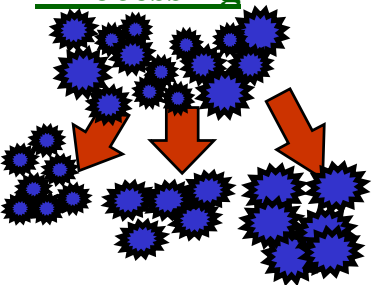
**Surfactants
1-4 nm thick**

Synthesis

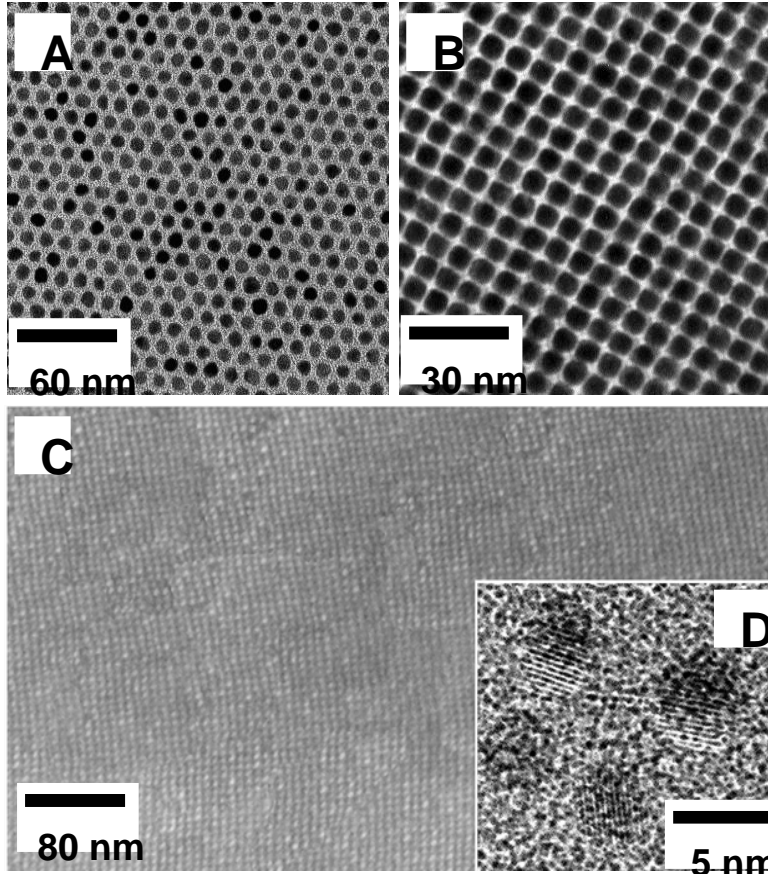


Reagents

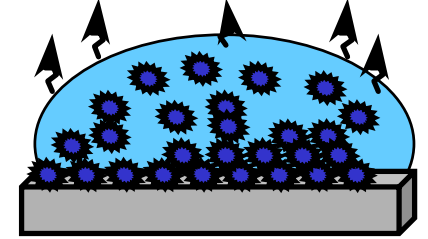
**Size Selective
Processing**



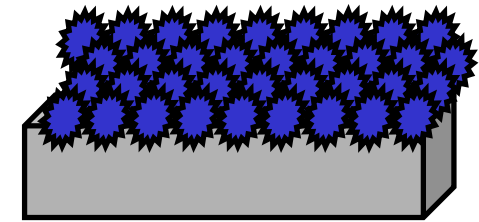
- (1) Synthesize, characterize and integrate nanostructured materials.
- (2) Probe the limits conventional materials/device scaling.
- (3) Harness mesoscopic properties for future technology.
- (4) Explore the potential of self-assembly for nanofabrication.



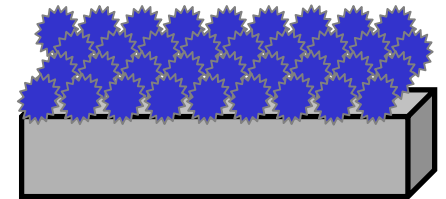
**Film Growth:
Self-Assembly**



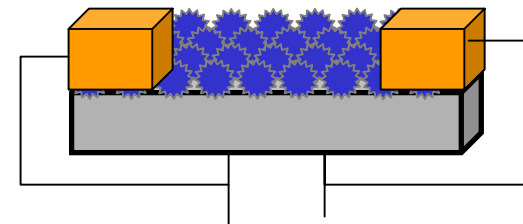
Nanocrystal Superlattice



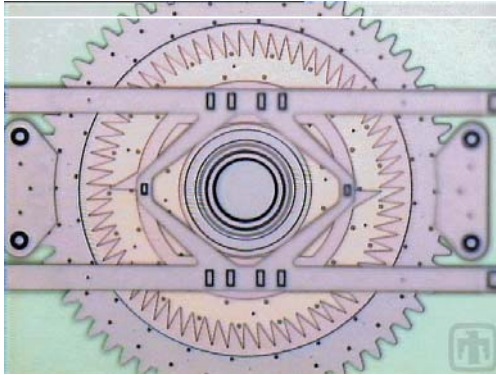
Annealed Superlattice



Patterning & addressing



Applications & Opportunities for High Energy Product magnets.



Micro/Nano Devices



Automotive and Avionic Components



Medical diagnostic system

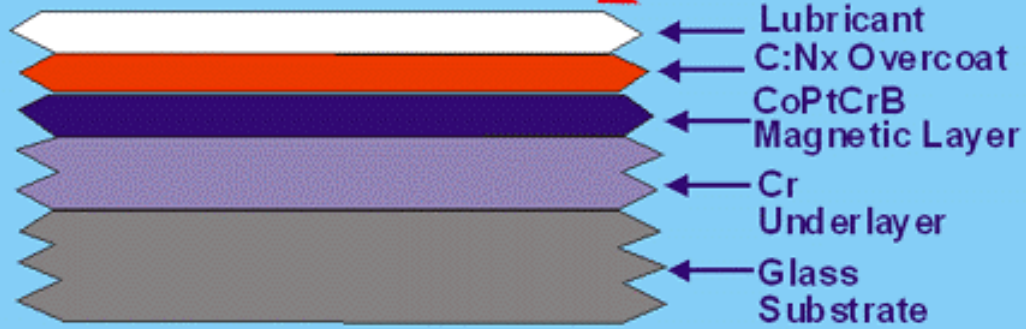
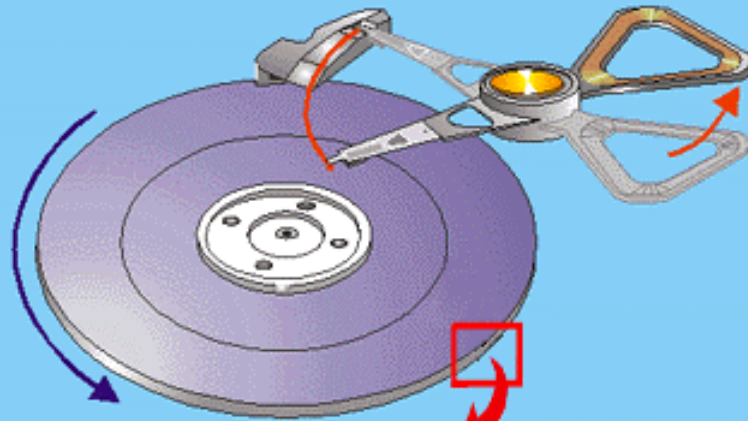


**Hard disk drives
Head actuators**



**Various actuators
in acoustic systems**

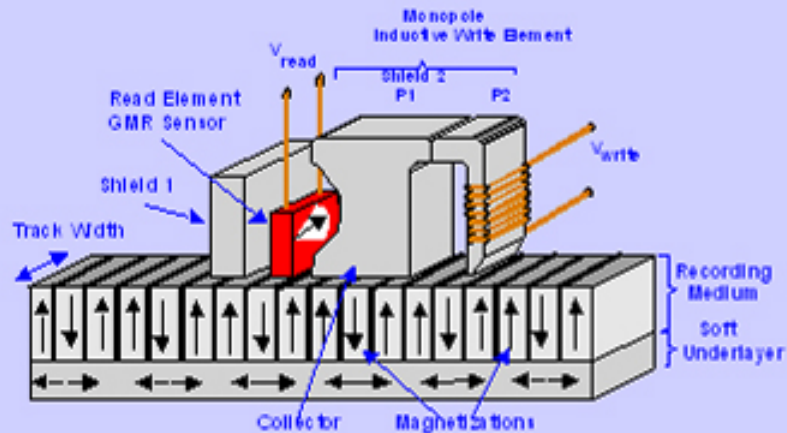
Disk Technology



Advanced Technologies To Delay Superparamagnetism

1. AFC media - implemented 1Q2001

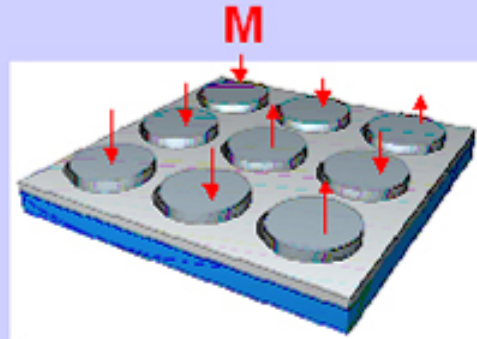
2. Perpendicular recording



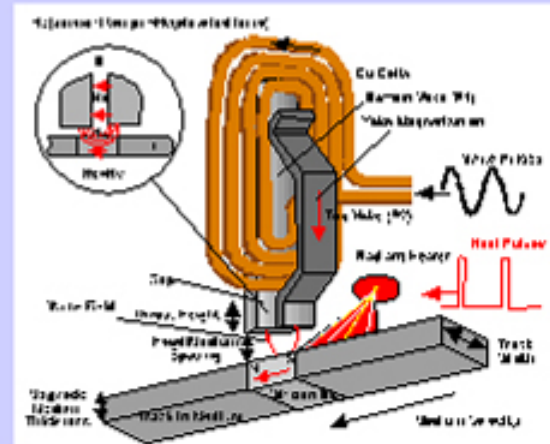
Reduces demagnetizing influence of adjacent bit fields, minimizes transition parameter. Involves new head configuration, return path soft underlayer, as NiFe, in media.

3. Reduce BAR (Bit aspect ratio)
20 ----> 4

4. Patterned media

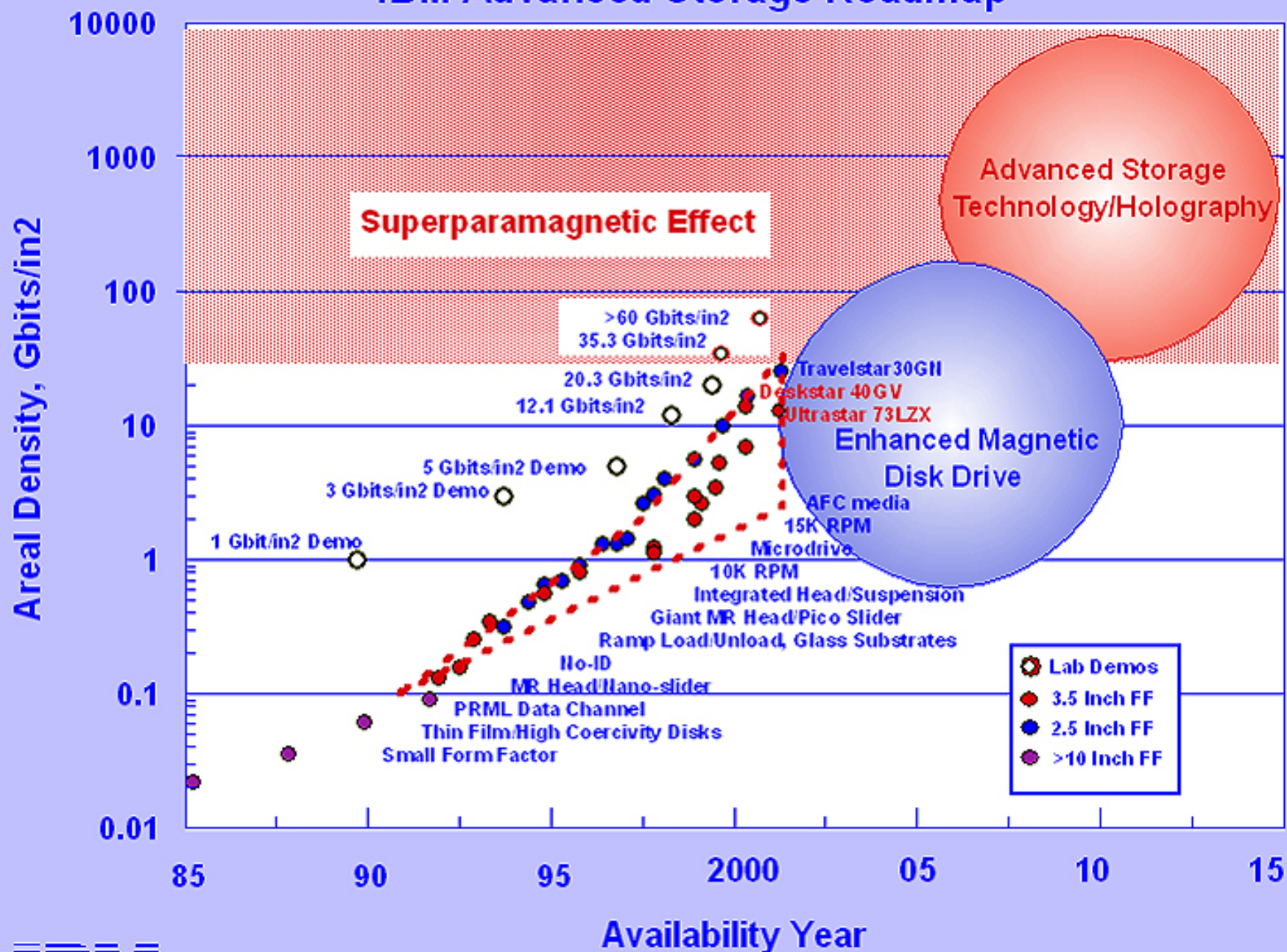


5. Thermally assisted writing



Required because of increased media coercivity (increases K_u to compensate for a reduced V). Involves new magnetic materials

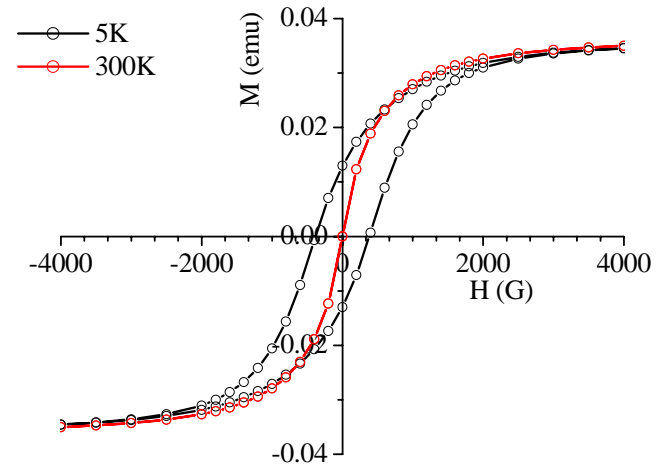
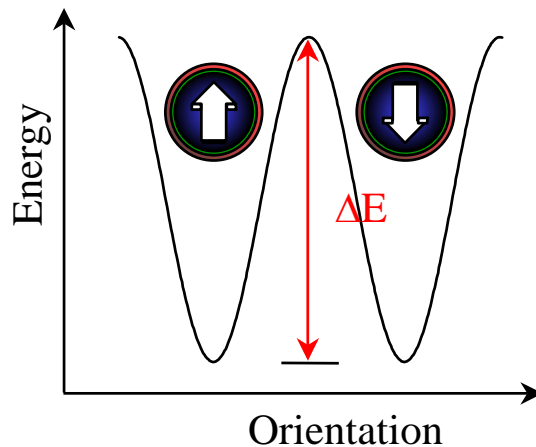
IBM Advanced Storage Roadmap



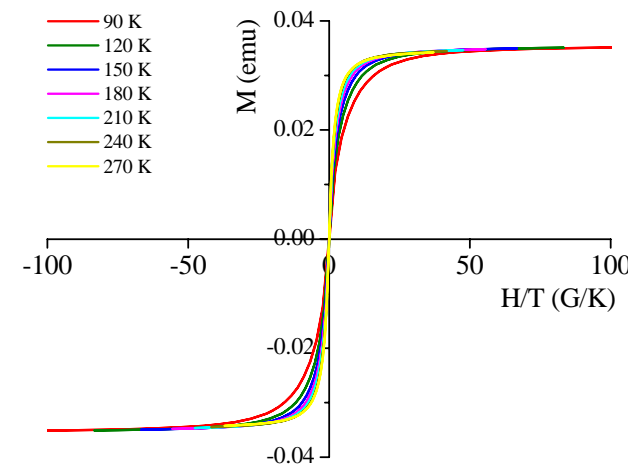
Superparamagnetism

- Single magnetic domain particles.
- Orientation determined by anisotropy energy, K .
- Energy barrier, $\Delta E = KV / k_B T$
- Remnant magnetization, M_{rem}

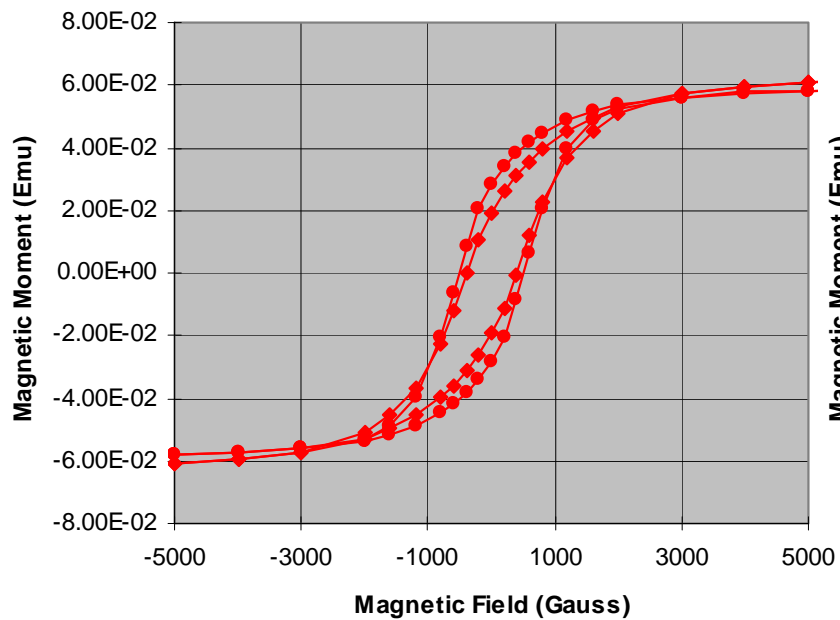
$$M_{rem}(t) = M_{sat} e^{-t/\tau} \text{ where } \tau = \tau_0 e^{-KV/k_B T}$$
- Blocking temperature, $k_B T_B \approx 25\Delta E$
- At $T \gg T_B$, particles are superparamagnetic.
- Zero hysteresis – Langevin equation
 - $M(H) = \coth(\mu H / k_B T) - k_B T / \mu H$
- At $T \ll T_B$, particles are ferromagnetic.



8nm MT Co

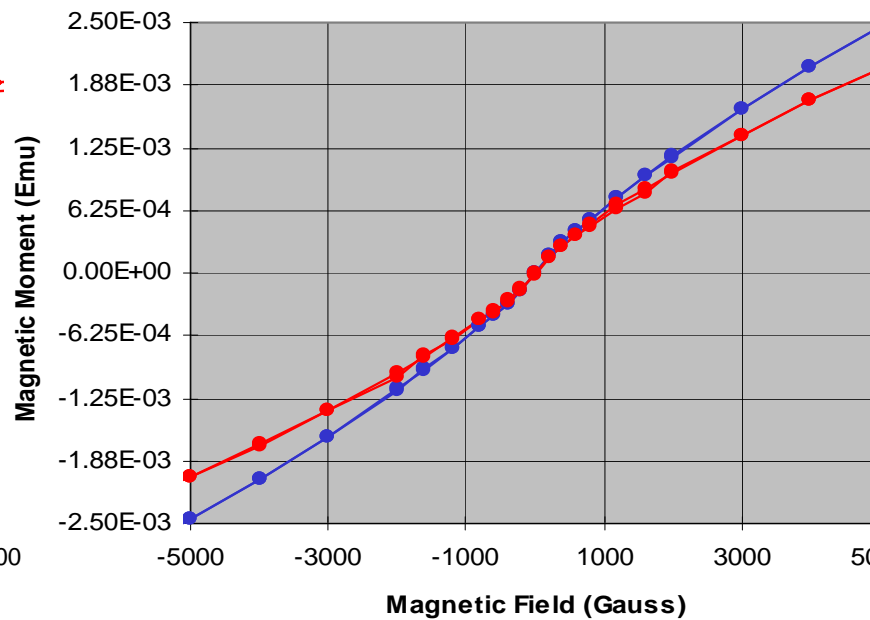


Magnetization - size dependence



◆ dipole interaction ● no dipole interactions

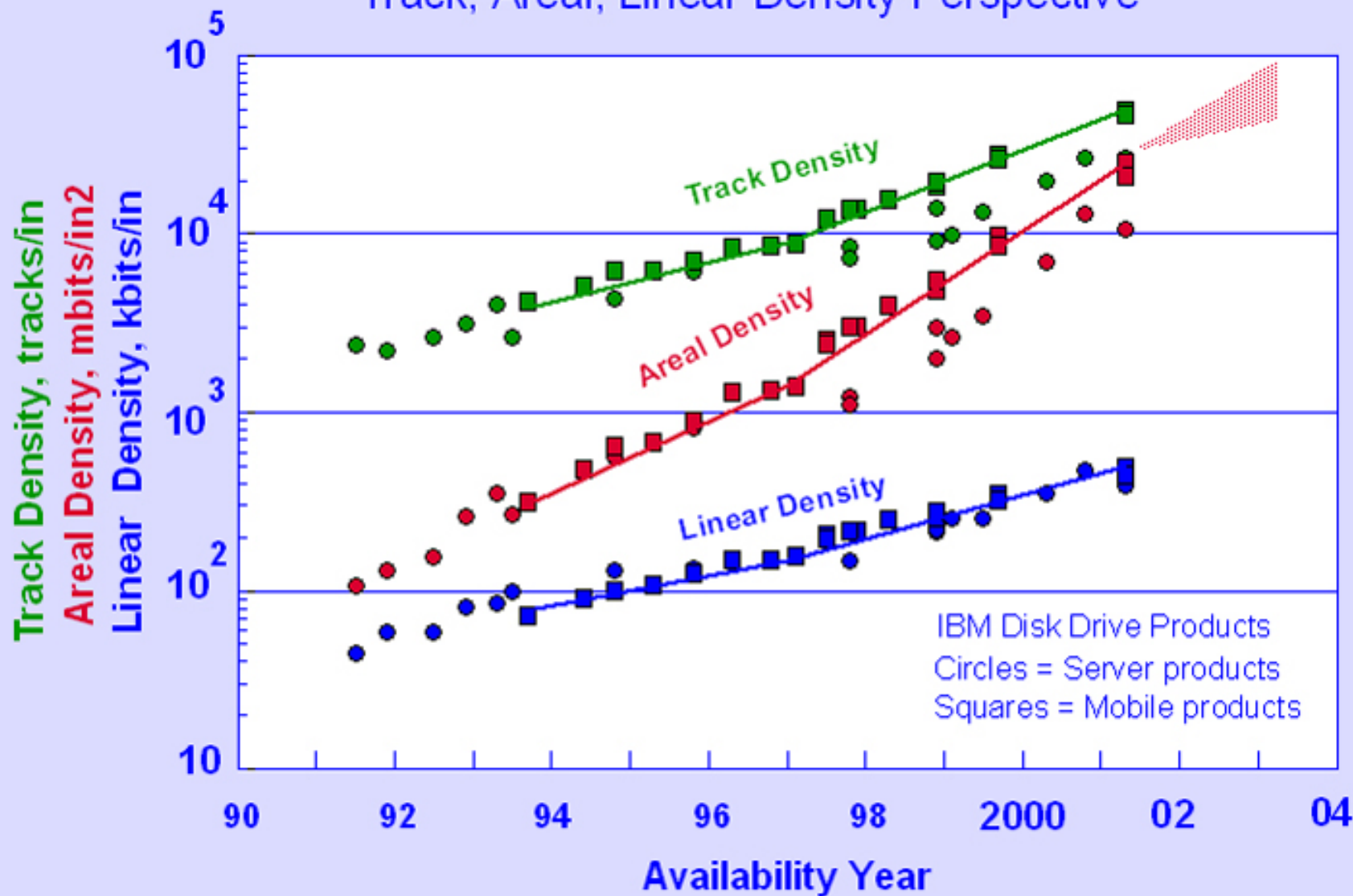
10nm fcc-Co particles



● dipole interactions ● no dipole interactions

2-2.5nm fcc-Co particles

Track, Areal, Linear Density Perspective

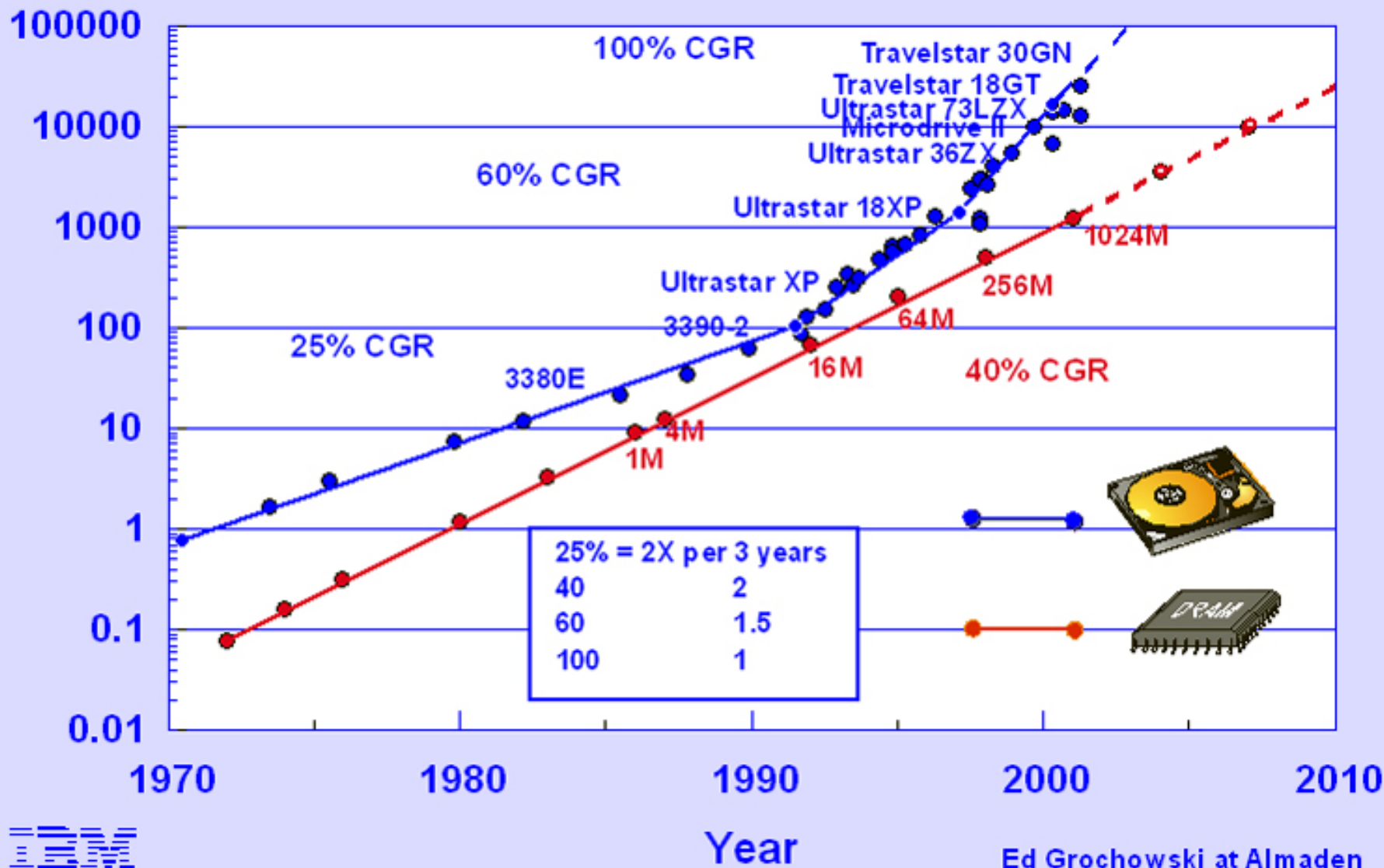


net2001c1_prz



Ed Grochowski at Almaden

Areal Density of Magnetic HDD and DRAM



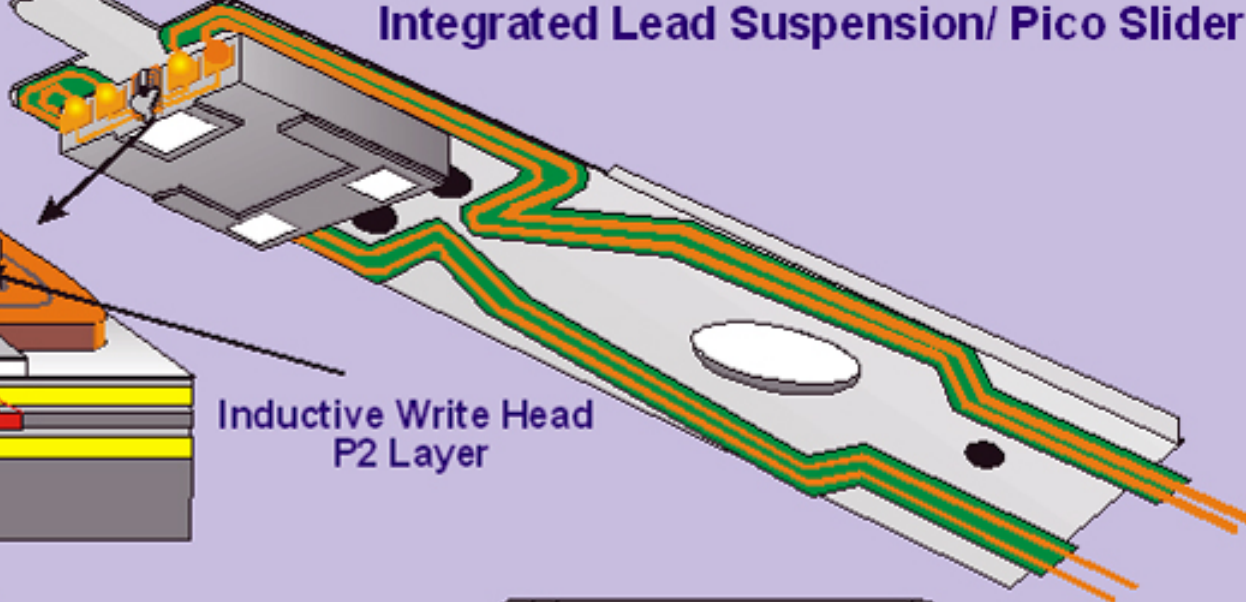
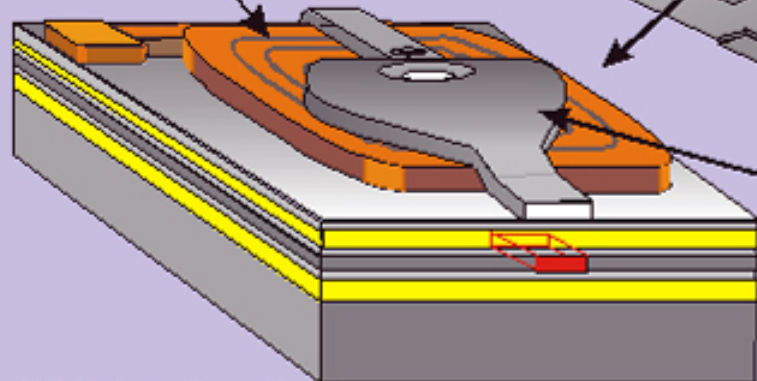
Areal Density, Mbits/inch2

AREAL2001E.PPT



Integrated Lead Suspension/ Pico Slider

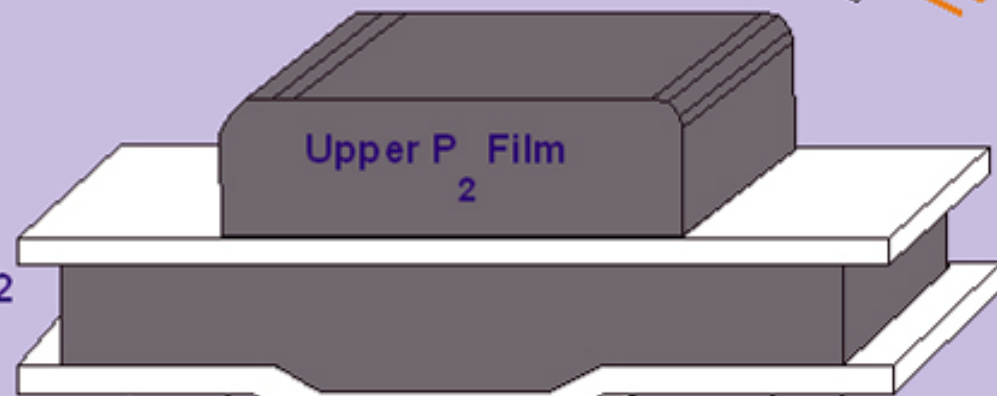
Copper Write Coils



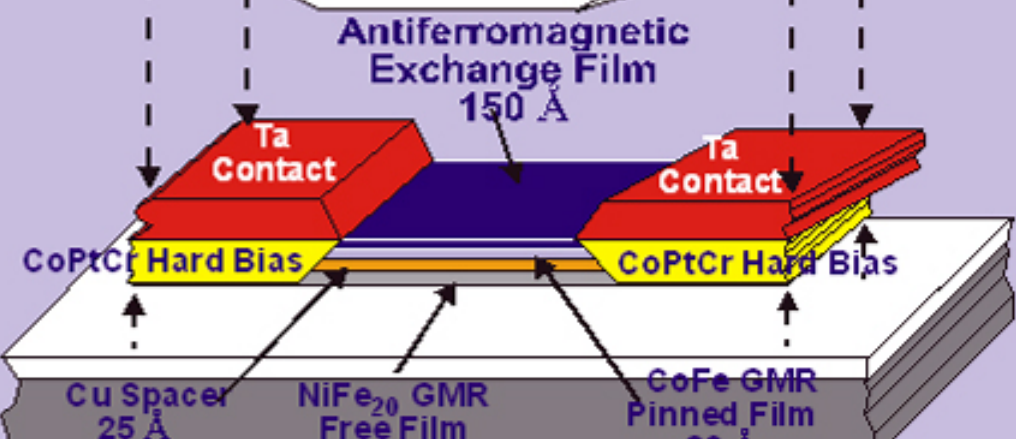
Head/Slider Section

Inductive Write

Lower P1-Shield 2



Spin Valve/GMR Read



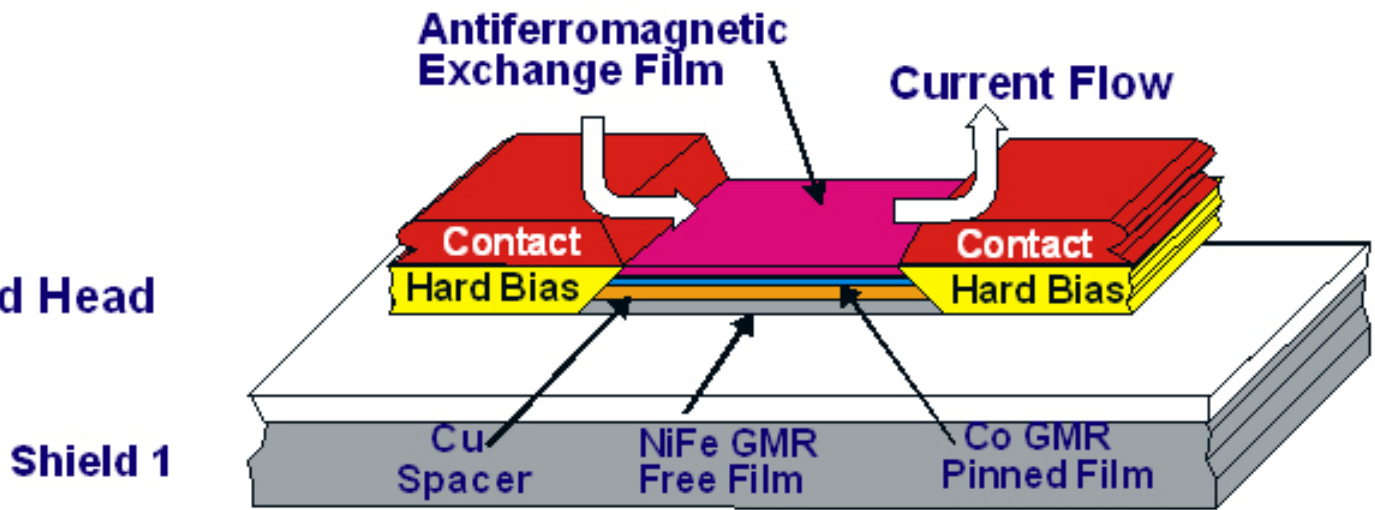
Shield 1

INSITE4e.CDR

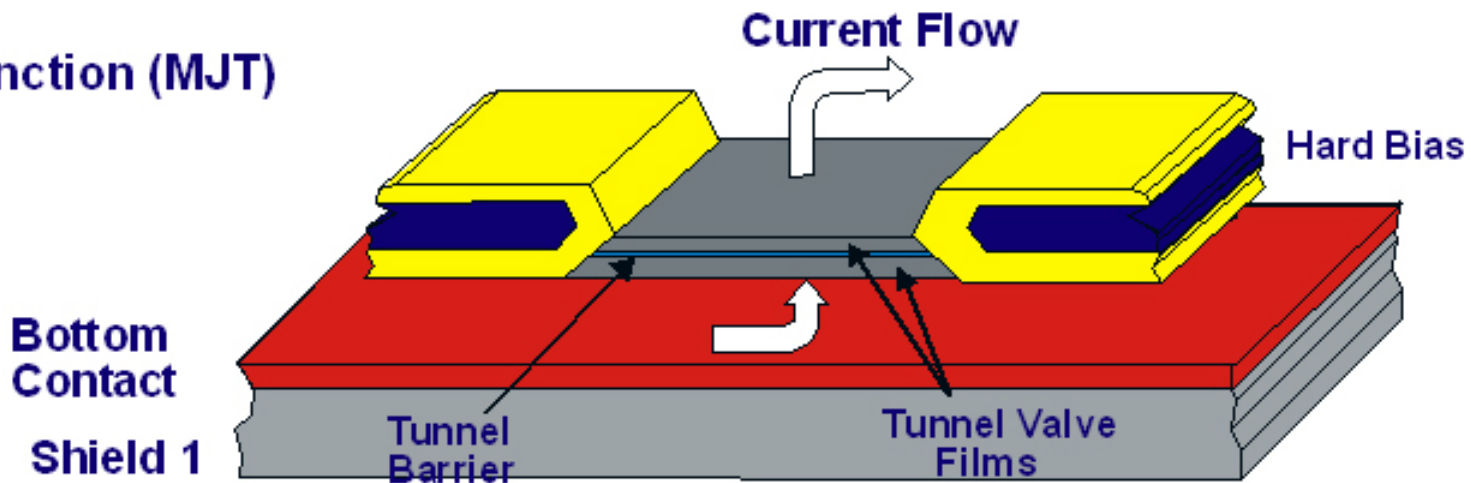


Read Head Design Technologies

Spin Valve (GMR) Read Head
CIP

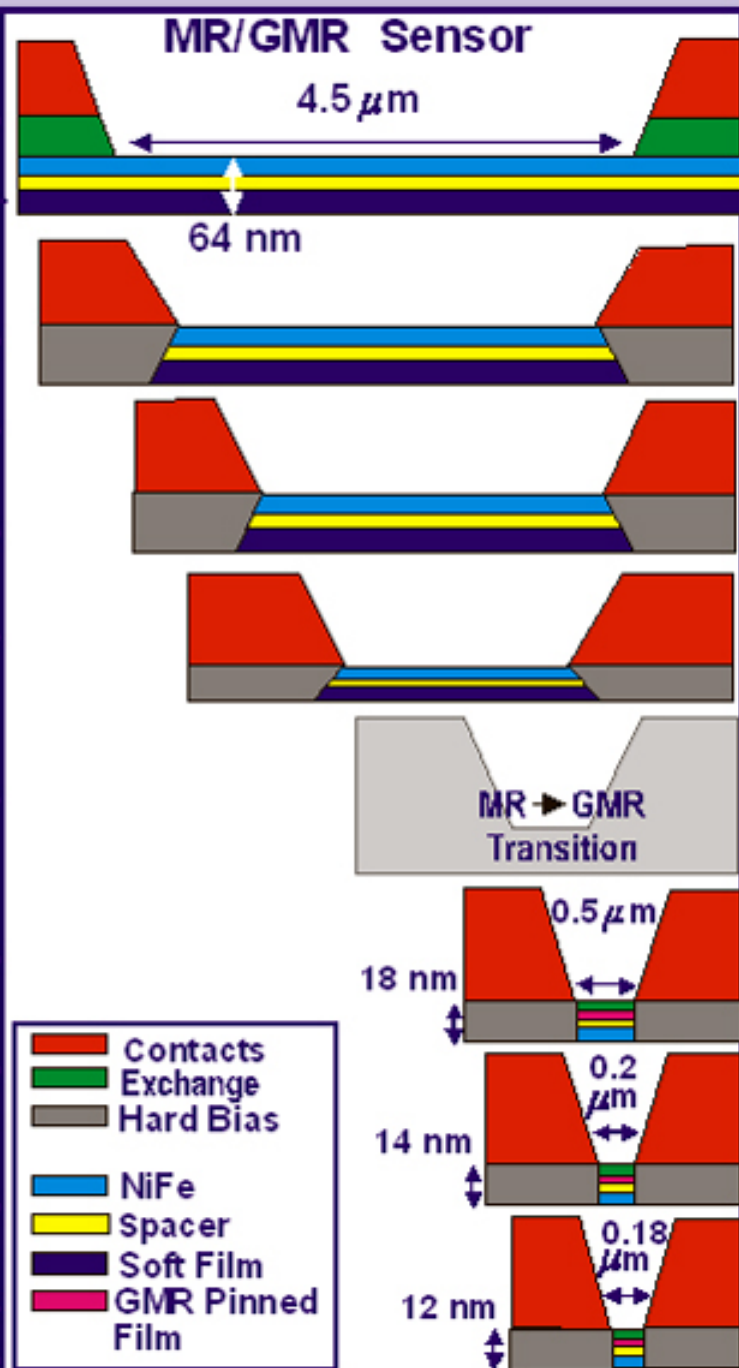


Magnetic Tunnel Junction (MJT)
Read Head
CPP



Projected IBM MR/GMR Read Head Evolution

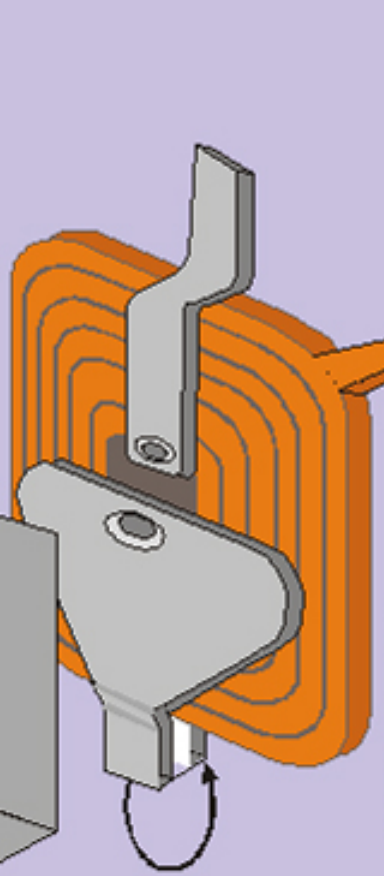
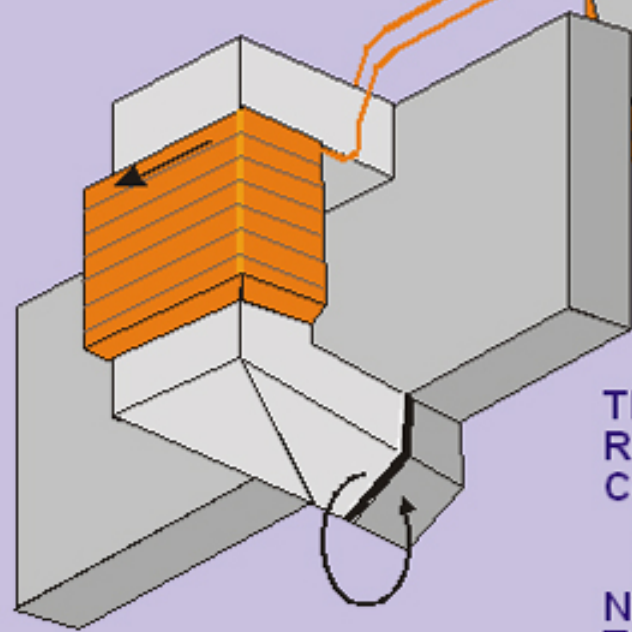
Year	Areal Density Gbits/in ²	Product
1991	0.132	Corsair
1992	0.260	Allicat
1993	0.354	Spitfire
1994	0.578	Ultrastar XP
1995	0.829 0.923	Ultrastar 2XP Travelstar 2LP
1996	1.32 1.45	Travelstar 2XP Travelstar VP
1997	2.64 2.68 3.12	Travelstar 5GS Deskstar 16GP Travelstar 8GN
1998	3.74 4.1 5.7	Travelstar 6GT Deskstar 25GP Travelstar 6GN
1999	5.3 10.1	Deskstar 37GP Travelstar 18GT
2000	7.04 14.5 17.1	Ultrastar 36LZX Deskstar 40GV Travelstar 30GT
2001	13.2 25.7	Ultrastar 73LZX Travelstar 30GN
2002	>30	
2004	>60	



Evolution of Magnetic Read/Write Sensors

Tunnel Junction Read Head
CPP Operation

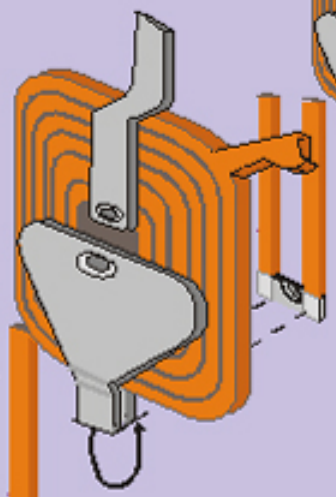
Ferrite Inductive MnFe
Read/Write Head
Wire wound coil
Machined Pole Pieces
Gap Width Controlled
By Films And Assembly
Tolerances



Thin Film Inductive
Read/Write Head
Coil, Pole Geometries
Controlled By Semi-
conductor Type Process
NiFe Poles
Two Contact Structure



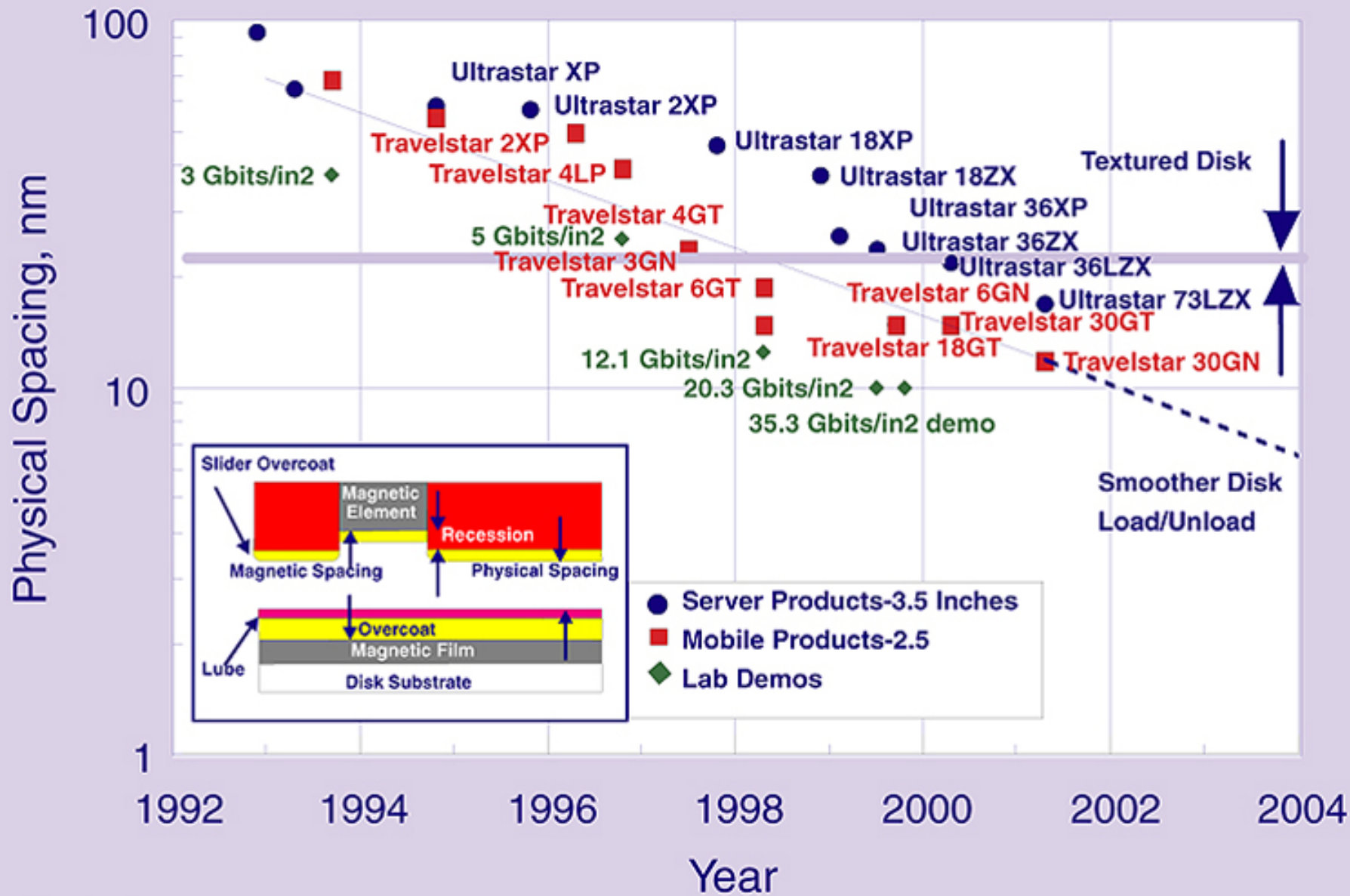
Thin Film Inductive Write
MR Read Head
Write Wide-Read Narrow
Four Contact Structure
SAL
NiFe MR Film



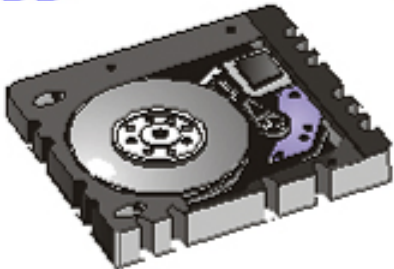



Thin Film Inductive Write
GMR Read Head
Write Wide-Read Narrow
Four Contact Structure
Pinned, Free Films
Antiferromagnetic
Exchange Film
CIP Operation



Physical spacing and disk surface evolution

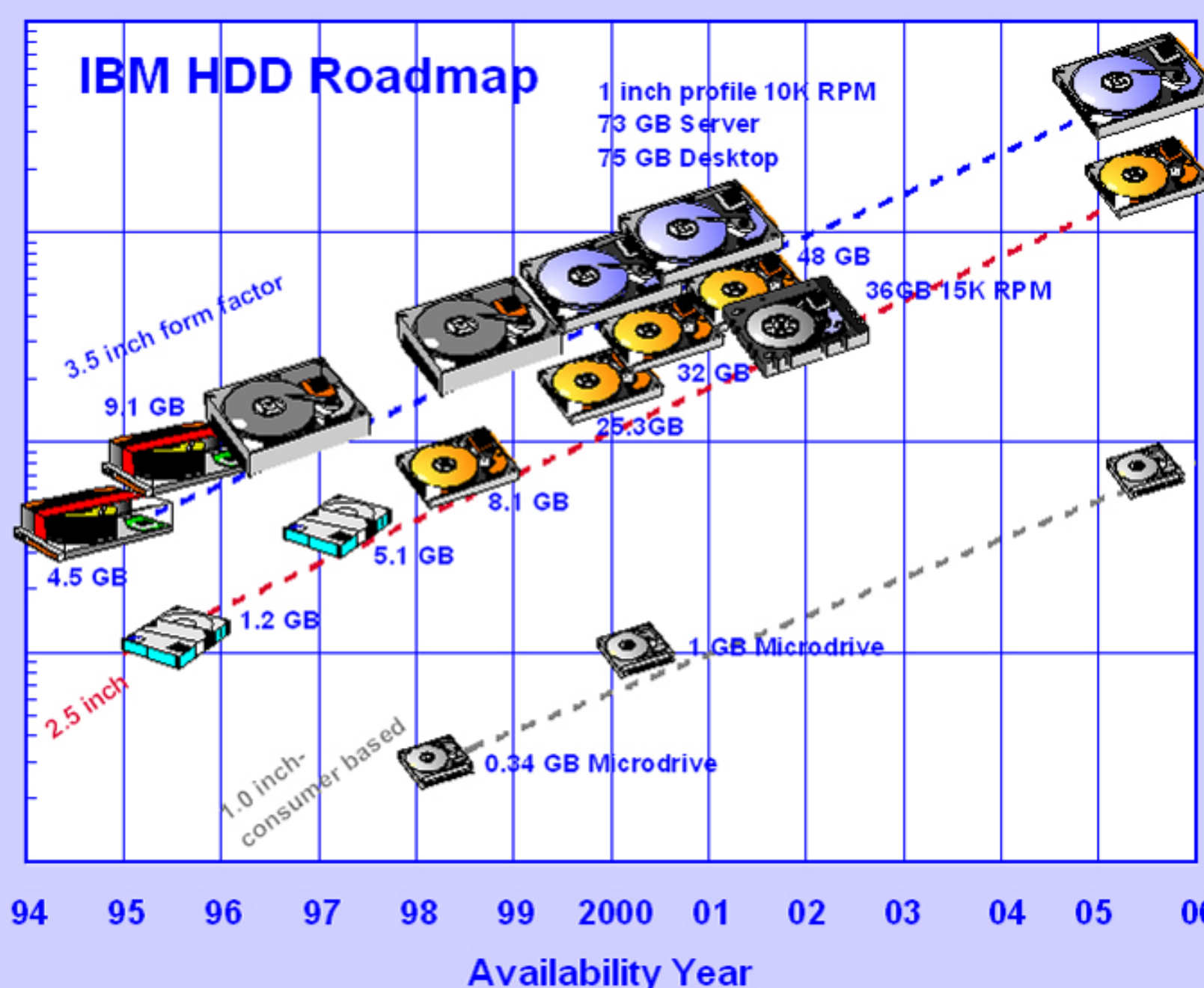


IBM HDD Design Projections

	1999	2000	2002	2004	2006
Server 3.5 Inch HDD 25.4 mm high 	36 GB 10000 RPM 4.9 ms Tseek	73 GB 10000 RPM 4.9 ms Tseek	73 GB 15000 RPM 4.0 ms Tseek		
Entry-Server 3.5 Inch HDD 25.4 mm high 	37 GB 7200 RPM 8.5 ms Tseek	75 GB 7200 RPM 8.5 ms Tseek	144 GB 10000 RPM 7.0 ms Tseek	300 GB 10000 RPM 4.0 ms Tseek	600 GB 15000 RPM 3.0 ms Tseek
Mobile 2.5 Inch HDD 9.5/12.5mm high 	25 GB 5400 RPM 12 ms Tseek	36 GB 5400 RPM 10.0 ms Tseek	50 GB 5400 RPM 9.0 ms Tseek	100 GB 7200 RPM 7.0 ms Tseek	200 GB 7200 RPM 5.0 ms Tseek
Consumer 1.0 Inch HDD 5.0 mm high 	0.34 GB 4500 RPM 15 ms Tseek	1.0 GB 3600 RPM 15 ms Tseek	2.0 GB 3600 RPM 15 ms Tseek	4.0 GB 4500 RPM 12 ms Tseek	8.0 GB 4500 RPM 10 ms Tseek

HDD Capacity, GBytes

IBM HDD Roadmap

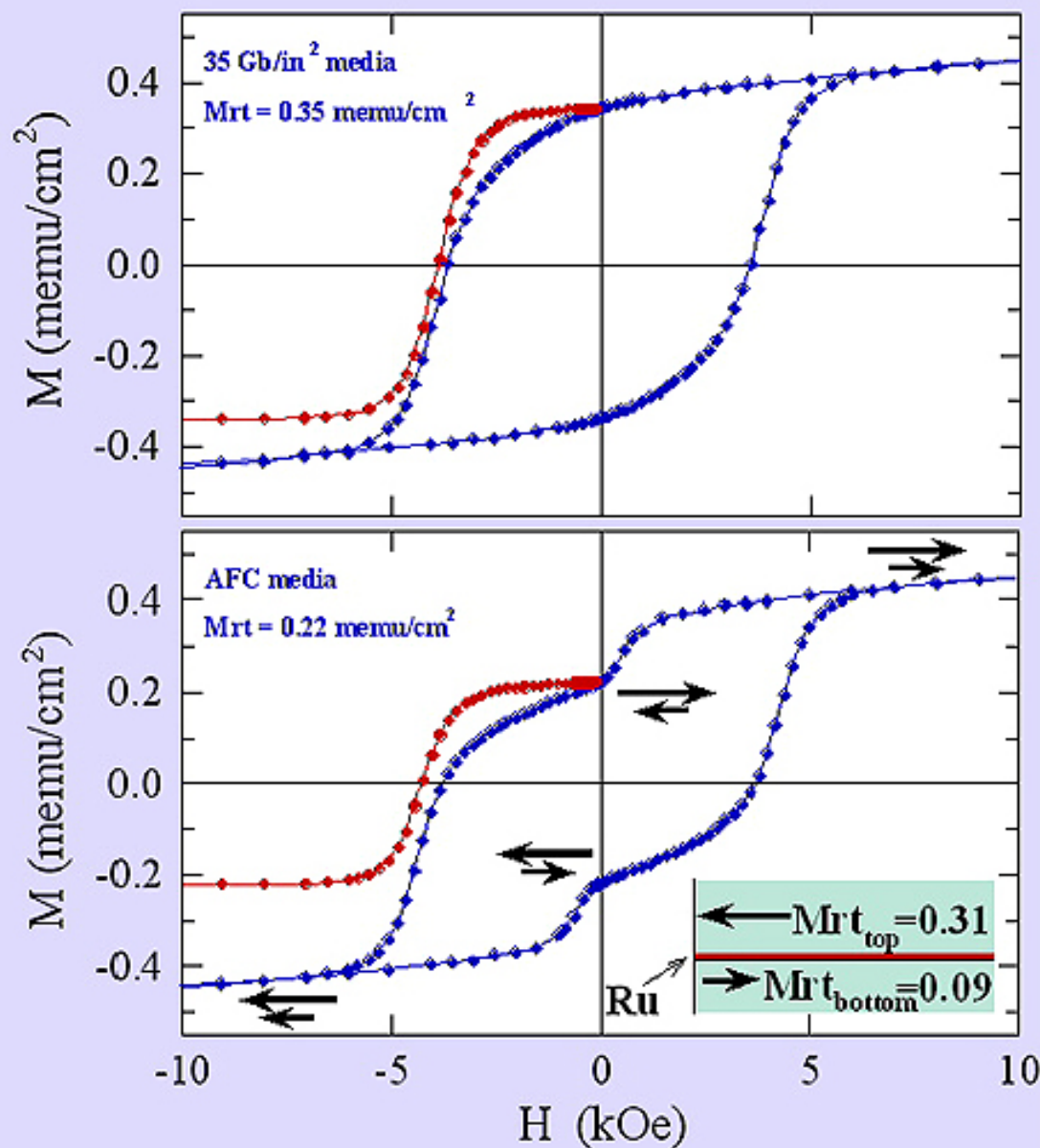
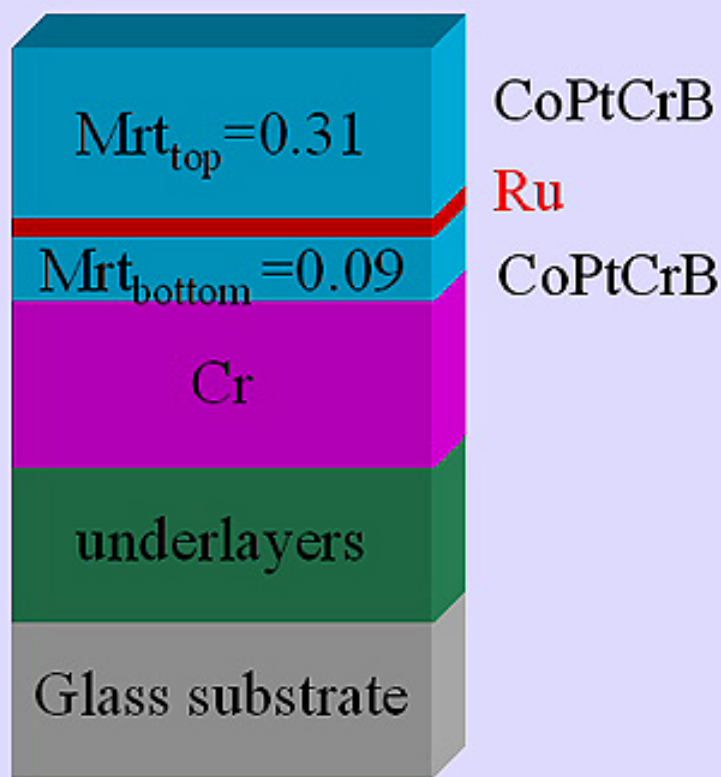


94 95 96 97 98 99 2000 01 02 03 04 05 06

Availability Year

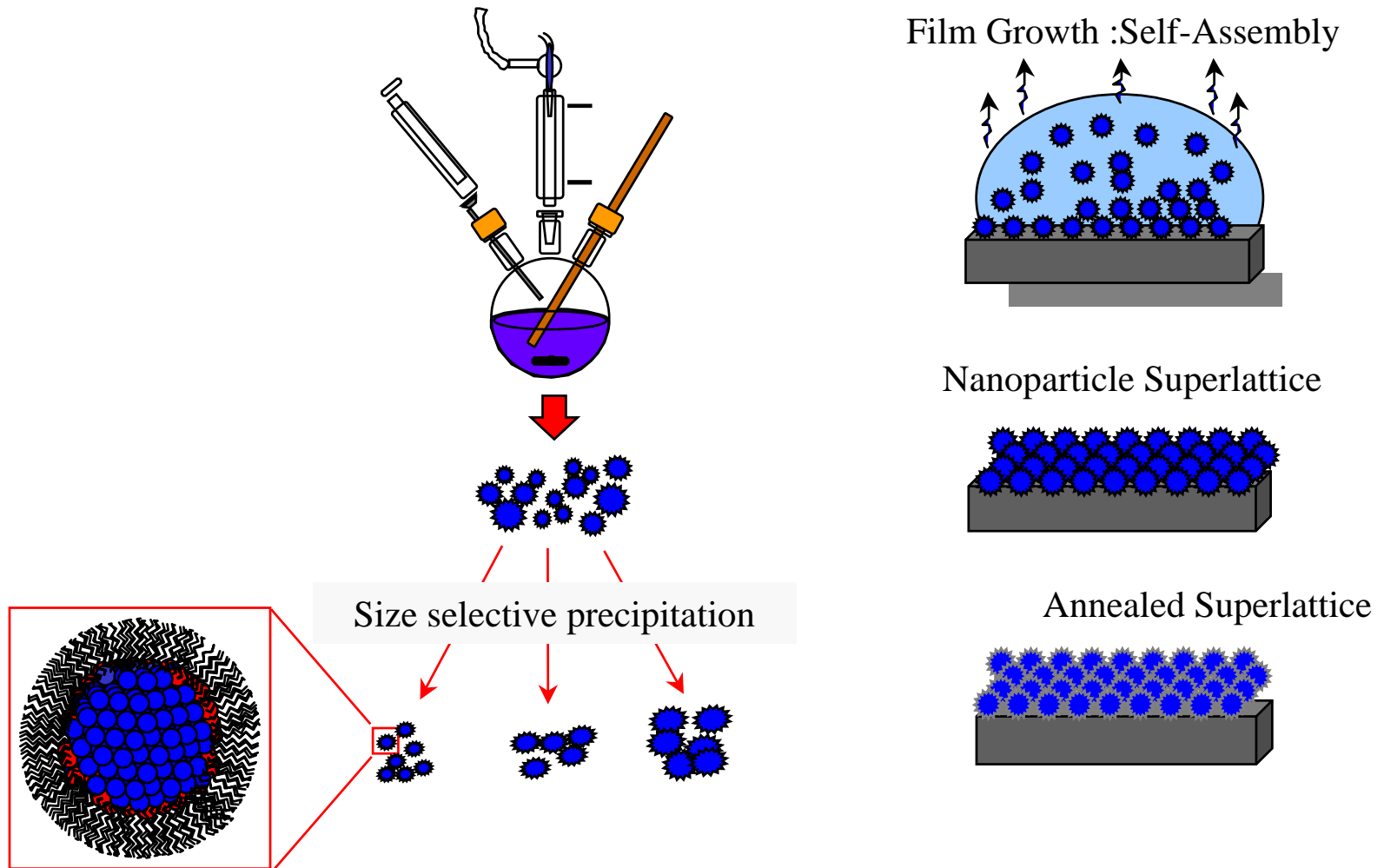


AFC media magnetization response to magnetic field

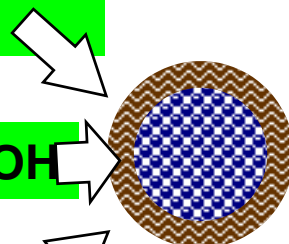
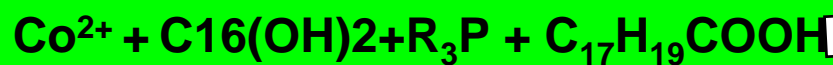
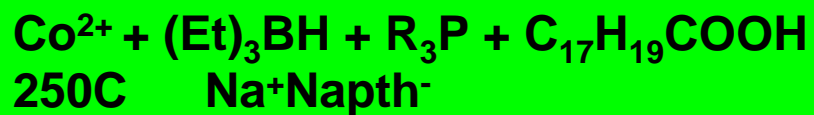


Synthesis and Self-assembly of Co nanoparticles

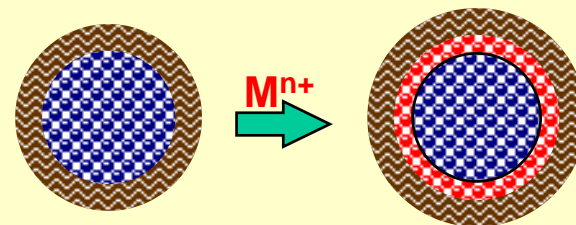
- High temperature (200 °C), solution phase synthesis.
- Rapid nucleation – growth controlled by coordinating ligands.
- Size distribution improved by size selective precipitation.



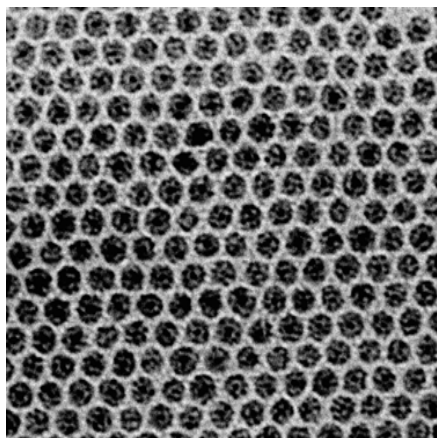
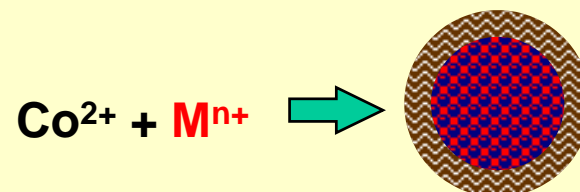
Synthesis of Transition Metal Nanocrystals



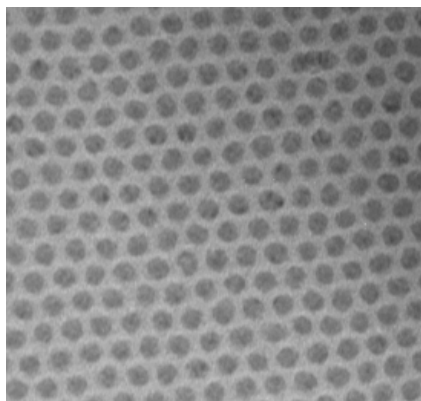
Sequential reduction of metals Core/Shell



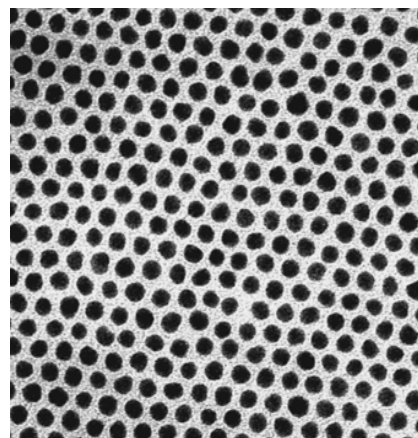
Simultaneous reduction of metals alloys



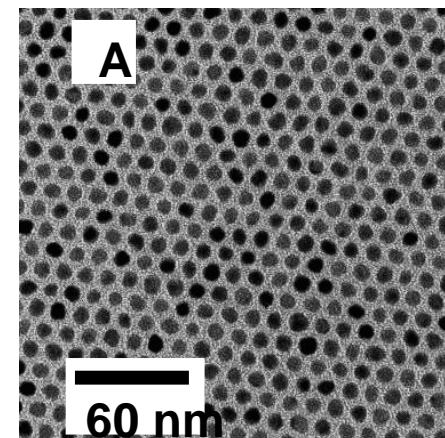
Co 8 nm



Ni 9 nm



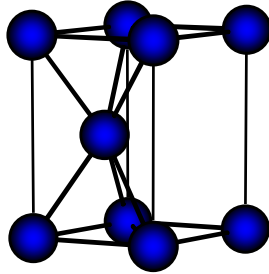
Co/Ni 9 nm



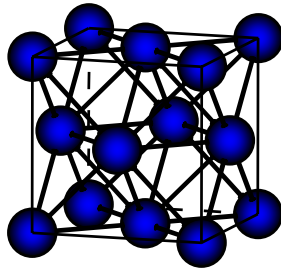
FePt 4 nm

Crystal phases of Cobalt

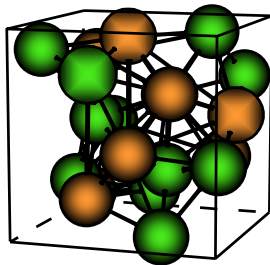
3 crystal phases are studied..



(1) hcp Co



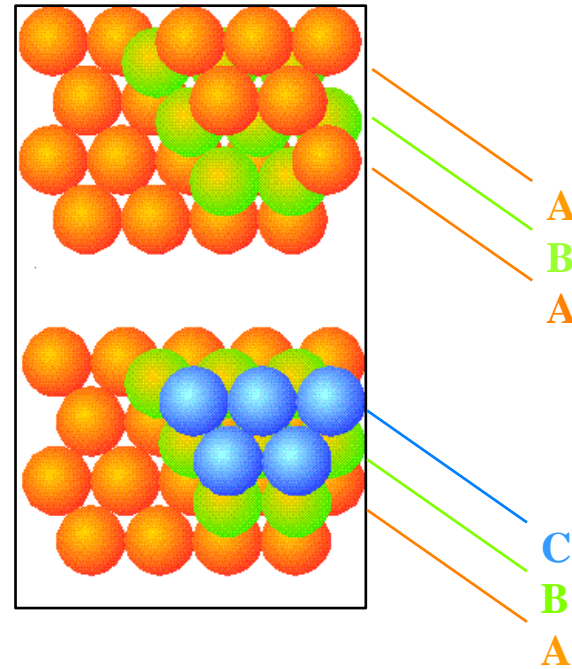
(2) fcc Co



(3) ϵ -Co

Fcc and hcp differ only in stacking sequence of close-packed layers.

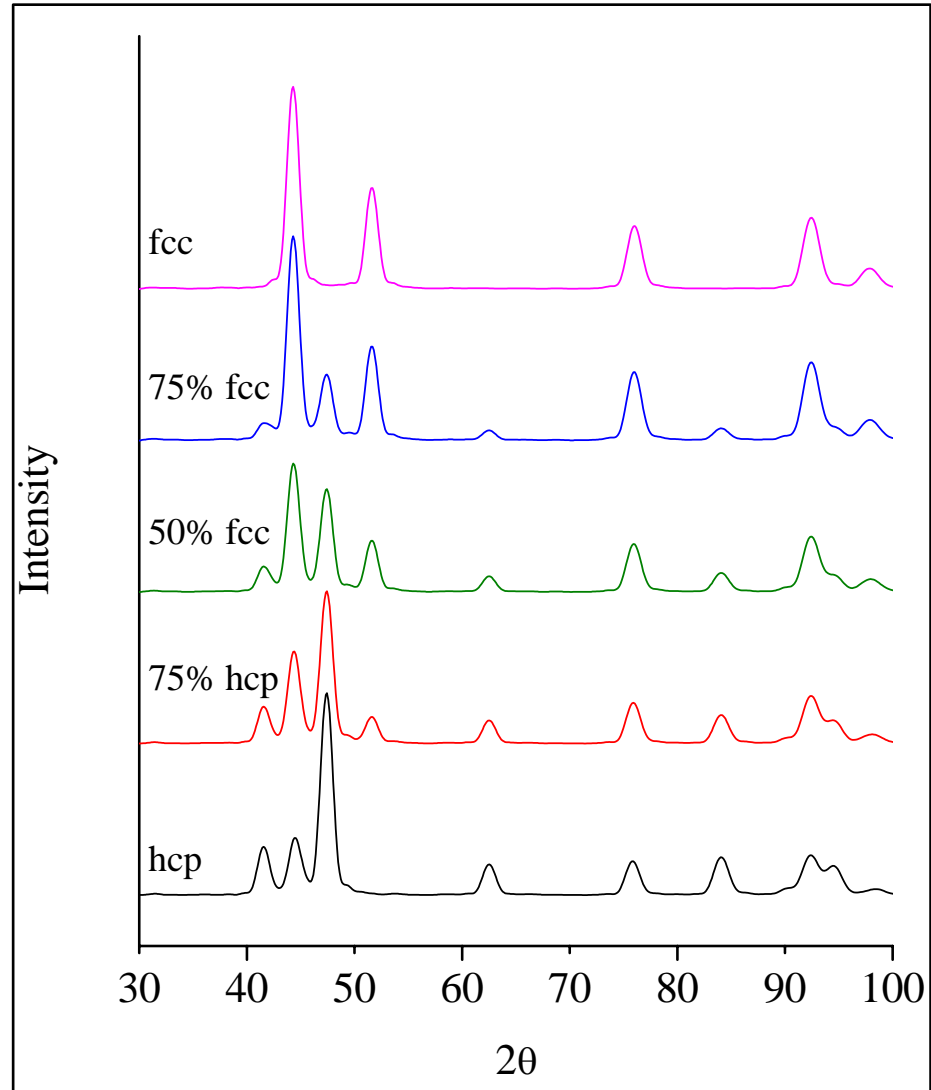
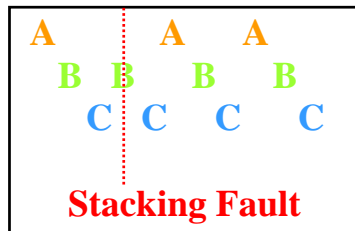
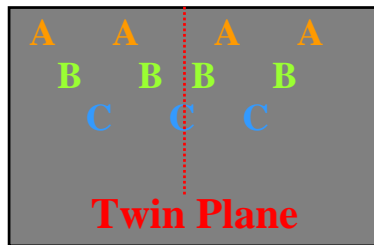
fcc: **A****B****C****A****B****C**... Hcp: **A****B****A****B****A****B**...



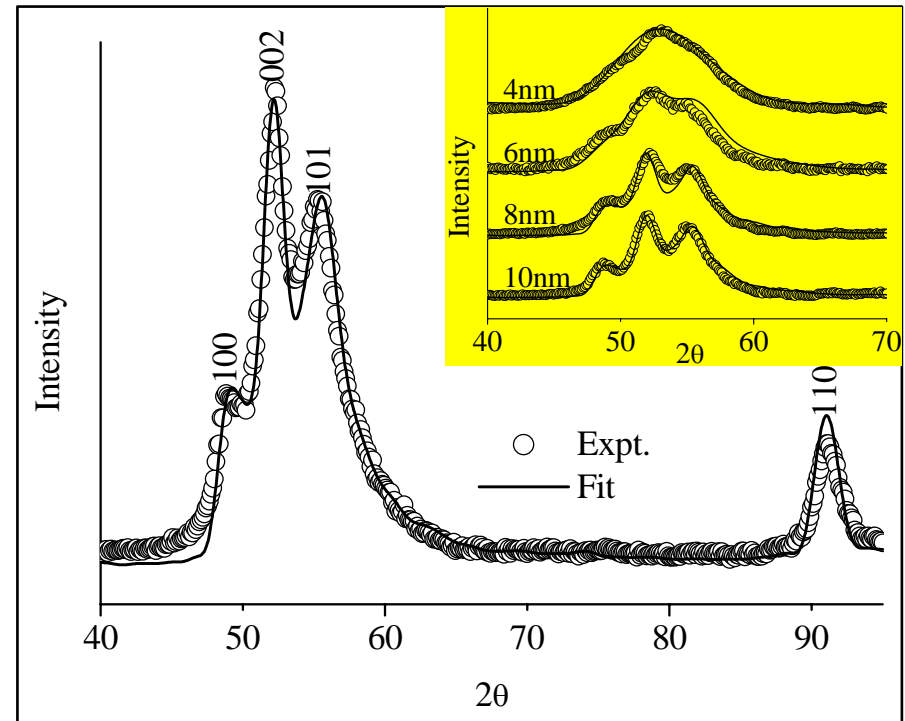
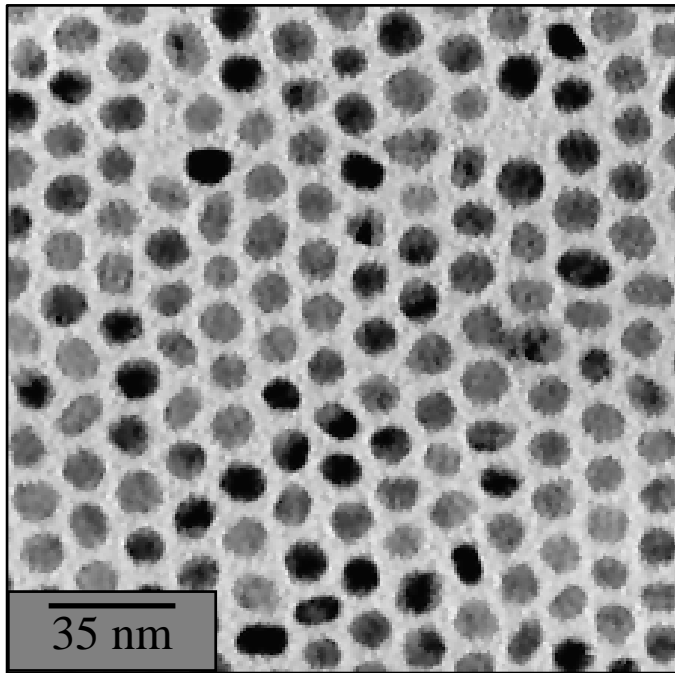
- Cubic unit cell
- Complex internal structure
- Set I - 8 atoms
- Set II - 12 atoms

XRD modeling of cobalt nanoparticles

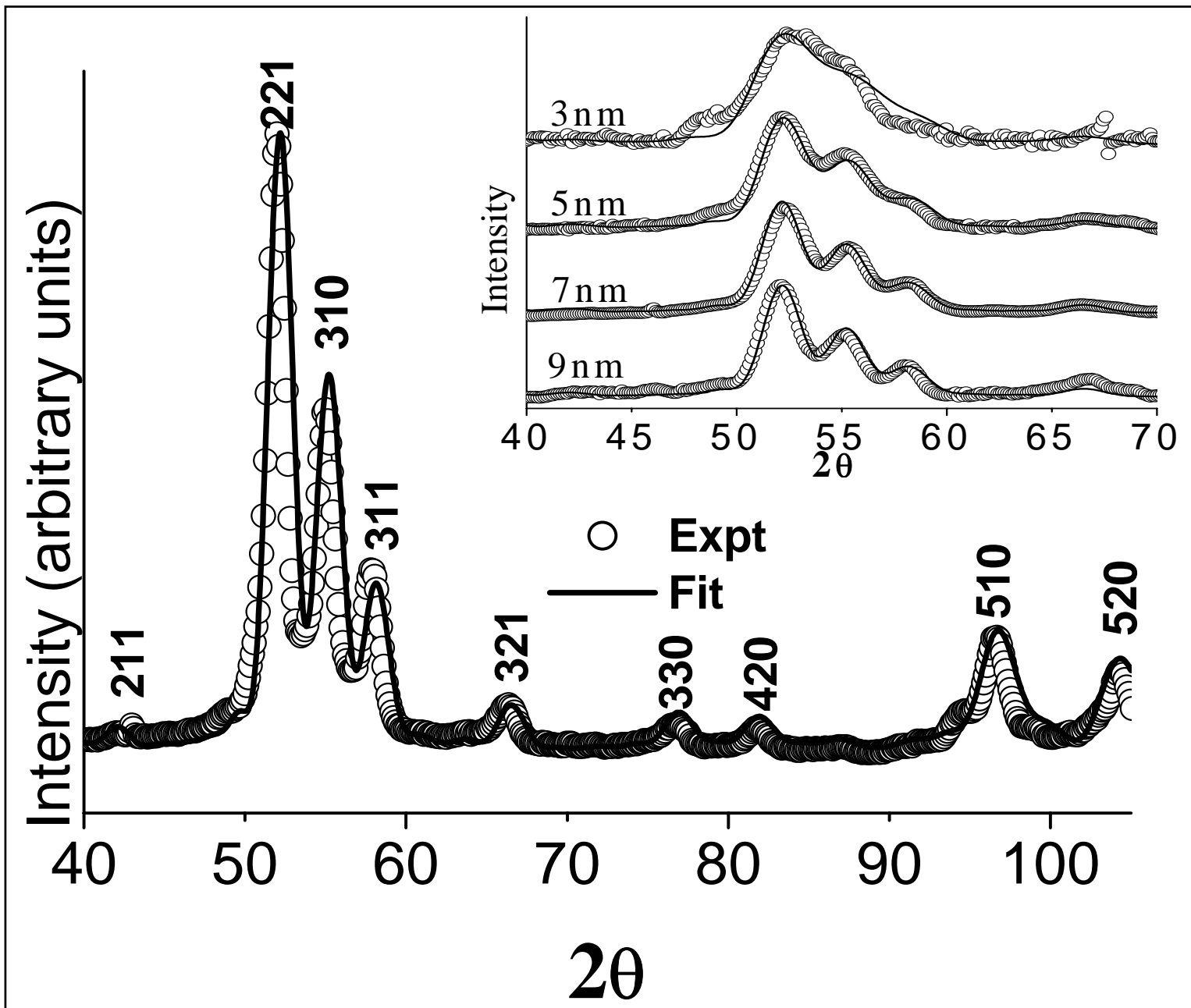
- Better fits obtained by including
 - Stacking faults
 - Twin faults
- Introduction of stacking faults generates mixed fcc/hcp structures.
- Leads to the inter conversion of fcc and hcp phases



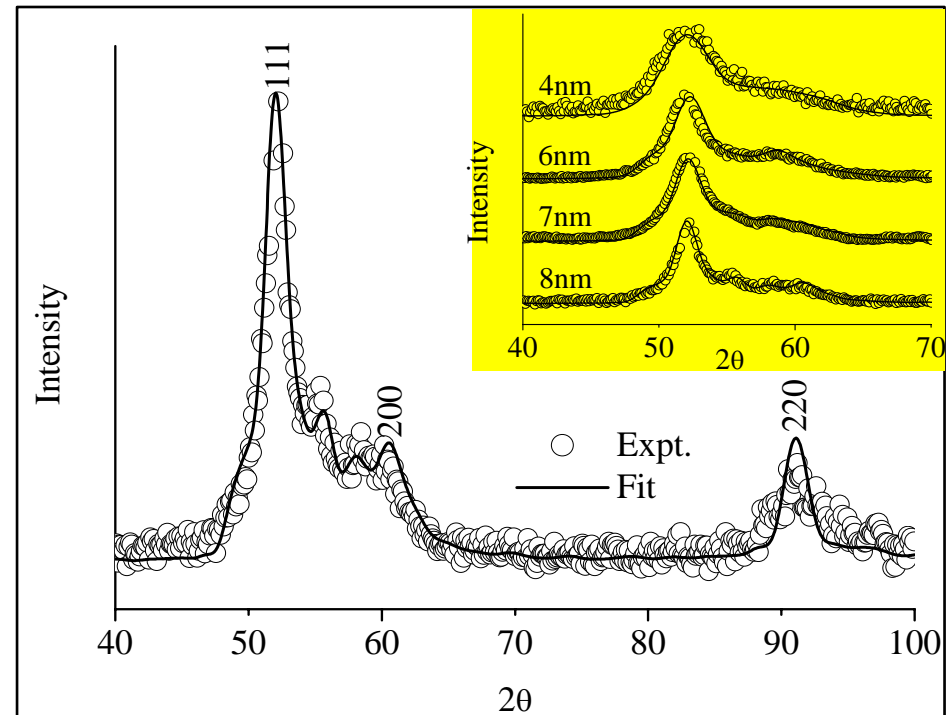
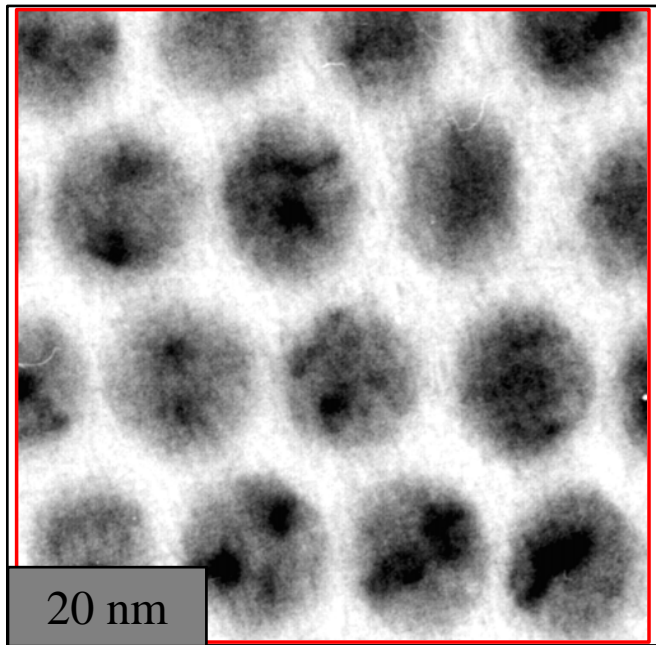
XRD Modeling of hcp nanoparticles



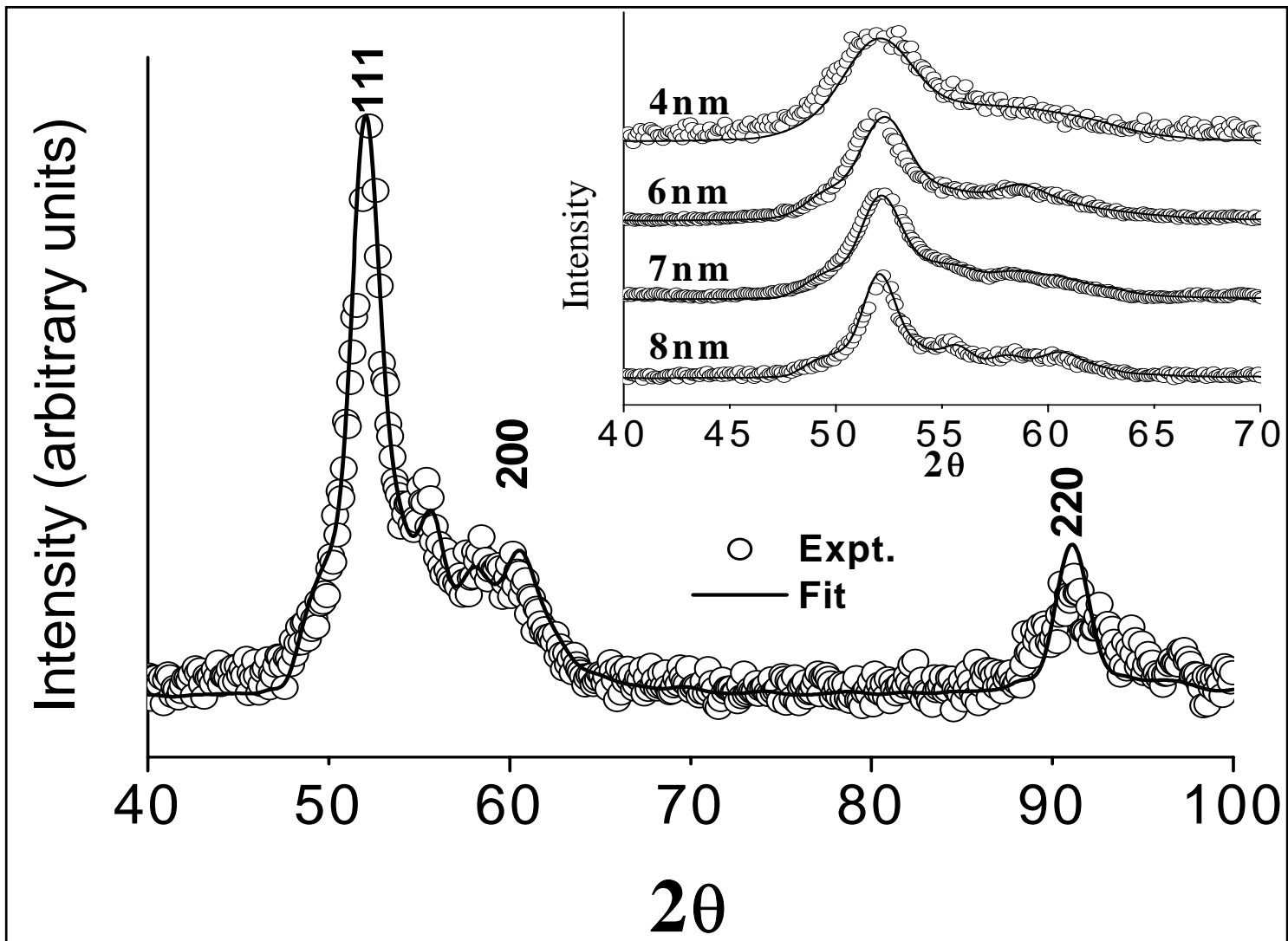
- TEM images show that hcp Co nanoparticles are slightly prolate.
- XRD fitting show extensive faulting/disorder.
 - Approximately one fault every 2.5 stacking planes.
 - Consistent across a variety of particle sizes.



XRD Modeling of fcc nanoparticles

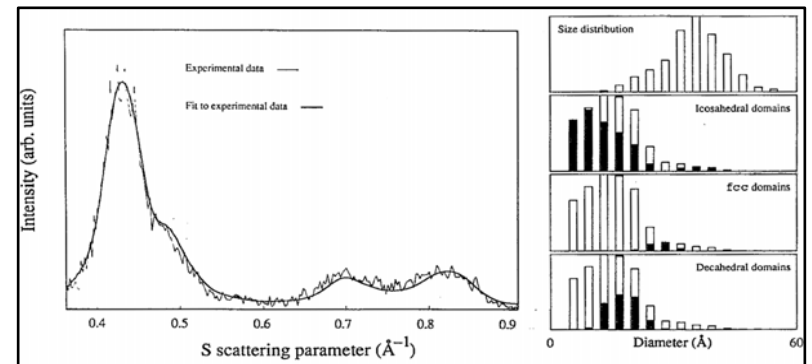
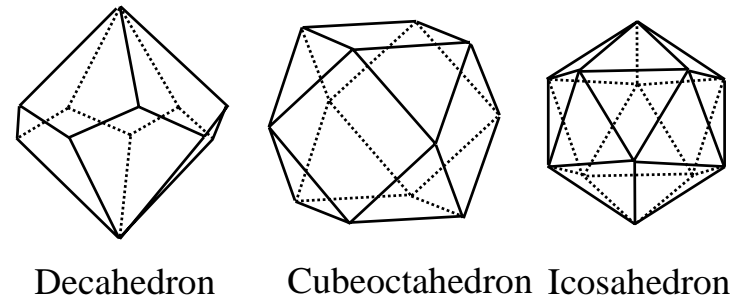
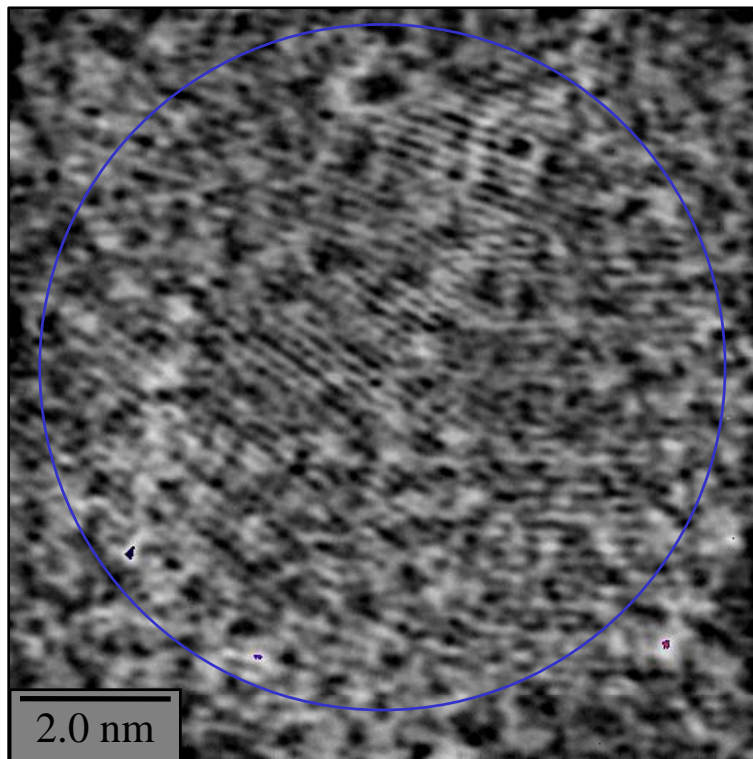


- TEM images show that fcc Co nanoparticles are spherical in shape.
- XRD fitting - one fault every 4 planes.
 - Bad fits at higher angles.
- Dark regions in TEM imply “multiple twinned” (MT) structures.

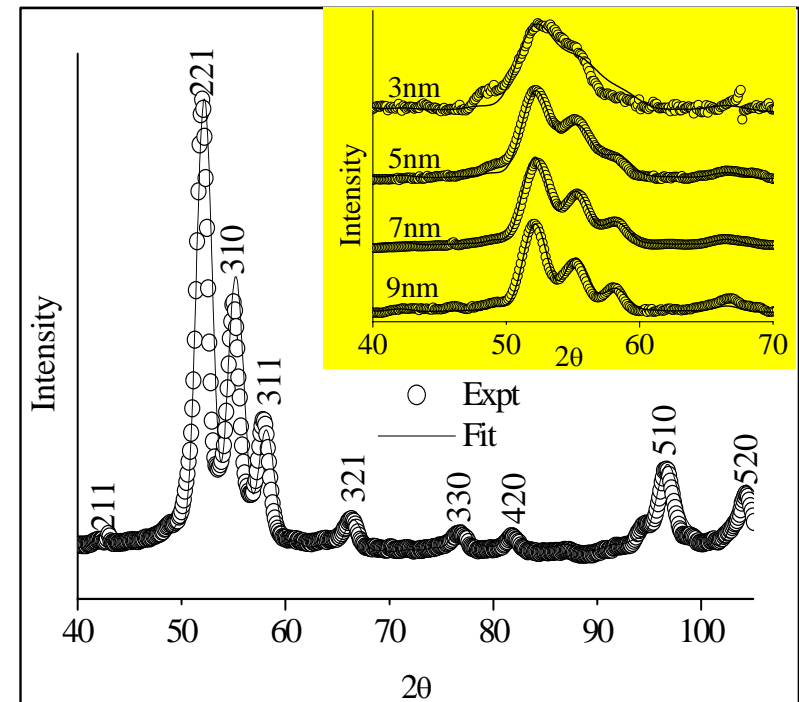
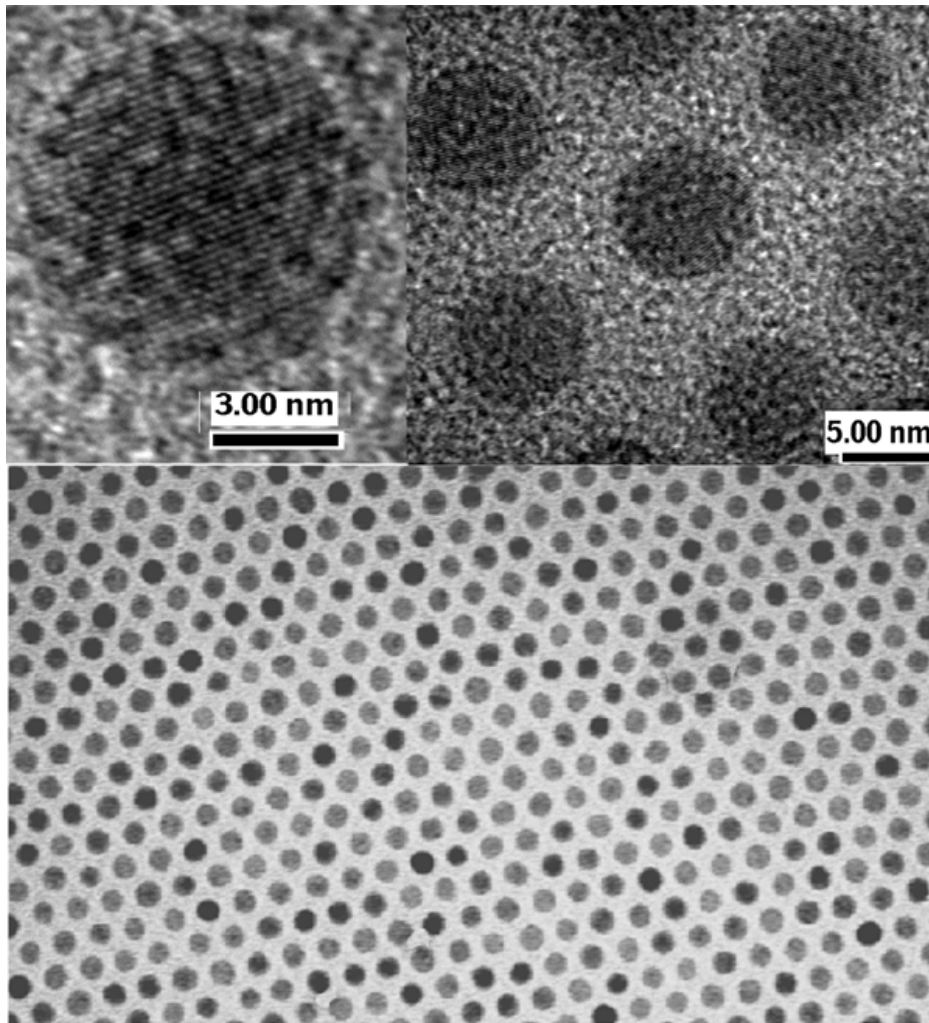


XRD Modeling of MT polyhedra

- Better fits have been reported for MT polyhedra
 - Highly faceted structures
 - Icosahedral, cubeoctahedral and decahedral structures suggested
- HR-TEM images also suggest the presence of multiple domains
 - Consistent with multiple twinning



XRD Modeling of ϵ -Co nanoparticles



- TEM images show that ϵ -Co forms as spherical nanoparticles with narrow size distributions.
- XRD fits - perfect crystalline internal structure.
- Supported by HR-TEM images of individual nanoparticles.

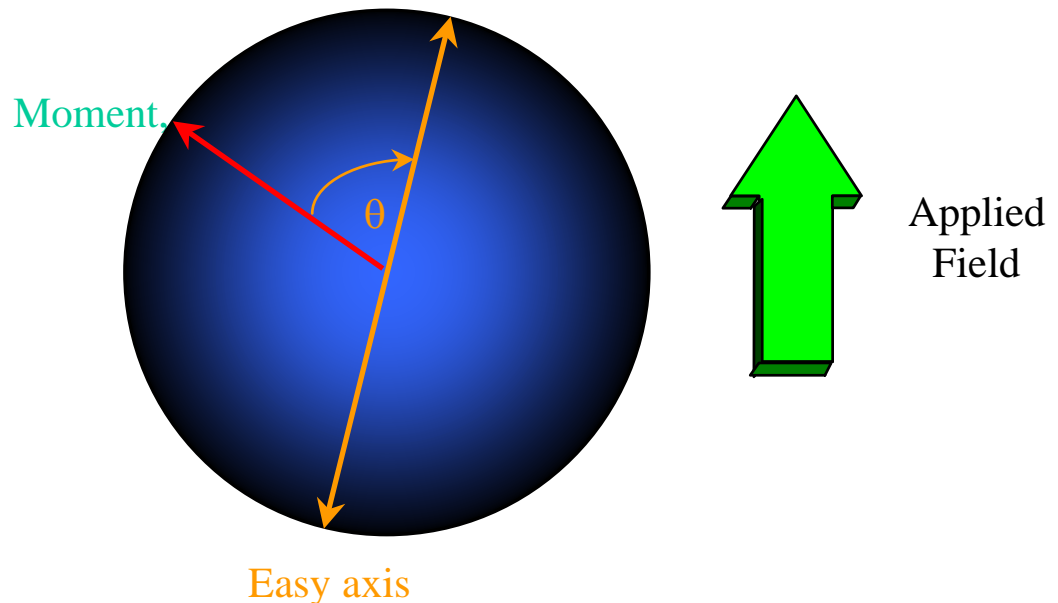
Modeling of the magnetization of Co nanoparticles

- Equilibrium partition function of nanoparticles in applied magnetic field.

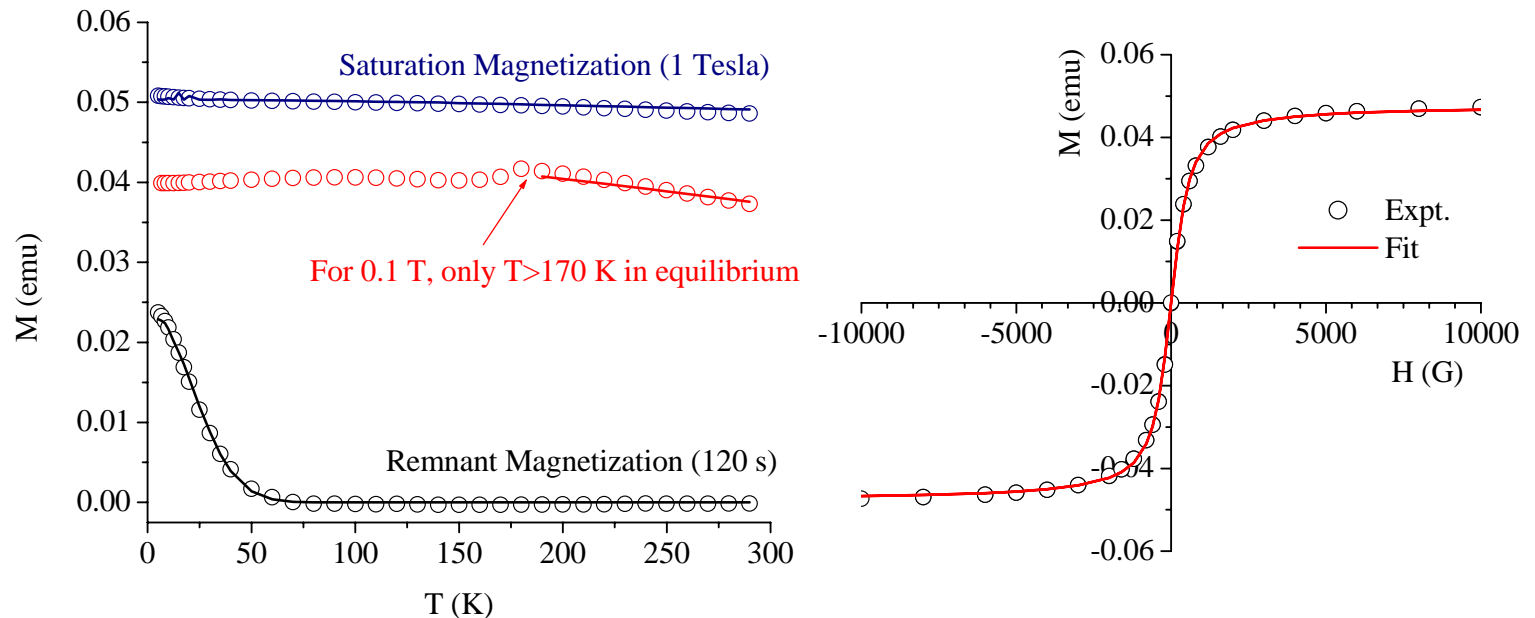
$$\langle M \rangle = \int dKp(K) \int dVp(V) \int dH_\theta \int dH_\phi \frac{\int d\mu_\theta \int d\mu_\phi M_{sat} (\hat{\mu} \cdot \hat{H}) e^{-E(\hat{H}, \hat{\mu}, K, V)/k_B T}}{\int d\mu_\theta \int d\mu_\phi e^{-E(\hat{H}, \hat{\mu}, K, V)/k_B T}}$$

$$E/V = -M_{sat} \hat{\mu} \cdot \hat{H} - KS_z^2$$

$$M_{rem}(t) = \int dKp(K) \int dVp(V) [\alpha M_{sat} e^{-t/\tau}] \quad \text{where} \quad \tau = \tau_0 e^{-KV/k_B T}$$

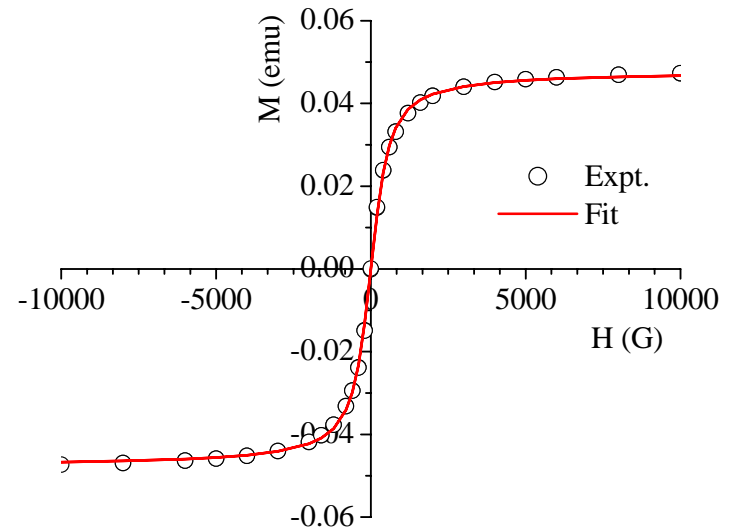
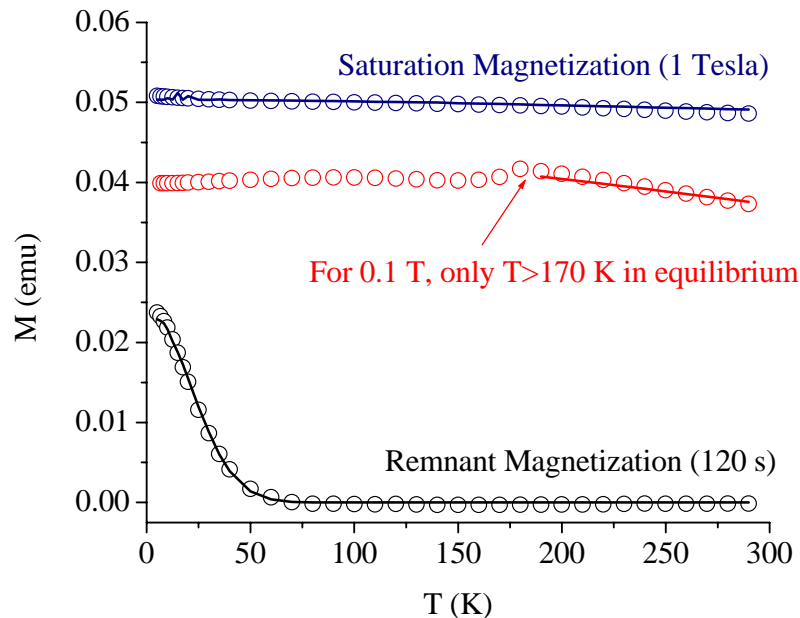


Magnetic modeling of MT Co nanoparticles



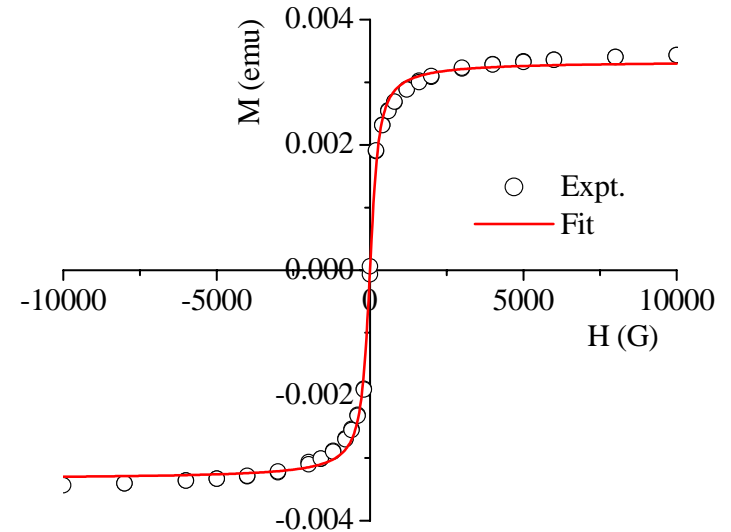
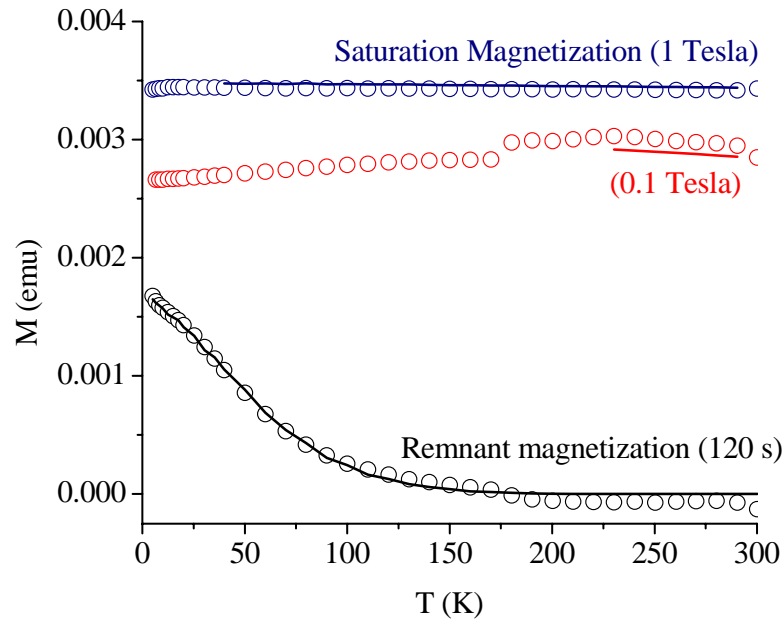
- TEM analysis - 7 nm diameter
- Magnetic fitting
 - Diameter 6.2 ± 0.5 nm
 - K $7.0 \times 10^5 \pm 3.5 \times 10^5$ ergs cm⁻³
- Smaller “magnetic” diameter accounted for by the presence of oxide layer.
- Anisotropy close to bulk fcc value
- Remnant magnetization is half saturation magnetization at low temperatures
 - Implies uniaxial symmetry.

Magnetic modeling of MT Co nanoparticles

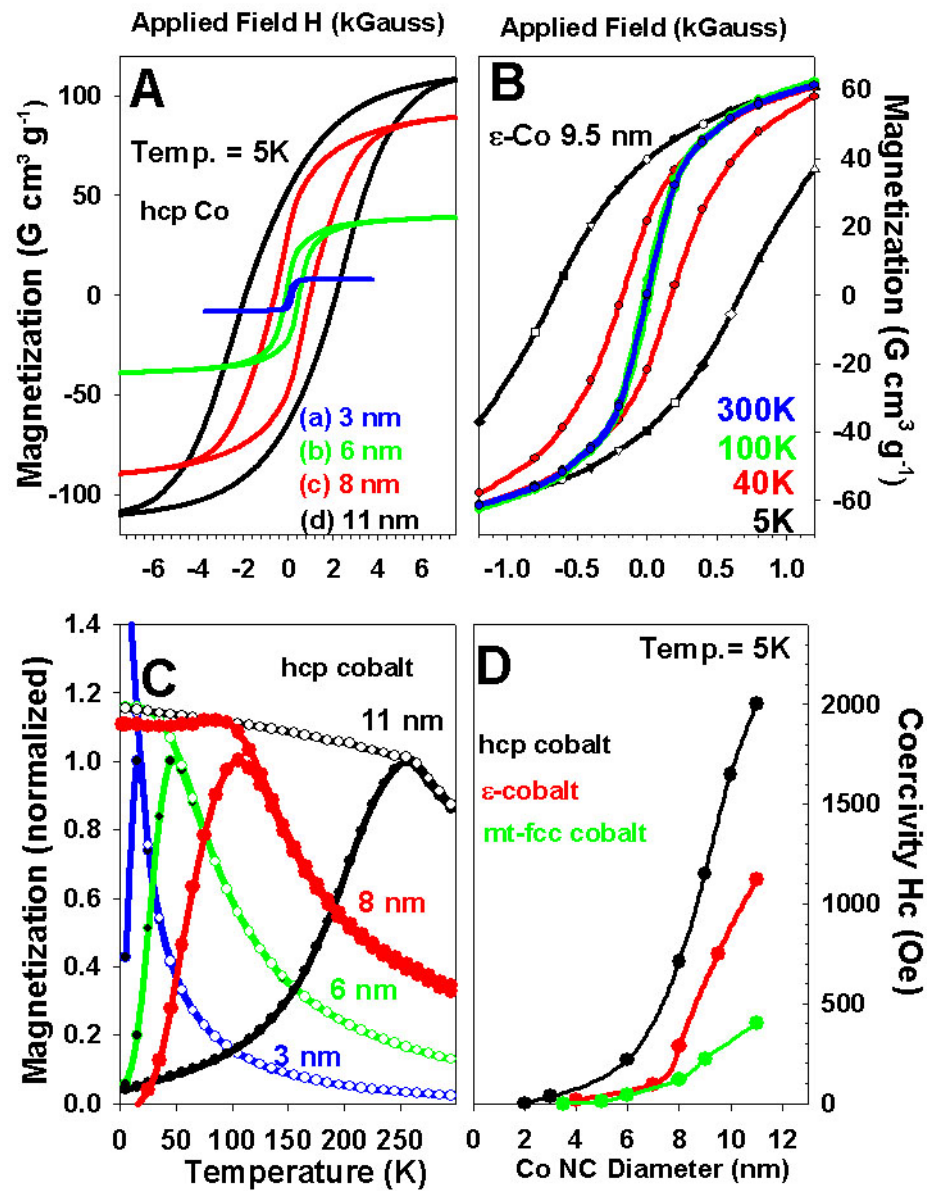


- TEM analysis - 7 nm diameter
- Magnetic fitting
- ◆ Diameter 6.2 ± 0.5 nm
 - ◆ K $7.0 \times 10^5 \pm 3.5 \times 10^5$ ergs cm^{-3}
- Smaller “magnetic” diameter accounted for by the presence of oxide layer.
- Anisotropy close to bulk fcc value
- Remnant magnetization is half saturation magnetization at low temperatures
- ◆ Implies uniaxial symmetry
 - ◆ Predicted for MT polyhedra

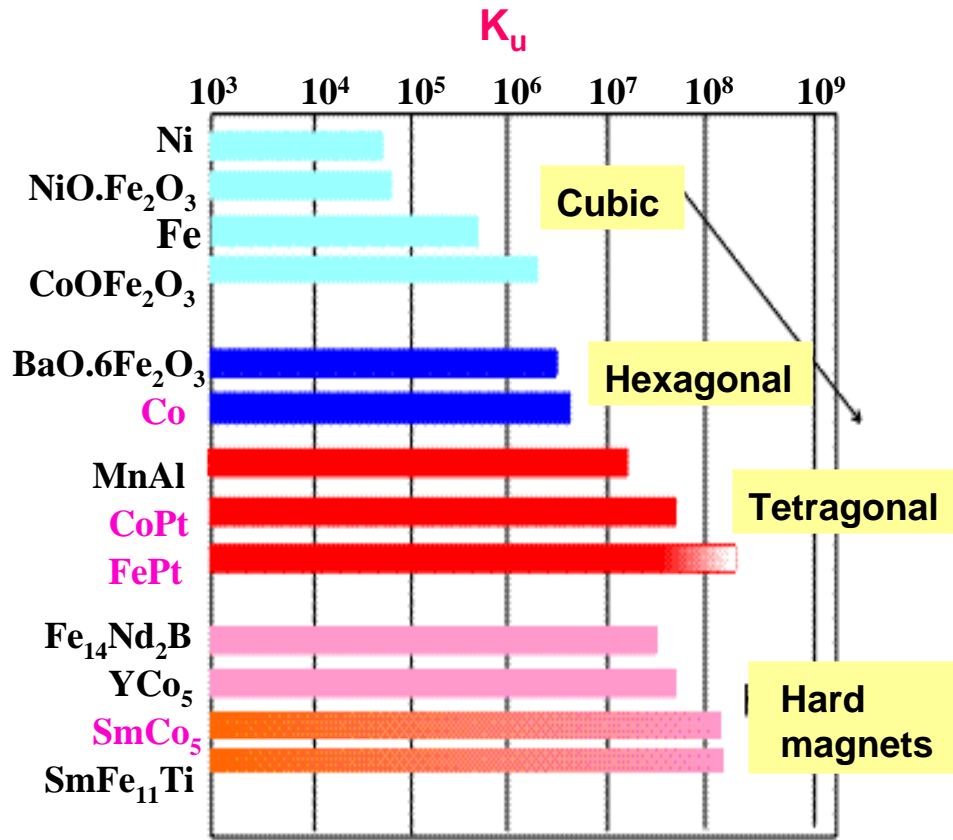
Magnetic modeling of ϵ -Co nanoparticles



- TEM analysis - diameter of 9.5 nm
- Magnetic fitting
 - Diameter 8.4 ± 0.9 nm
 - Anisotropy $7.1 \times 10^5 \pm 4.0 \times 10^5$ ergs cm^{-3}
- Anisotropy also close to bulk fcc value
- Remnant magnetization is half saturation magnetization at low temperatures
 - Implies uniaxial symmetry.



Materials Selection: $K_u V \gg kT$

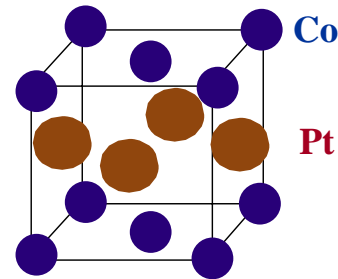


$K_u V \gg kT$

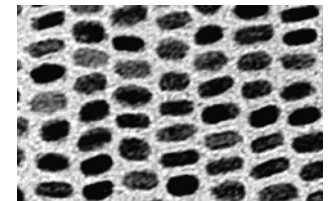


$K_u V < kT$

Crystal Anisotropy
 Shape Anisotropy
 Exchange Anisotropy
 Strain Anisotropy



CoPt L₁₀ structure (tetragonal)

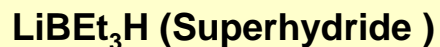
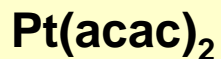


Shape ?

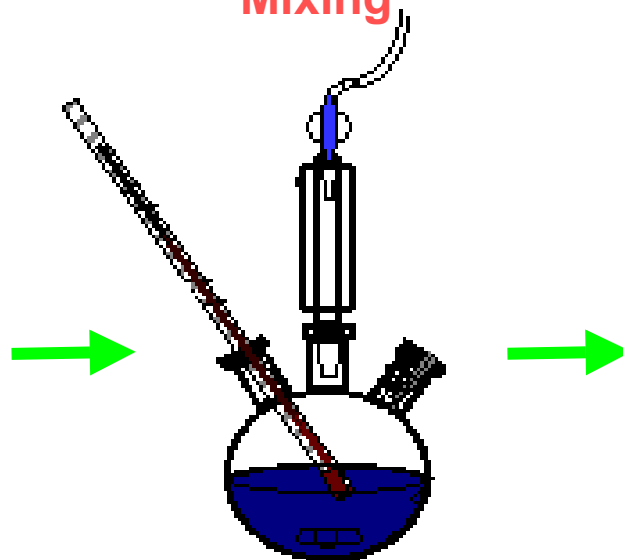
Solution phase synthesis

Example: FePt nanopartilces

Starting Materials

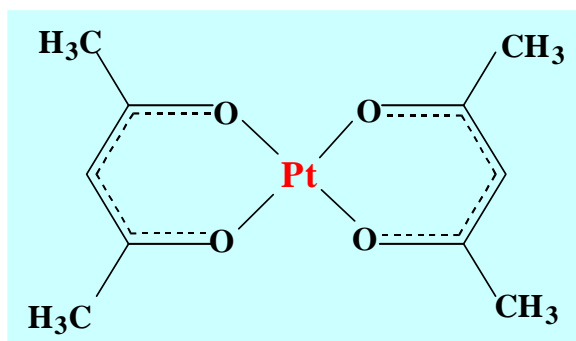
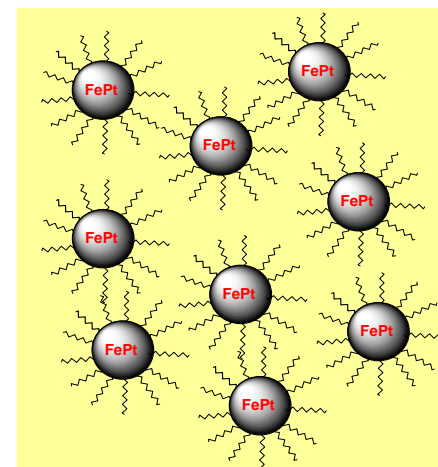


Mixing



200-260°C

Particle dispersion

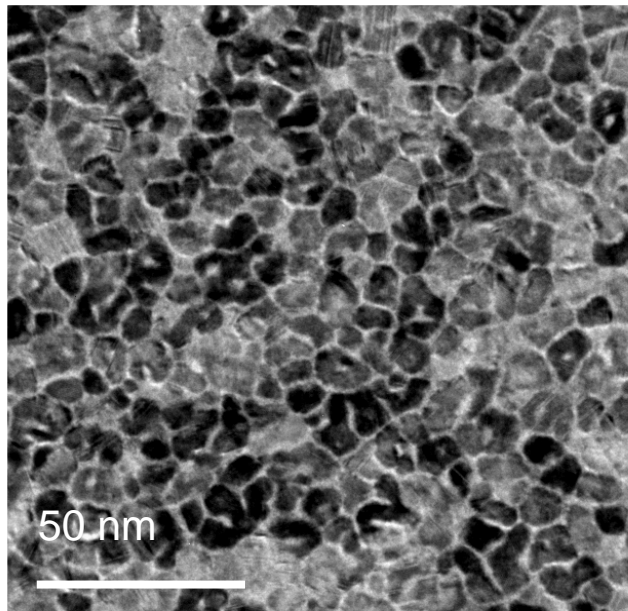


S. Sun, C. B. Murray,
IBM Yorktown

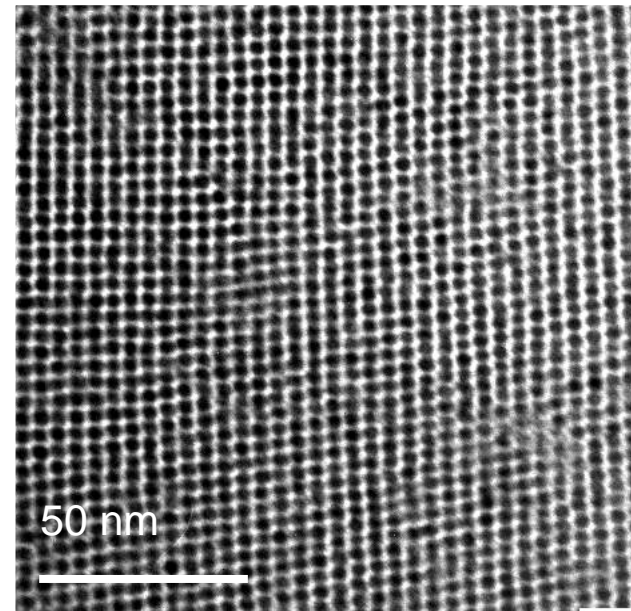
Nanoparticles for magnetic storage

- Narrow size distribution \rightarrow higher thermal stability
- Smaller particles \rightarrow narrower transition widths

35 GBit/in² prototype media
8.5 nm grains
 $\sigma_{\text{area}} \cong 0.6$

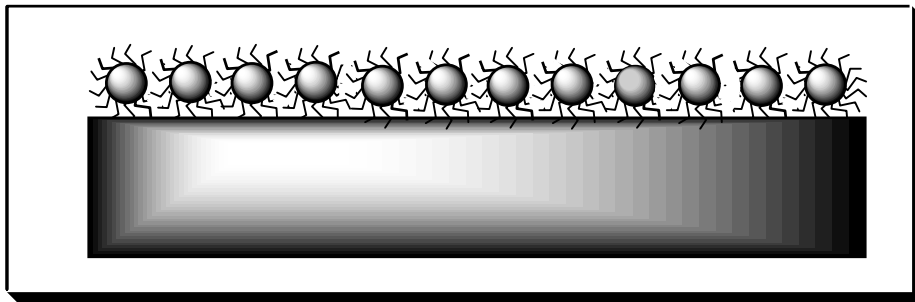


Nanoparticle arrays
4 nm FePt particles
 $\sigma_{\text{area}} \cong 0.05$

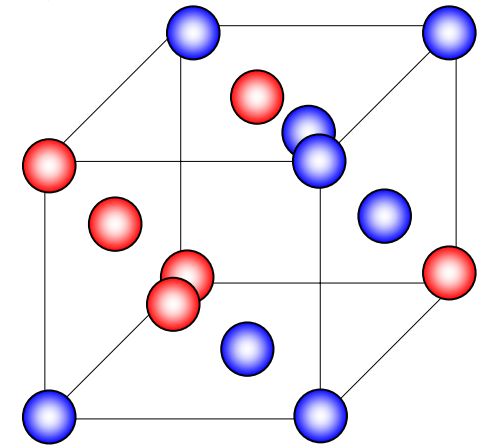


Magnetic properties

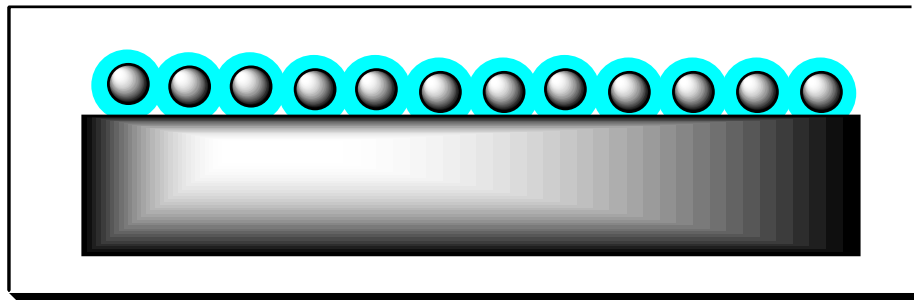
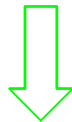
- Annealing leads to formation of ordered, ferromagnetic phase



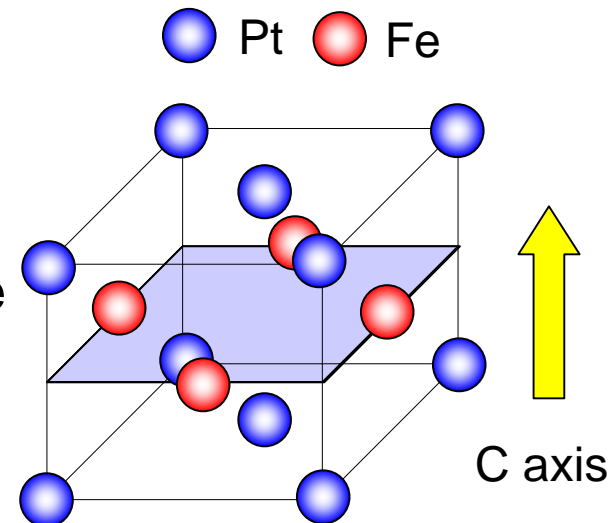
Chemically disordered
fcc structure
Superpara-
magnetic



Annealing at 550C



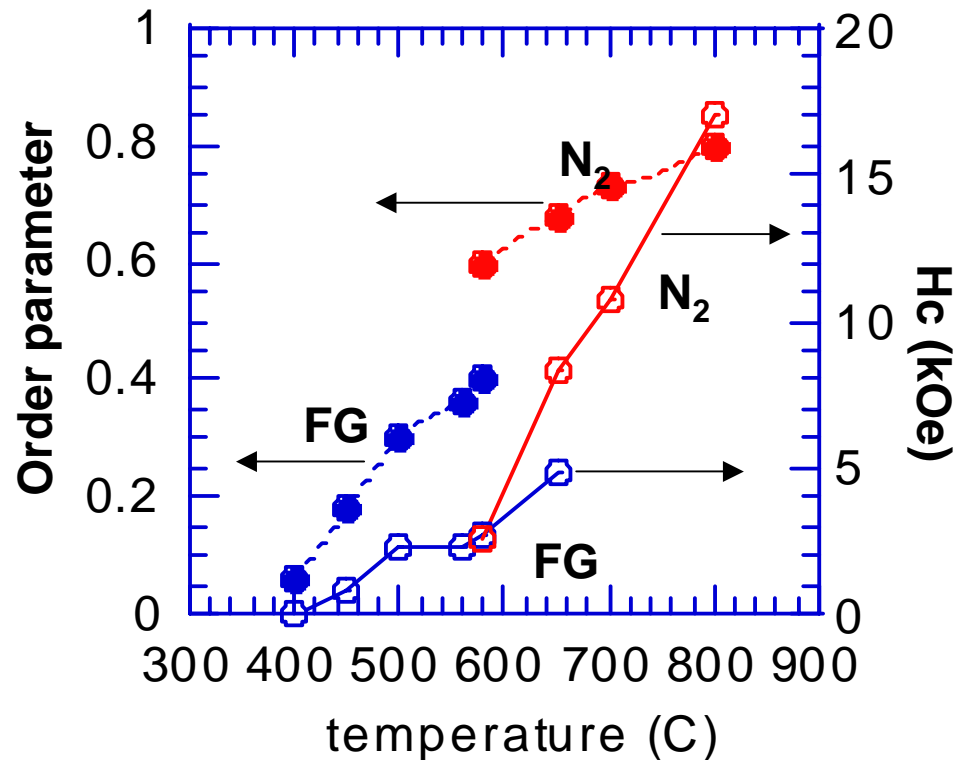
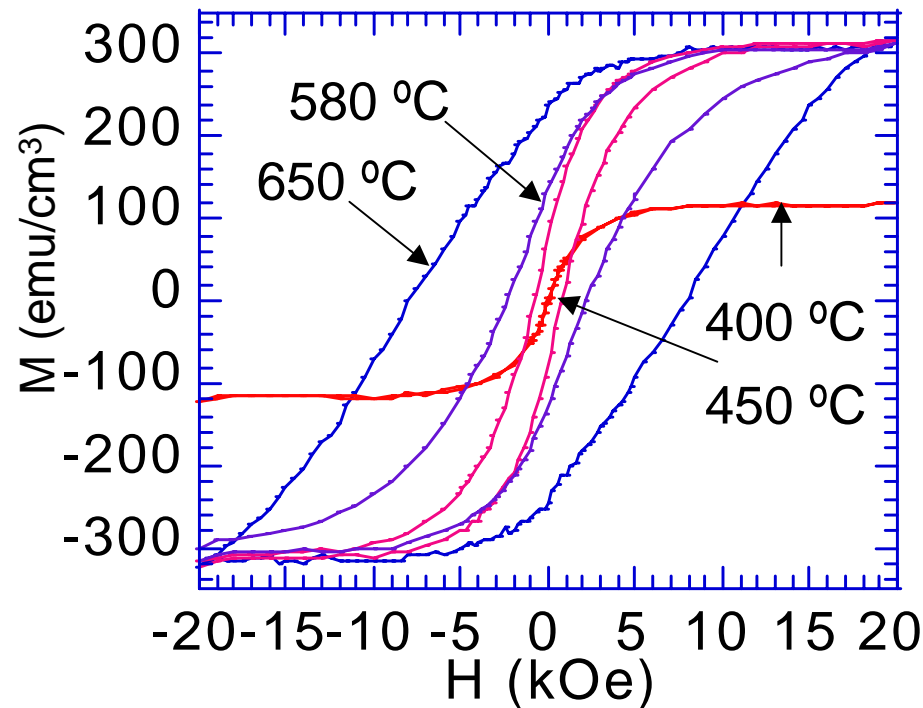
Chemically ordered
fct structure
Ferro-
magnetic



Magnetic properties

- Order parameter and coercivity increase with annealing temperature and duration

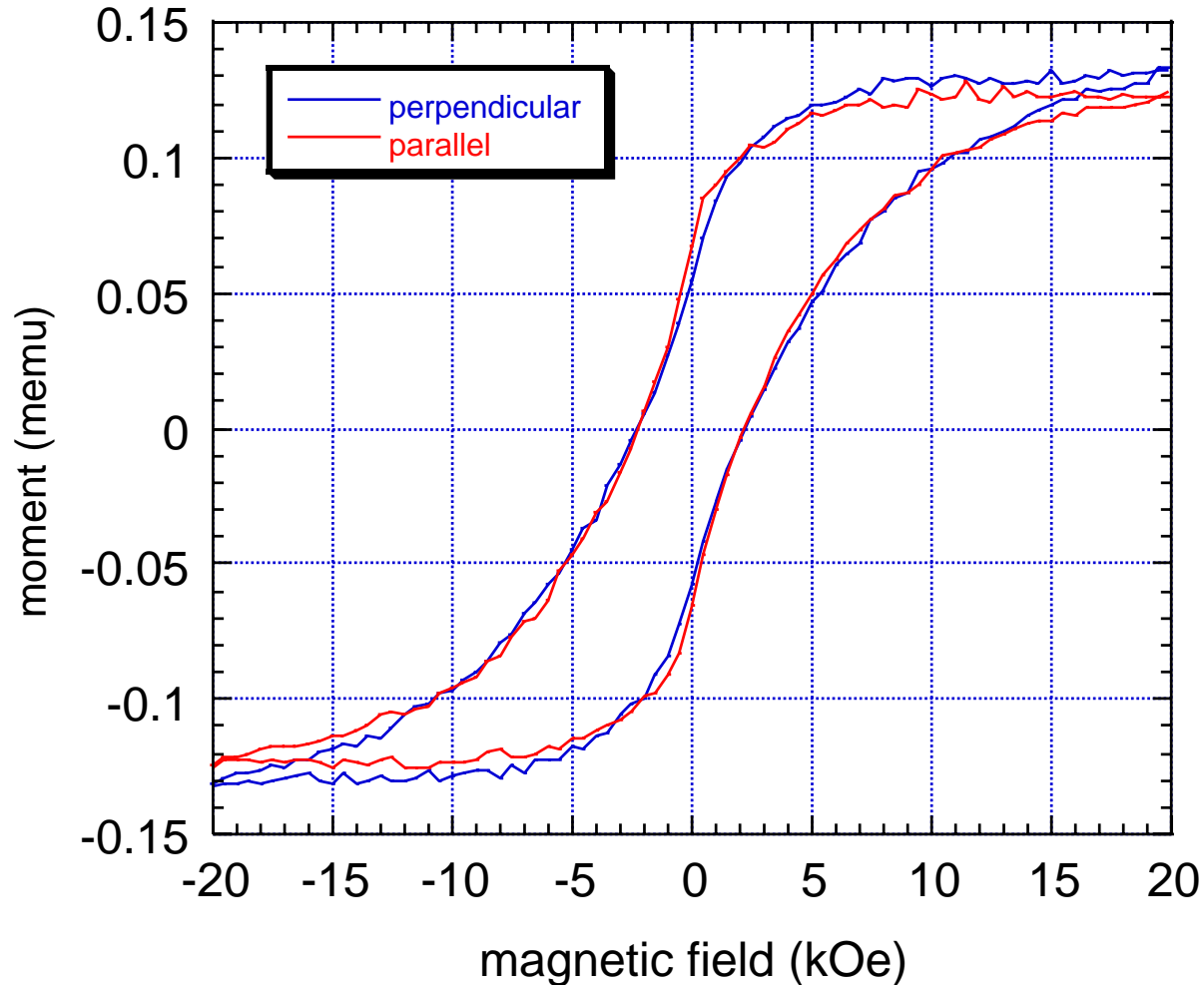
3 layer samples of 6 nm FePt particles



XRD data M. Toney, IBM Almaden

VSM Hysteresis loops

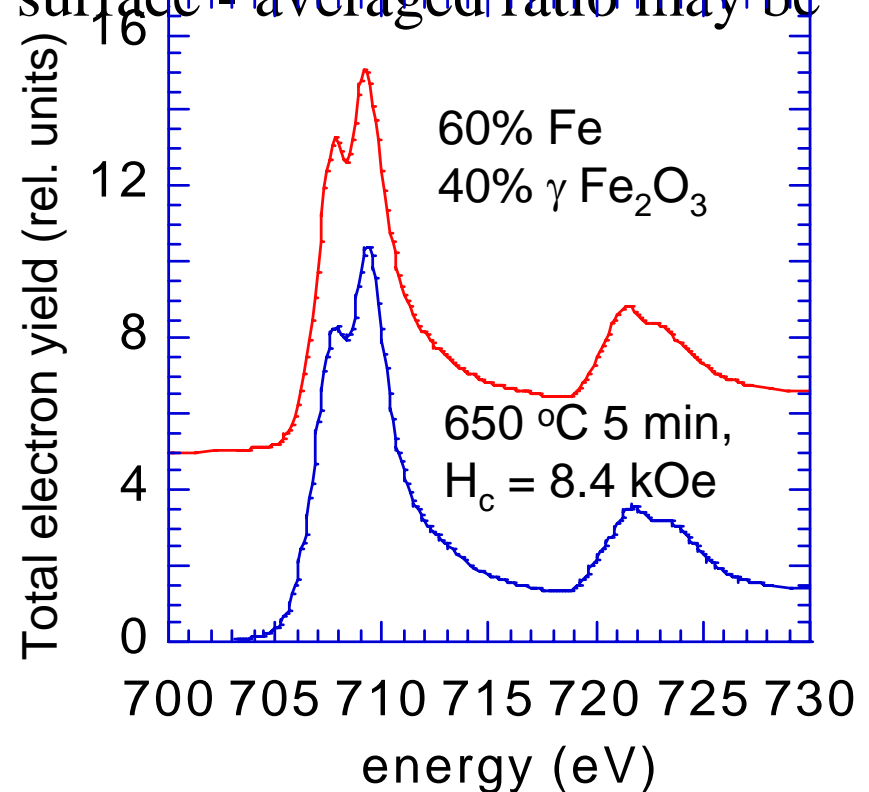
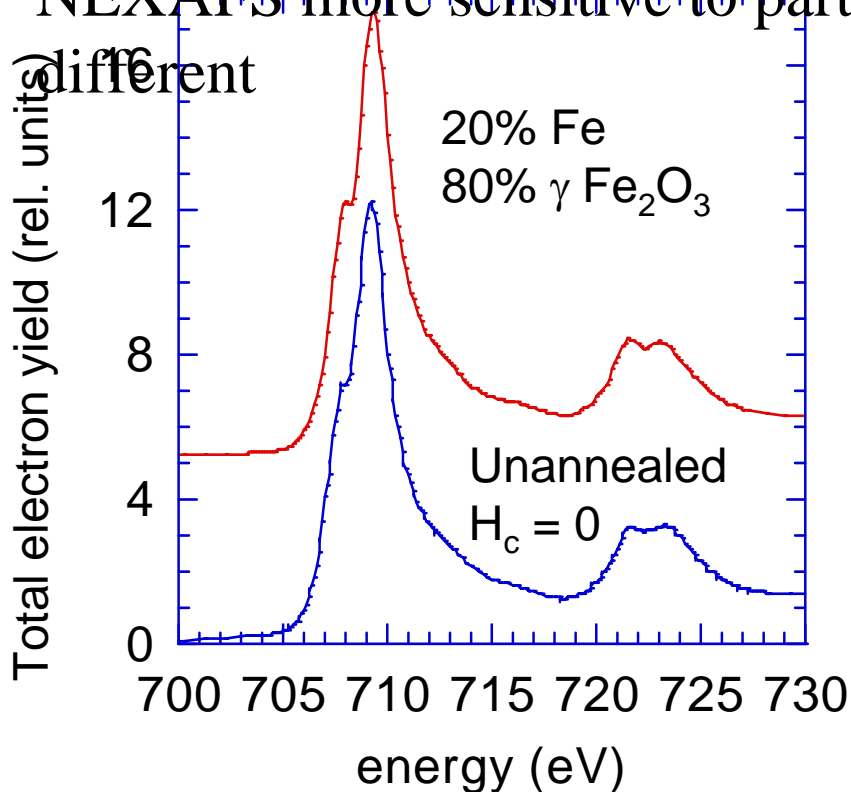
3 layers, annealed in N_2 at 580 C for 30 min, FePt samples from $FeCl_2$



“3D” random assembly of 4nm particles

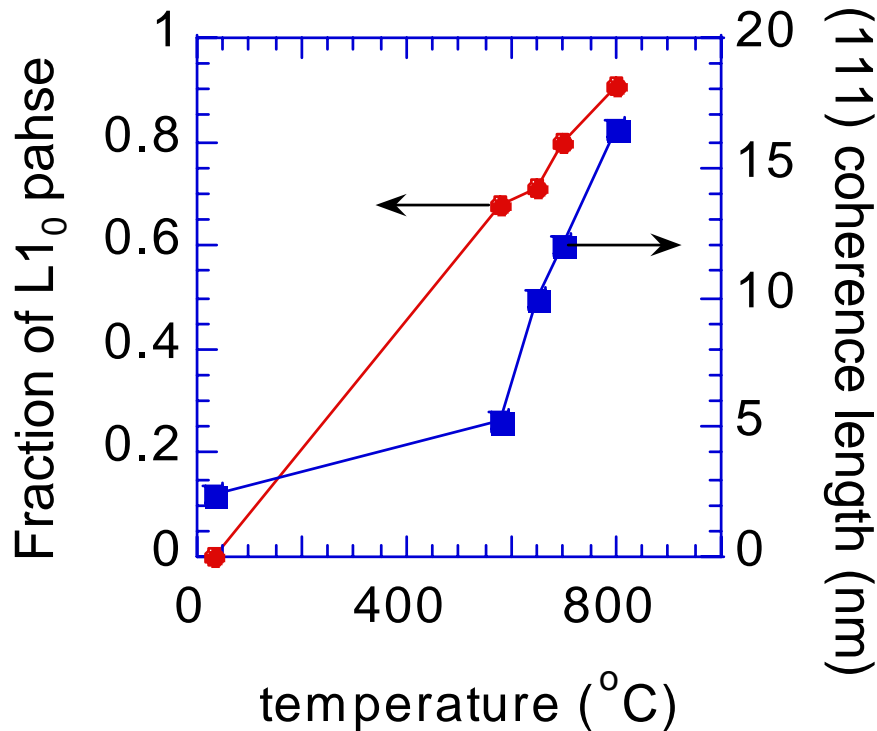
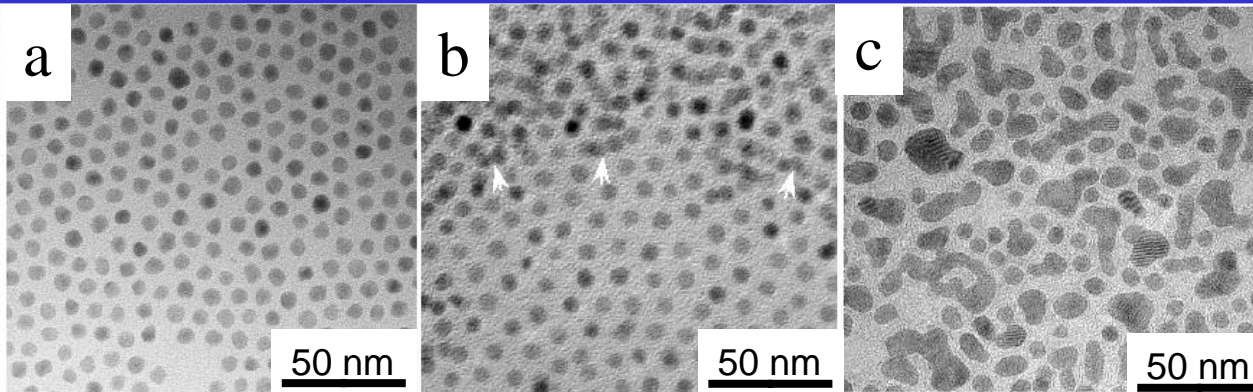
Chemical analysis

- Near Edge X-ray Absorption Fine Structure (NEXAFS) spectroscopy shows iron oxide fraction that is reduced upon annealing
- NEXAFS more sensitive to particle surface - averaged ratio may be different



Special thanks to Robin Farrow for providing iron oxide reference samples.

Structural properties

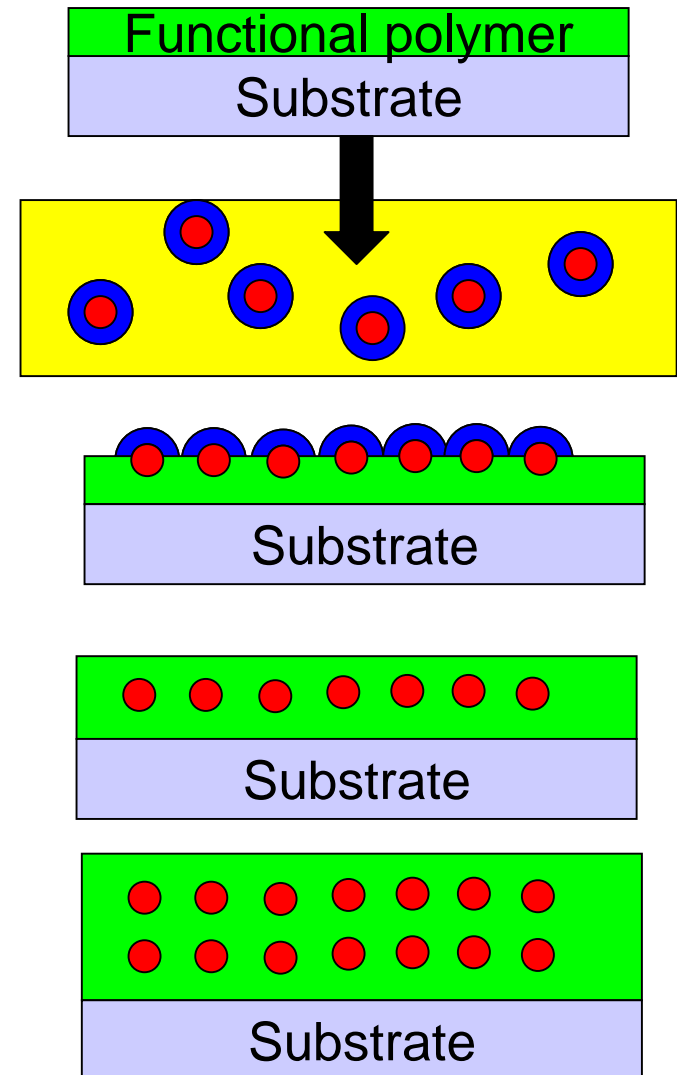


TEM images courtesy of Zu-Rong Dai

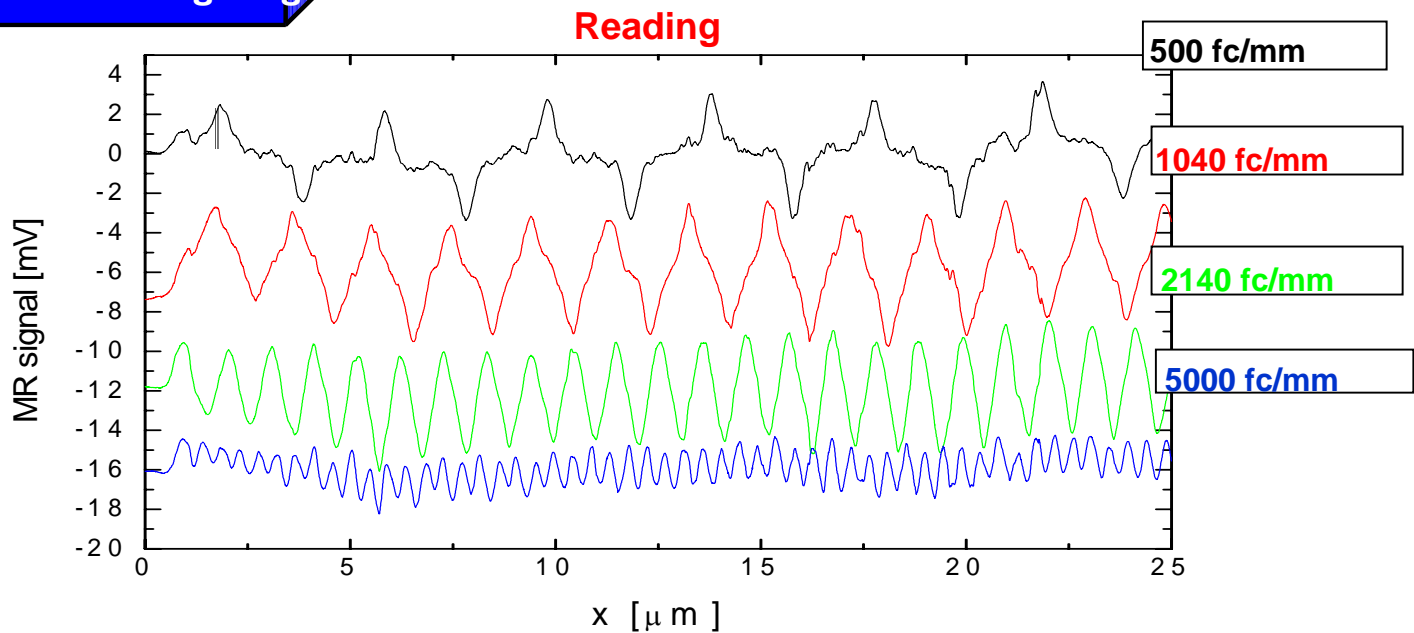
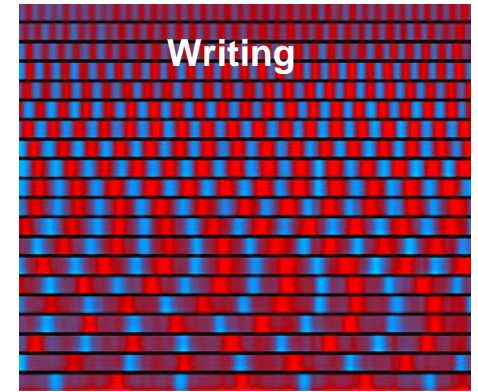
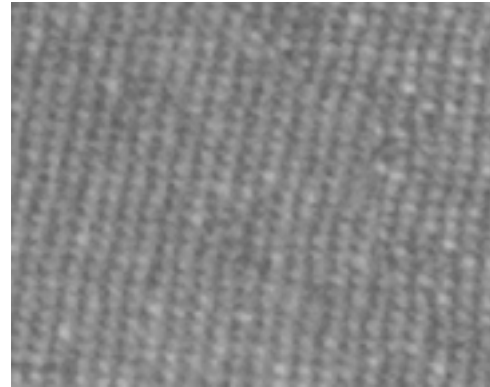
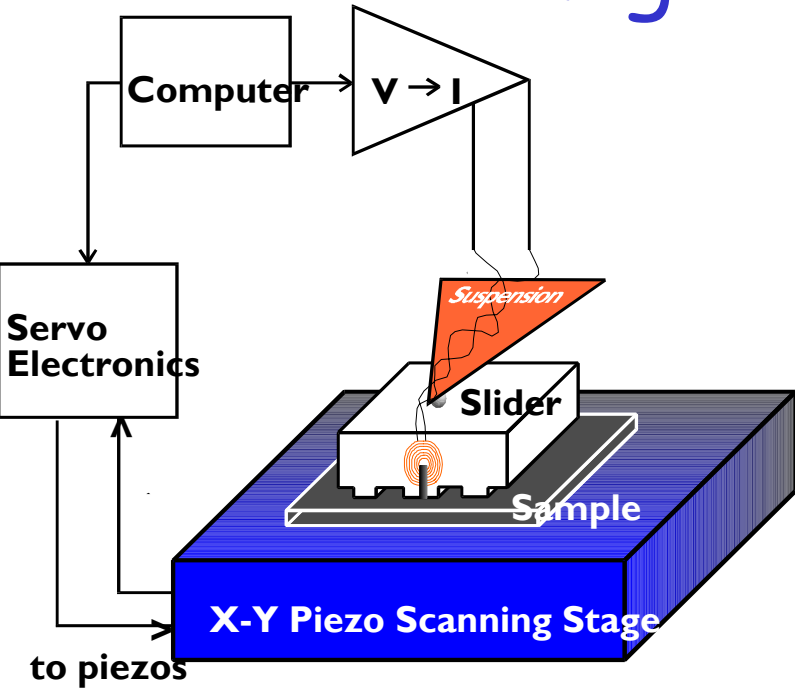
- X-ray scattering and TEM used to study structural properties
- 3 layers of 4 nm particles annealed in N₂

Polymer-mediated self assembly

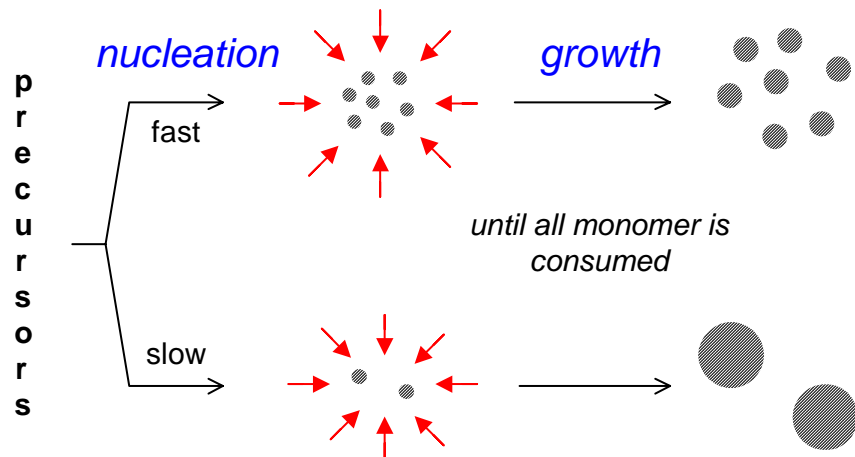
- Substrate surface is functionalized
- Dipped into dispersion of stabilized nanoparticles
- Ligand exchange leads to formation of strongly bound layer of nanoparticles
- New layer of functional molecule replaces stabilizer
- Repeat process to form multilayers



Magnetic recording



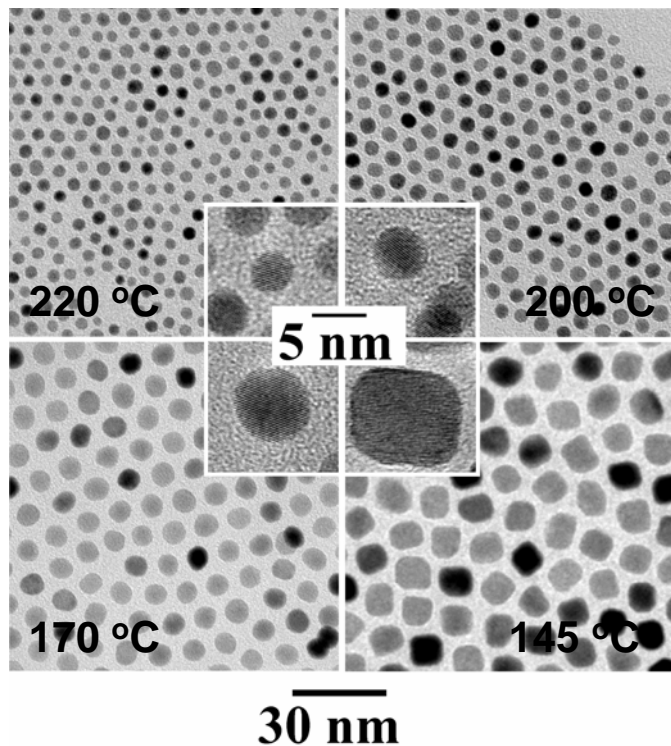
Size control of nanocrystals in the absence of Ostwald ripening



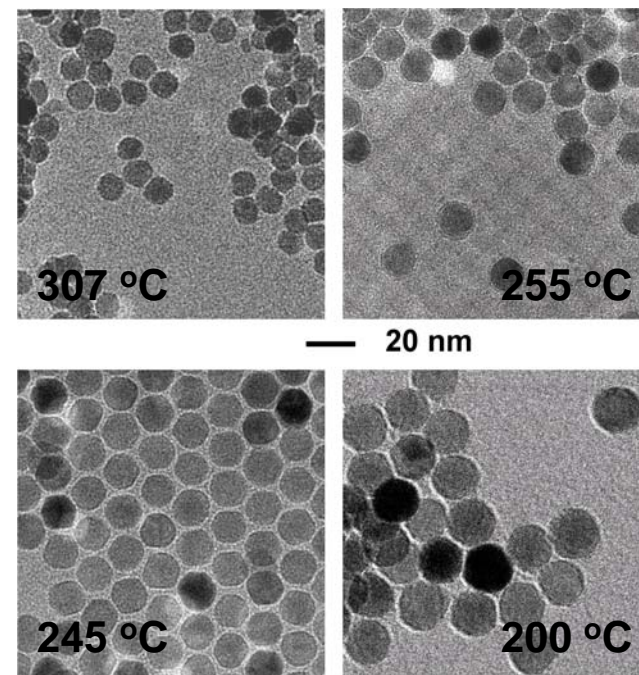
Factors influencing the nucleation rate

- reaction temperature
- concentrations of precursors
- concentrations of surfactants

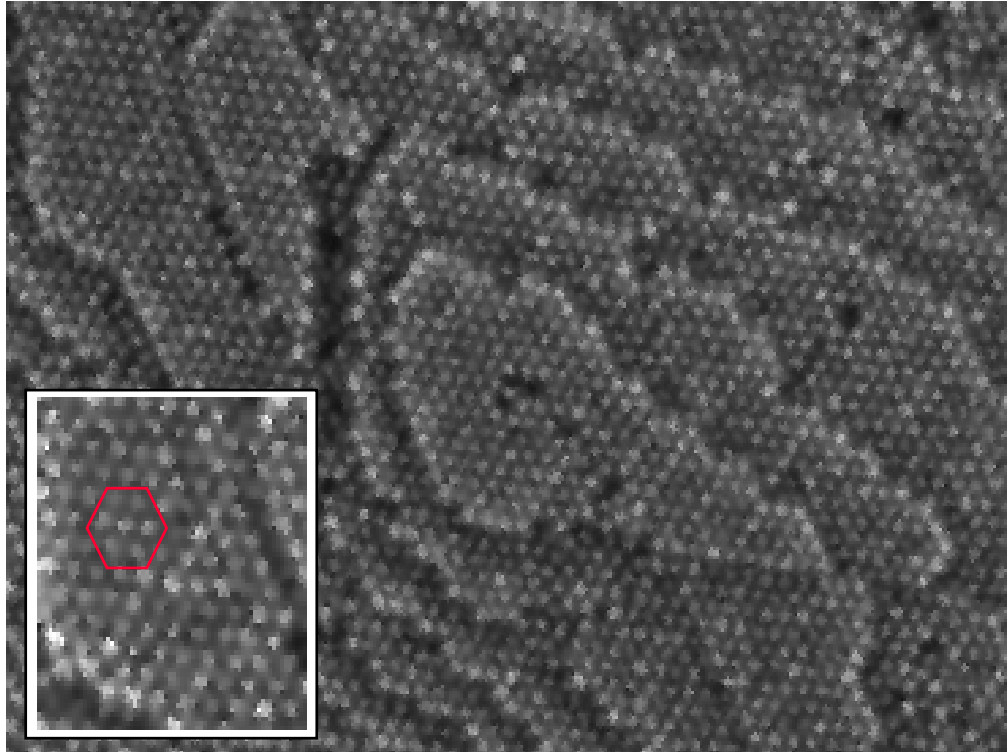
CoPt₃ nanocrystals



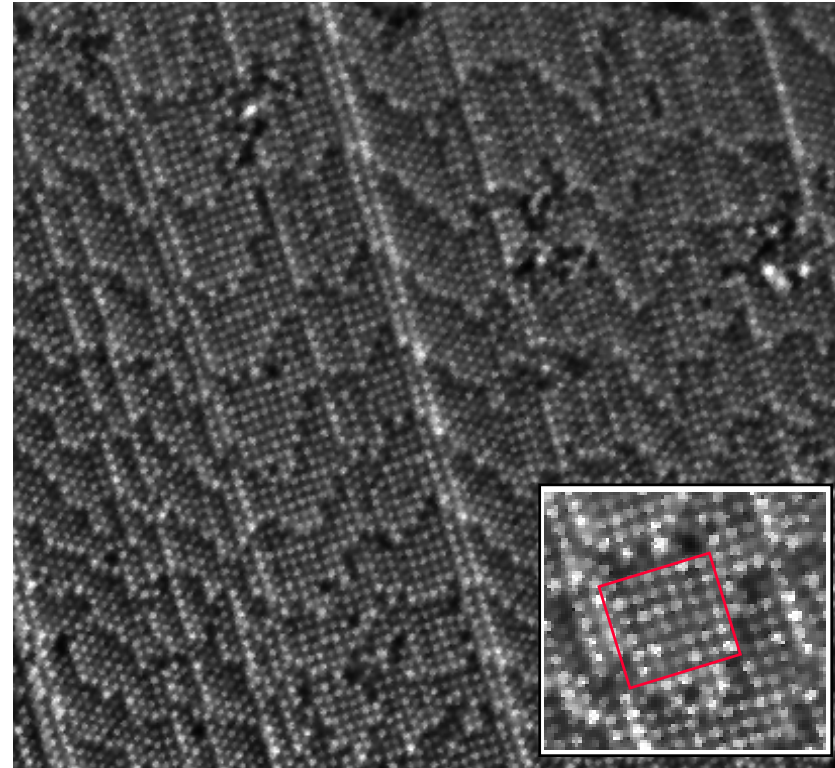
Fe₂O₃ nanocrystals



Cobalt Nanocrystal Superlattices (T. Betley et al)



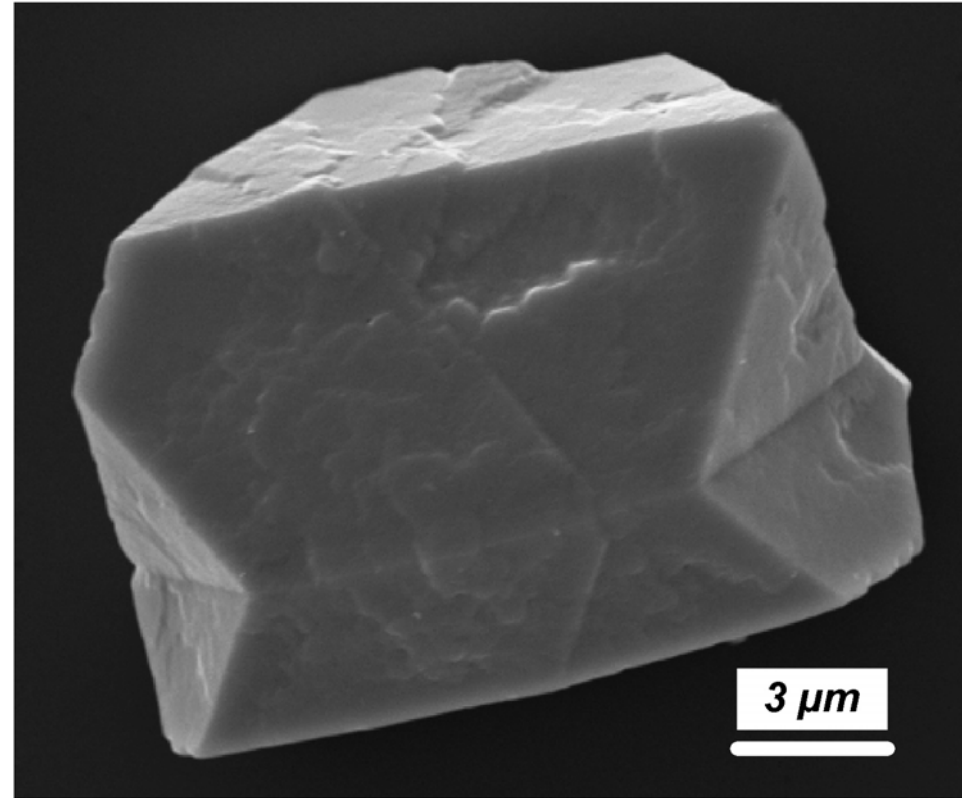
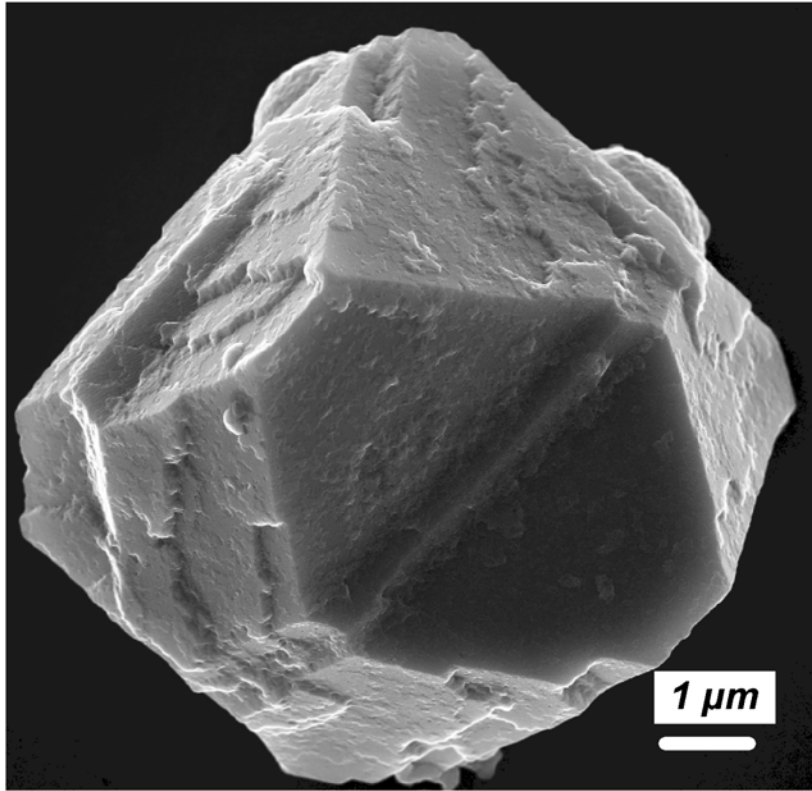
Hexagonal packing



Cubic packing

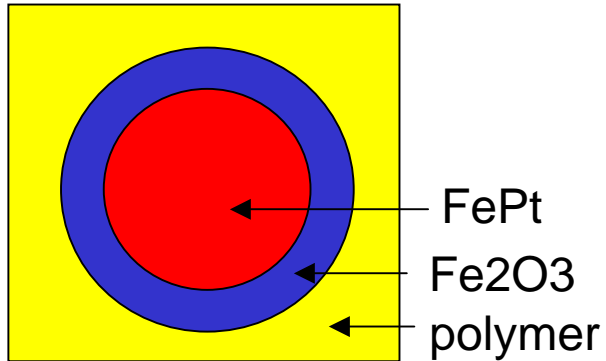
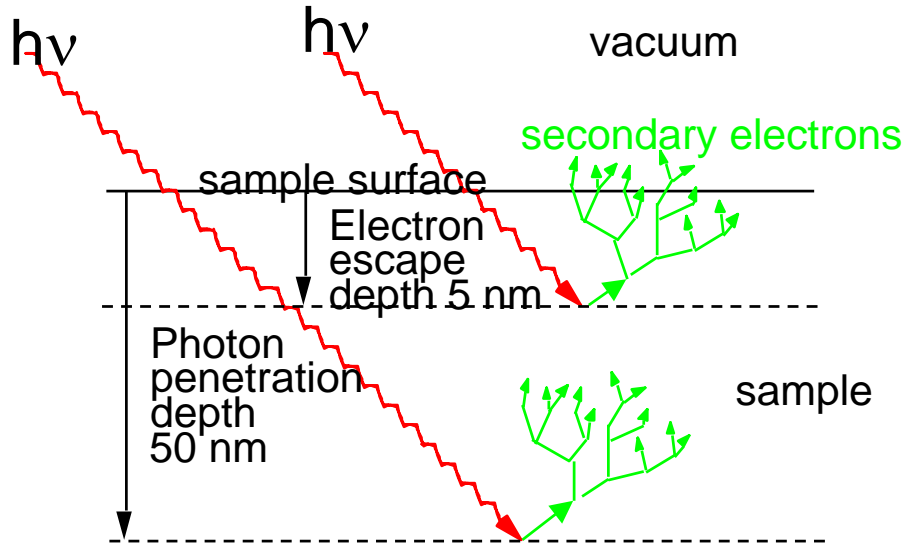
10 nm Cobalt NCs

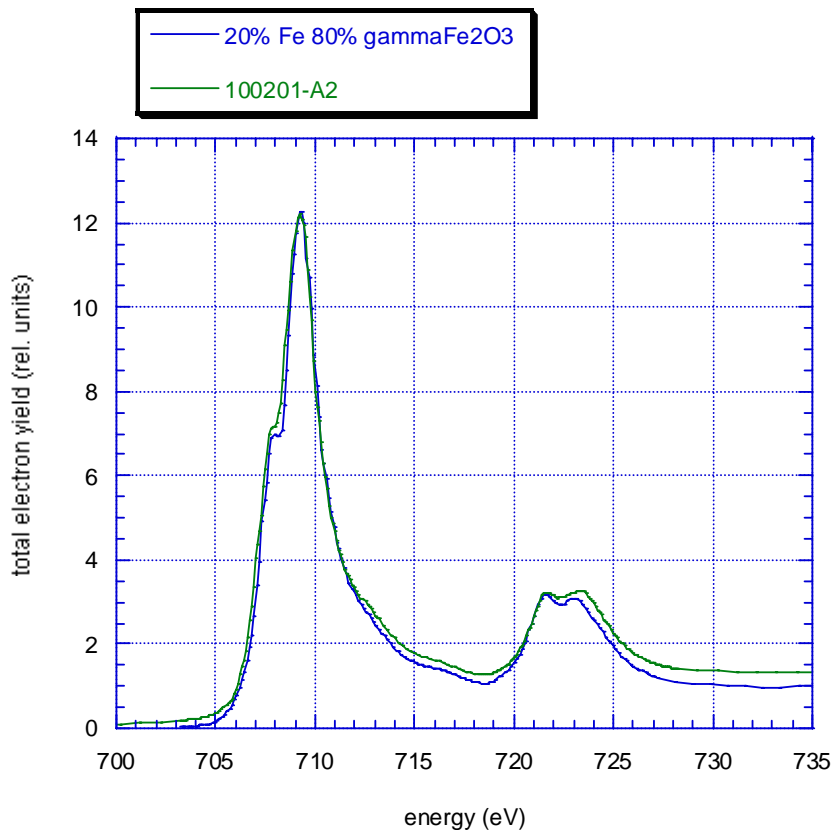
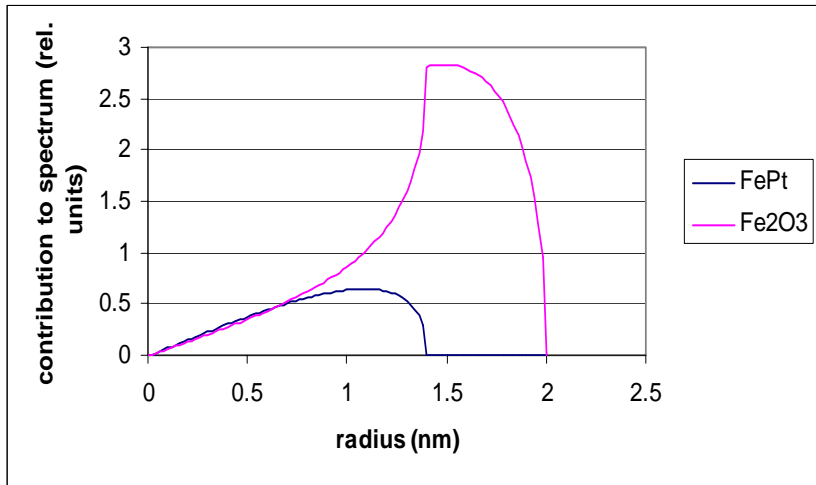
Three-dimensional colloidal supercrystals of CoPt_3 nanocrystals



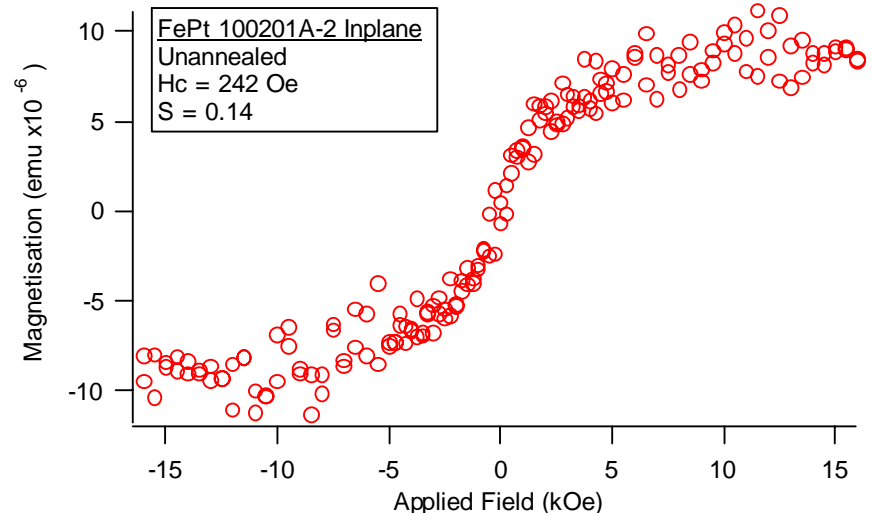
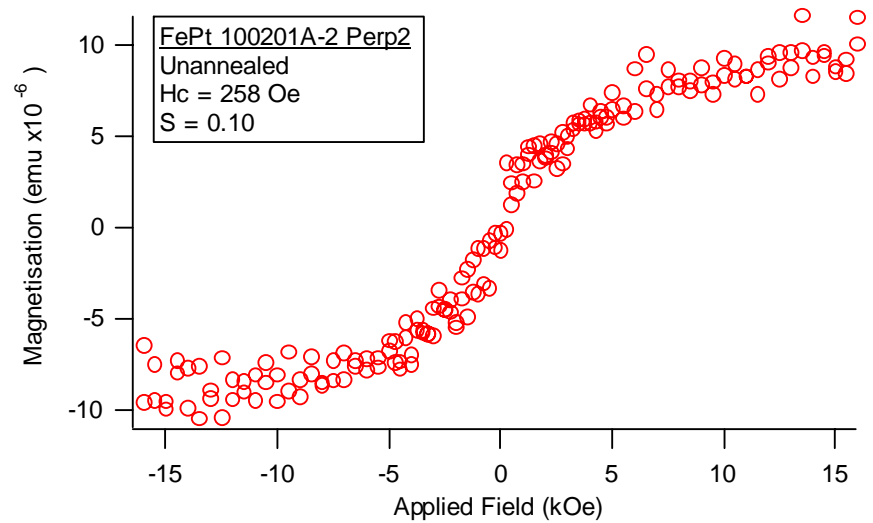
*Institute of Physical Chemistry, University of Hamburg,
Hamburg, Germany*



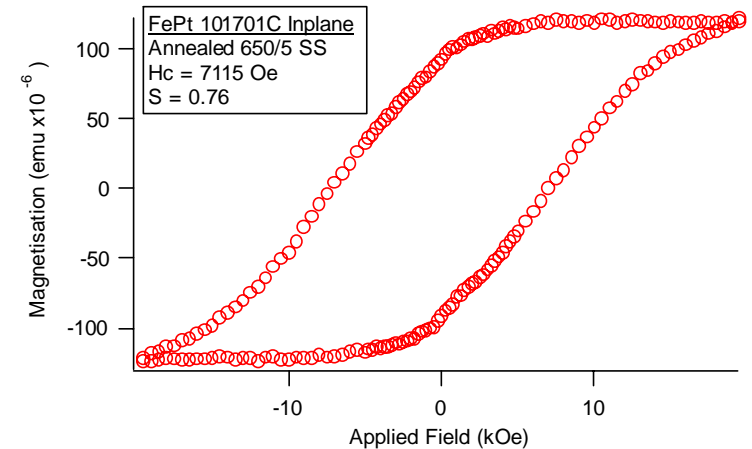
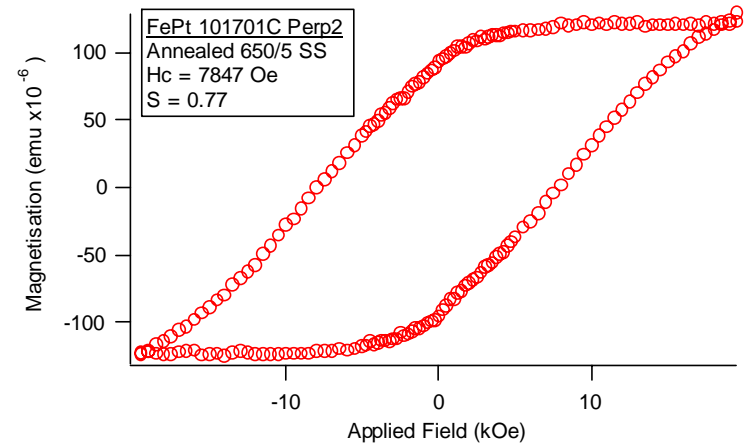
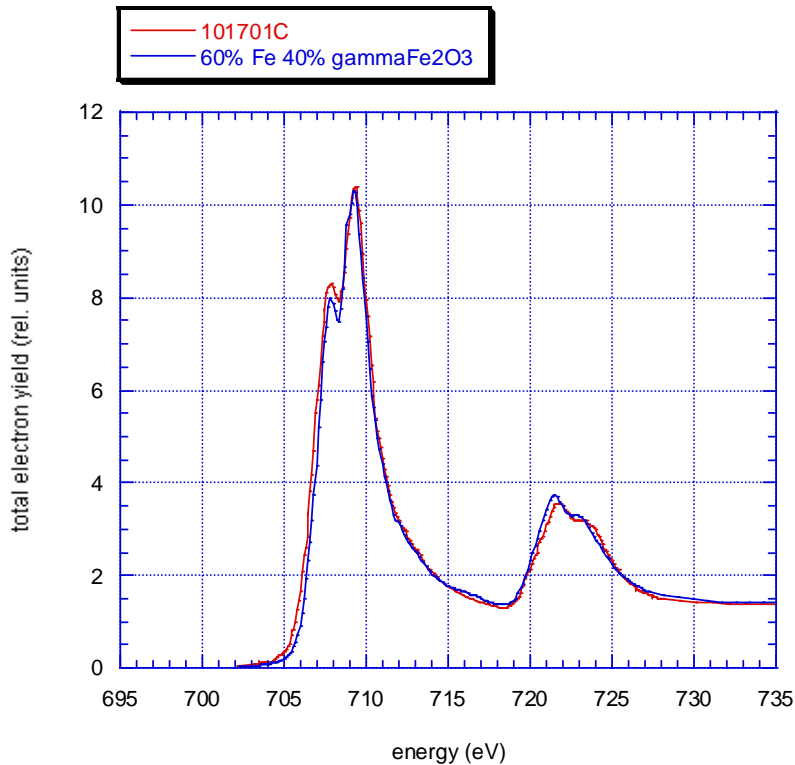
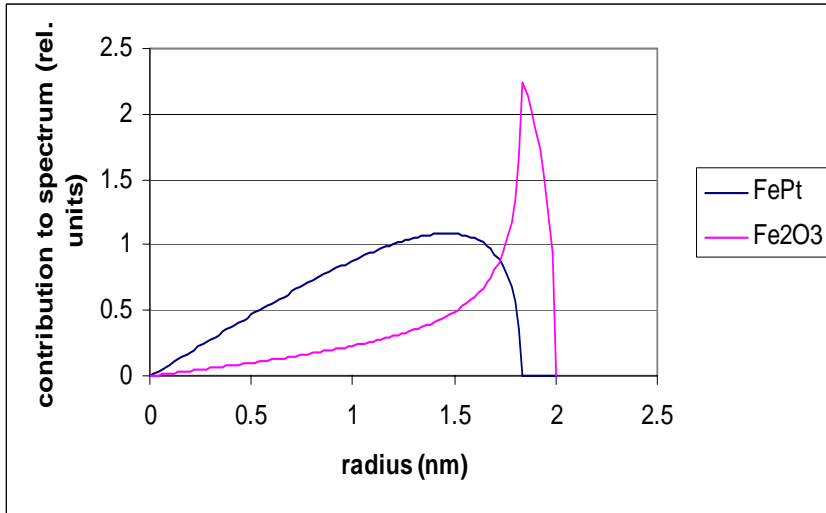


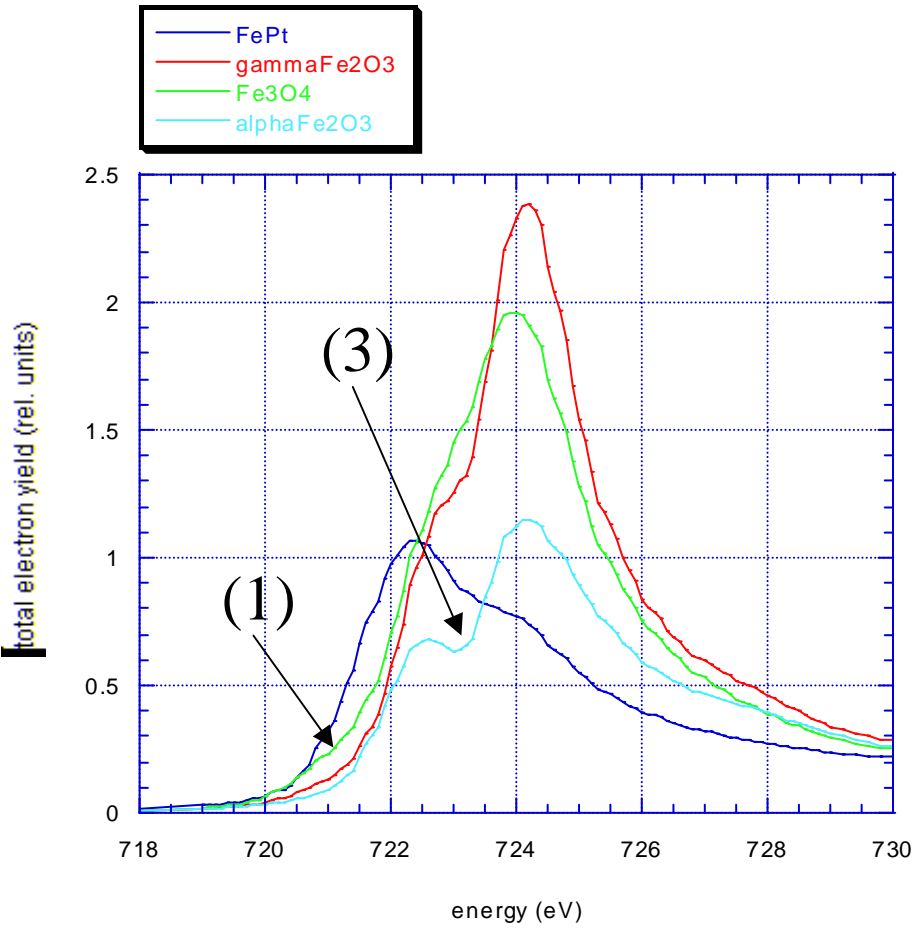


For the unannealed particles the ratio in the spectra can be estimated as 20%Fe, 80% Fe₂O₃ (I am still not sure what oxide we have, maybe a mixture). On the left is the contribution to the spectra as a function of radius. A 3nm diameter FePt metal core with a 0.5nm thick oxide shell would produce such a spectrum.

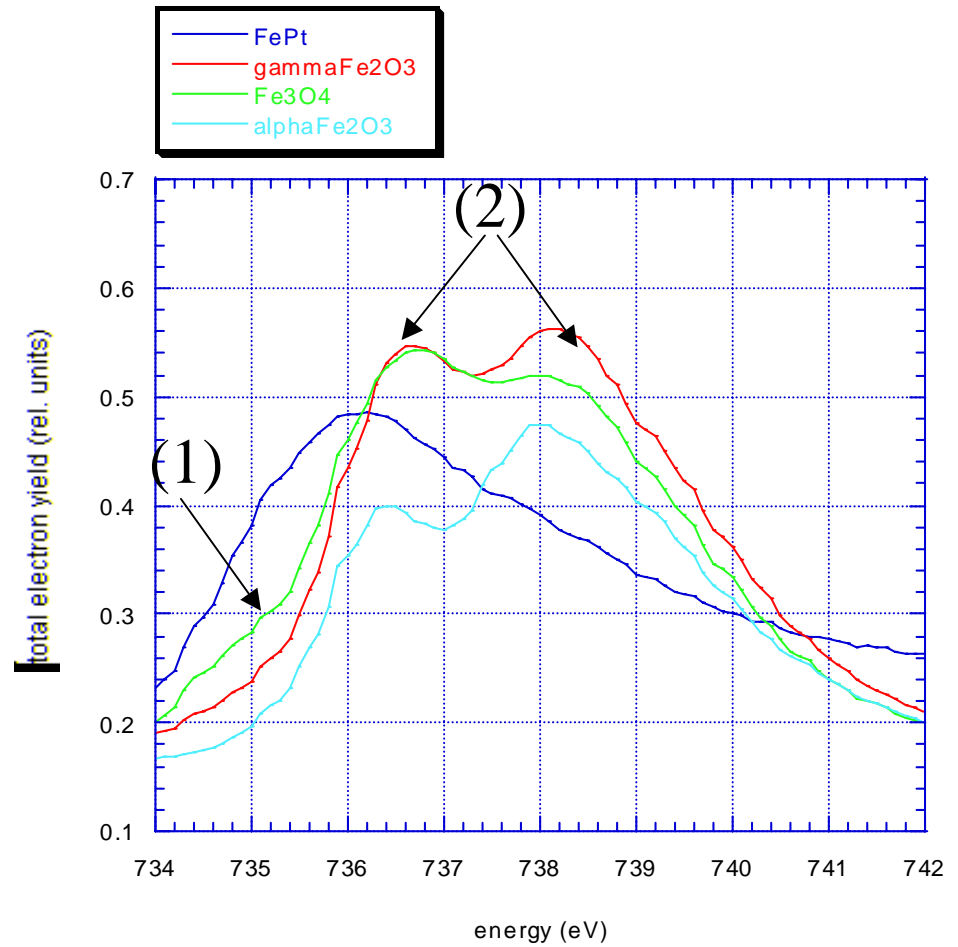


For the annealed particles the metal ratio is much higher, here an example for 650C/5min anneal. On the left is the contribution to the spectra as a function of radius. A 3.6 nm diameter FePt metal core with a 0.2nm thick oxide shell would produce such a spectrum.

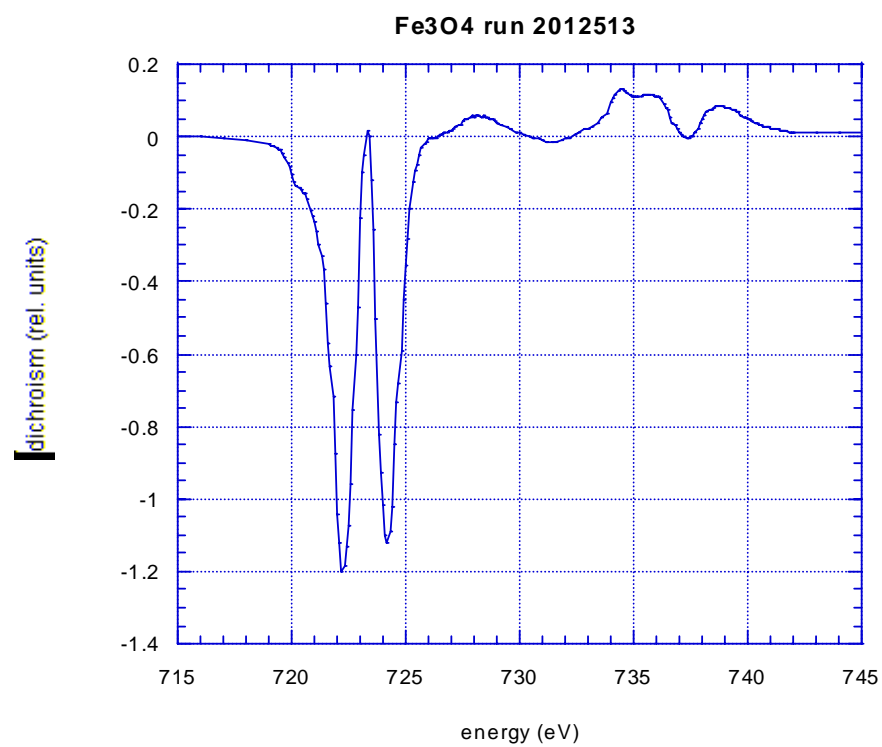
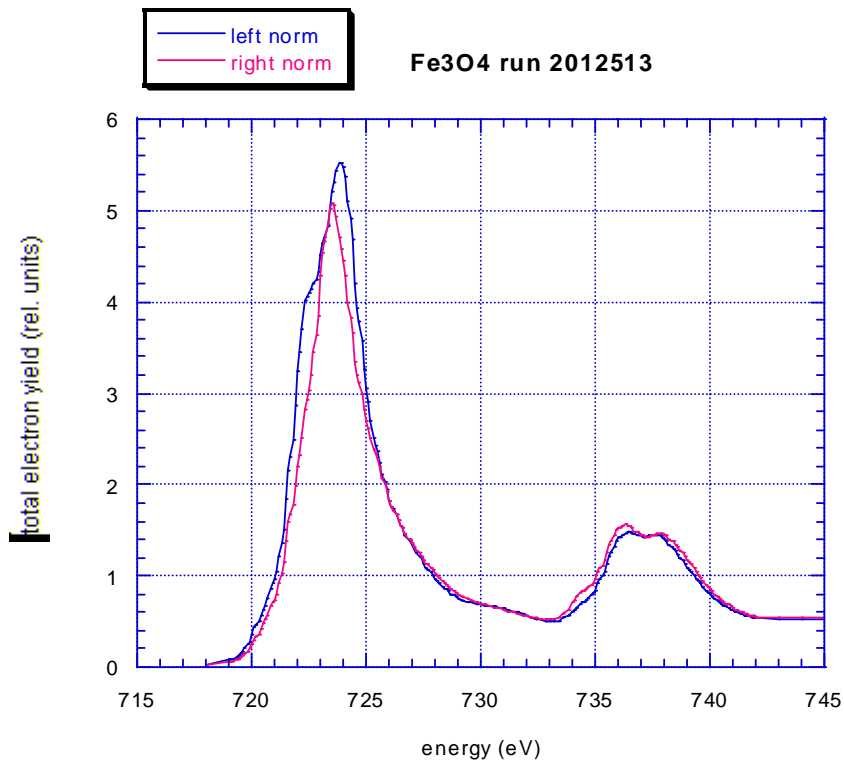




L3

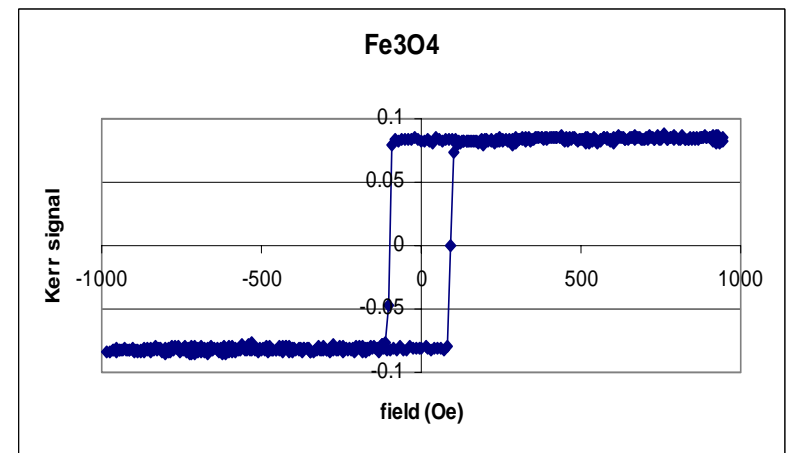
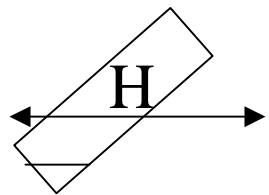


L2

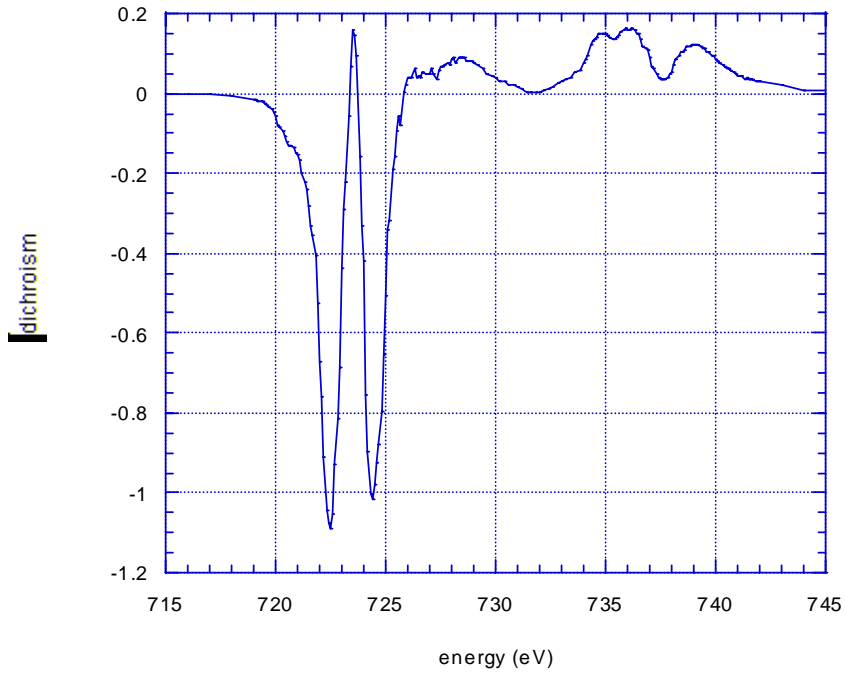


Fe3O4 sample from Robin
 XMCD in 500 Oe, 20 degrees incidence
 along easy axis
 run 20125013

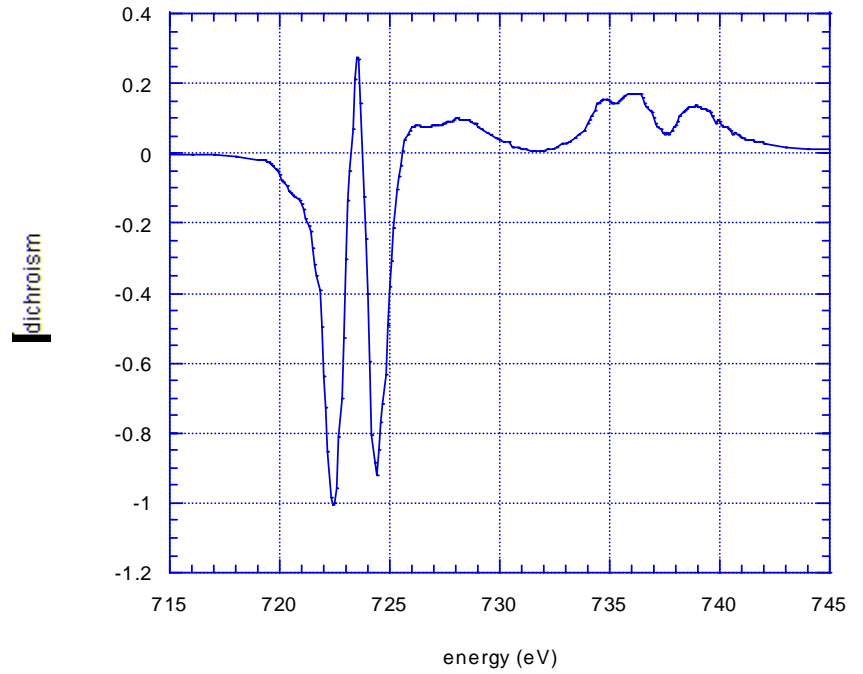
Polar Kerr



201240_20sum



Fe3O4 Robin run 20124021



Fe3O4 sample from Robin
XMCD in 500 Oe, 20 degrees incidence
along easy axis
test reproducibility - is very good

Three layers of PEI-E066 on Si(110) annealed under Ar + H(5%) for 30 min. The samples have been immersed into acetone for 1 min and dried.

030902-A, 400C

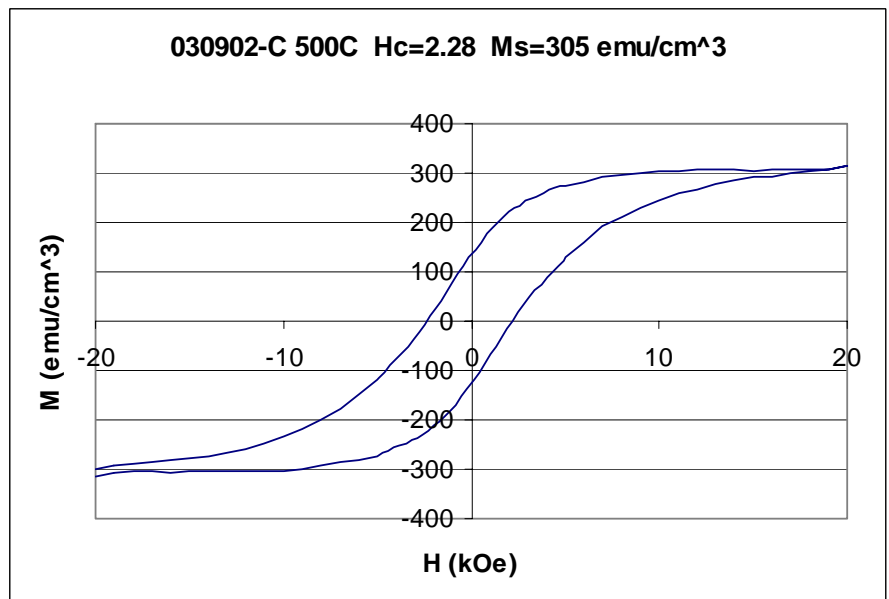
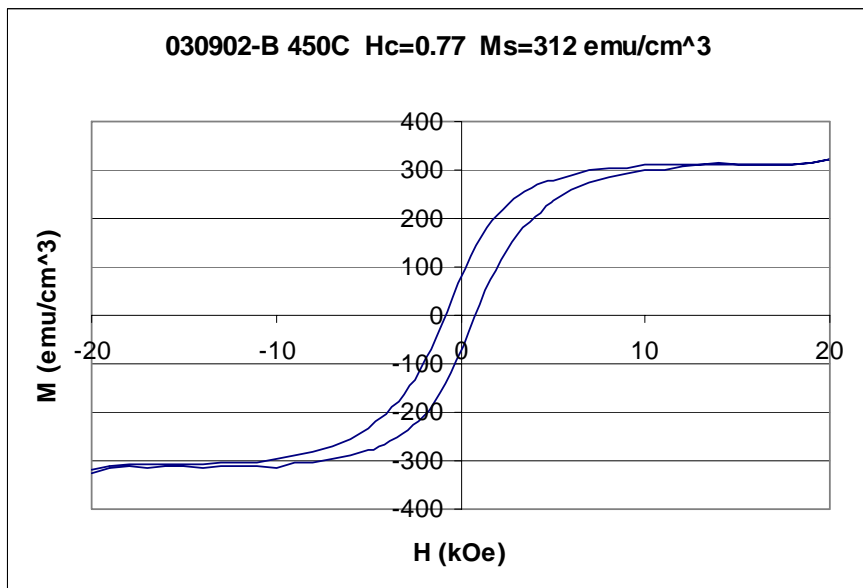
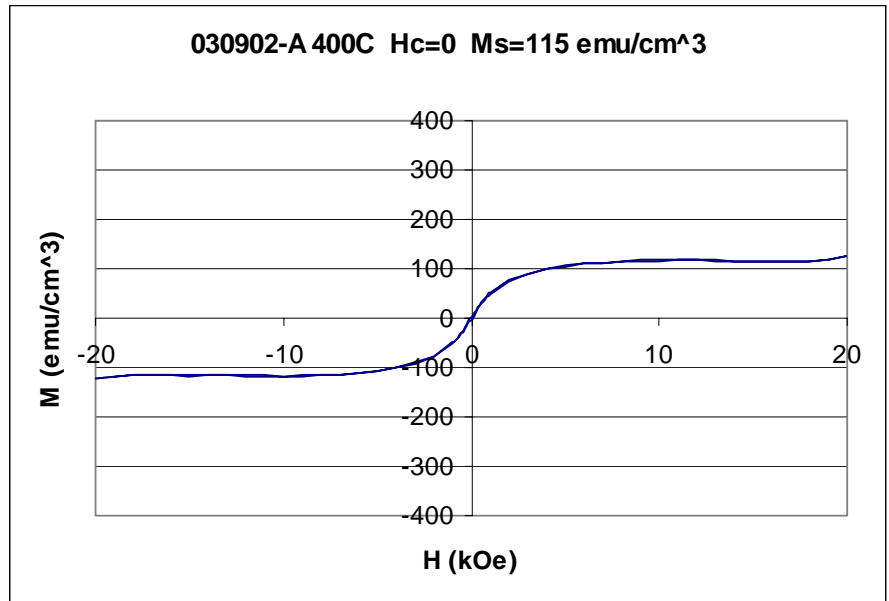
030902-B, 450C

030902-C, 500C

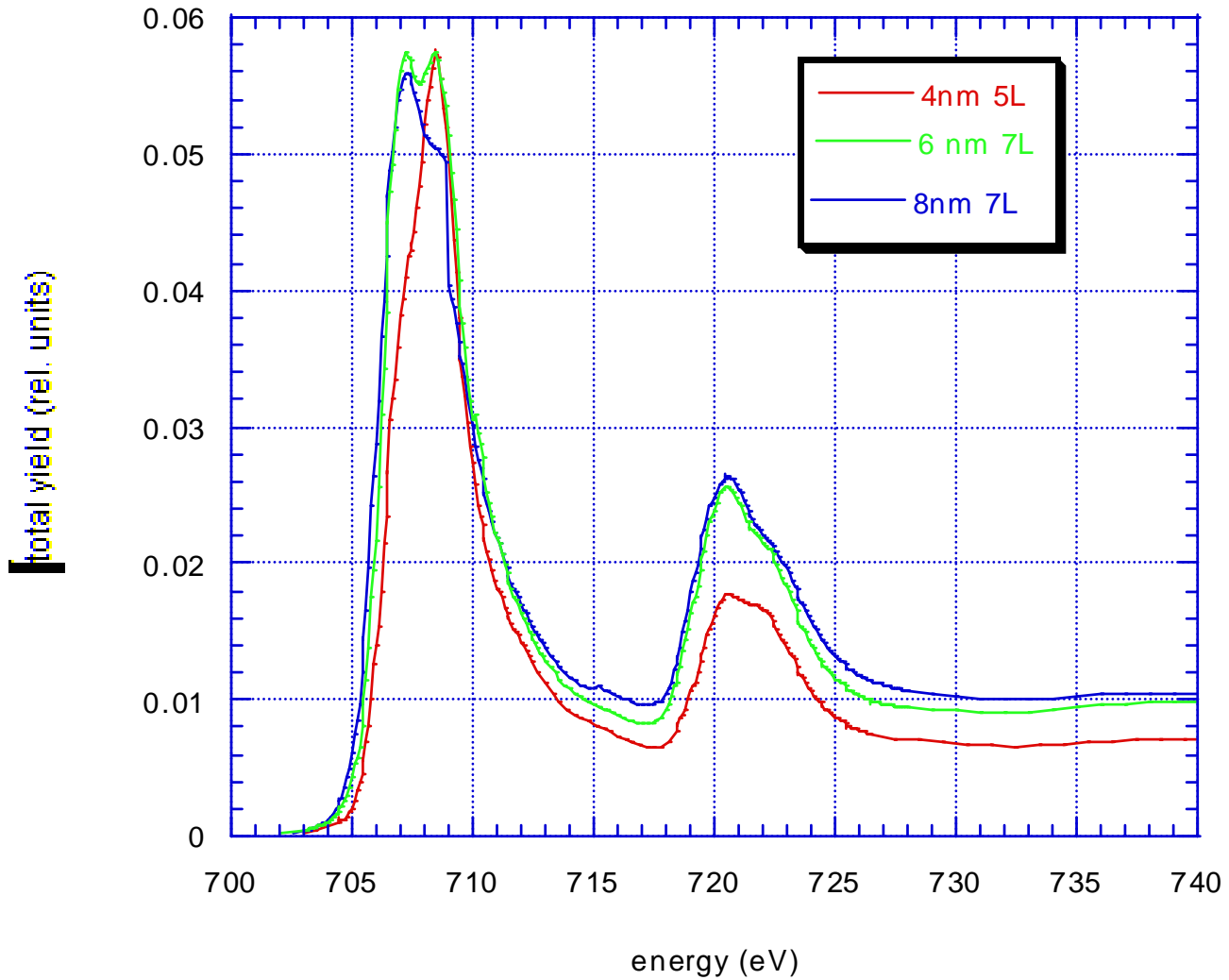
030902-D, 530C

030902-E, 560C

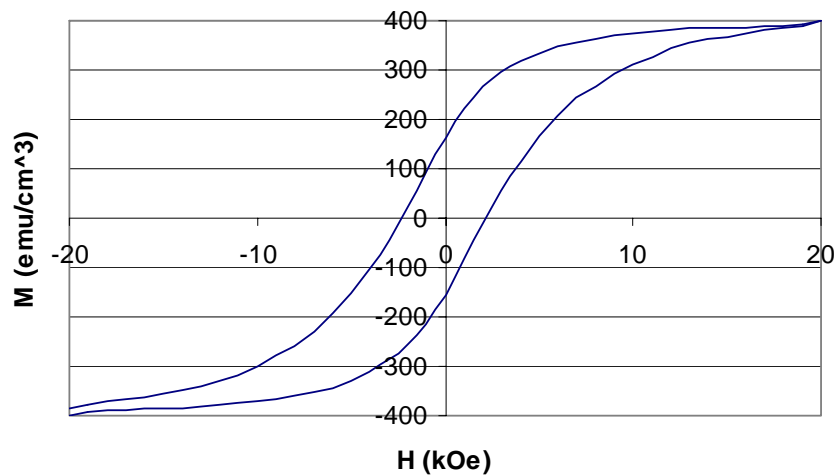
030902-F, 580C



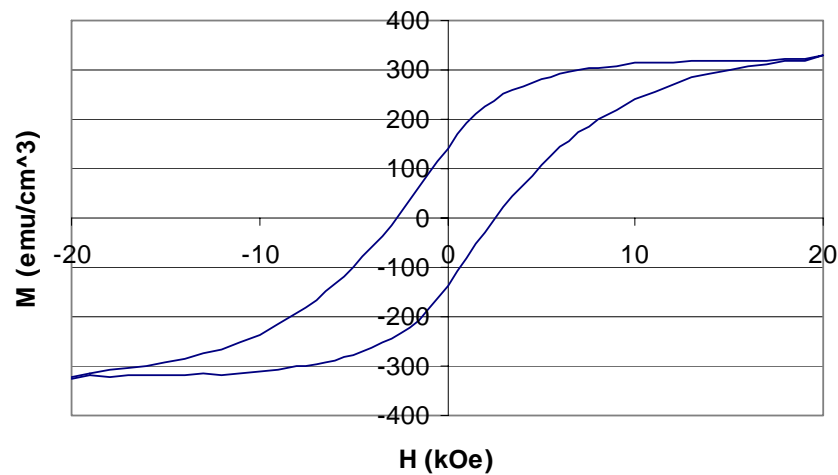
And here the comparison between 8nm, 6nm, and 4nm.



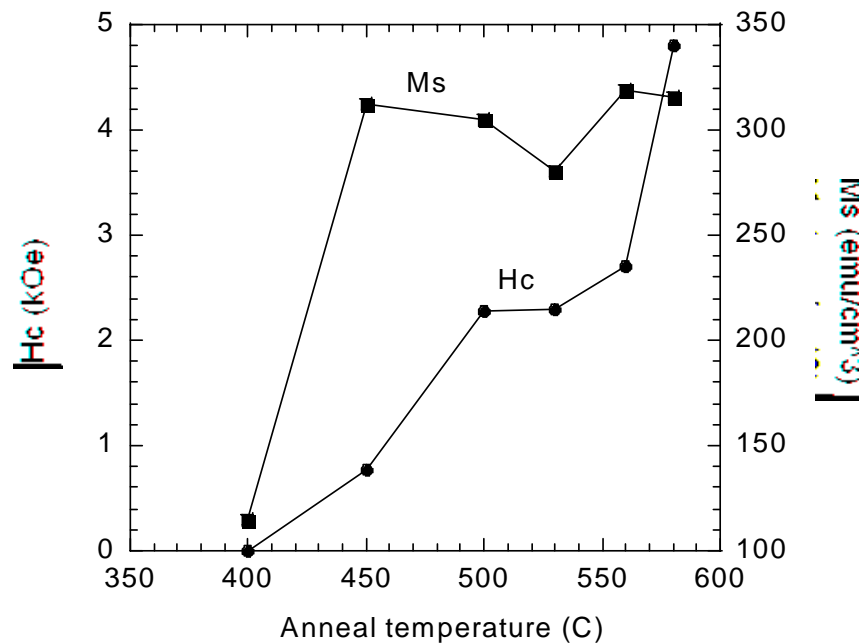
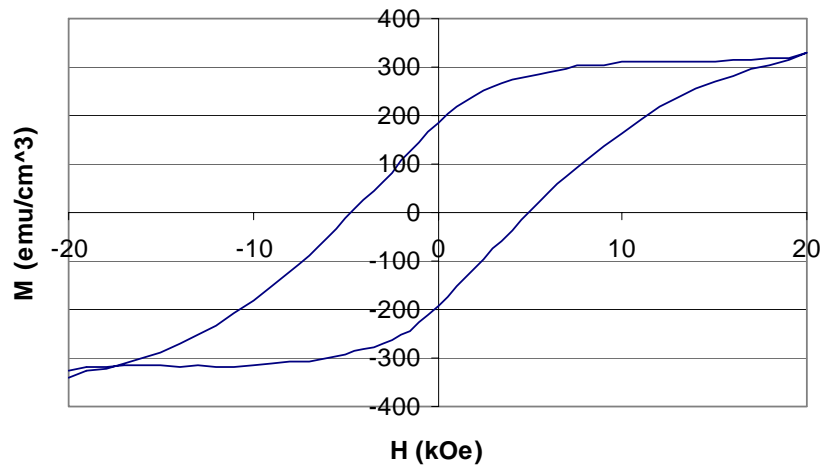
030902-D 530C Hc=2.3 kOe Ms=380 emu/cm³

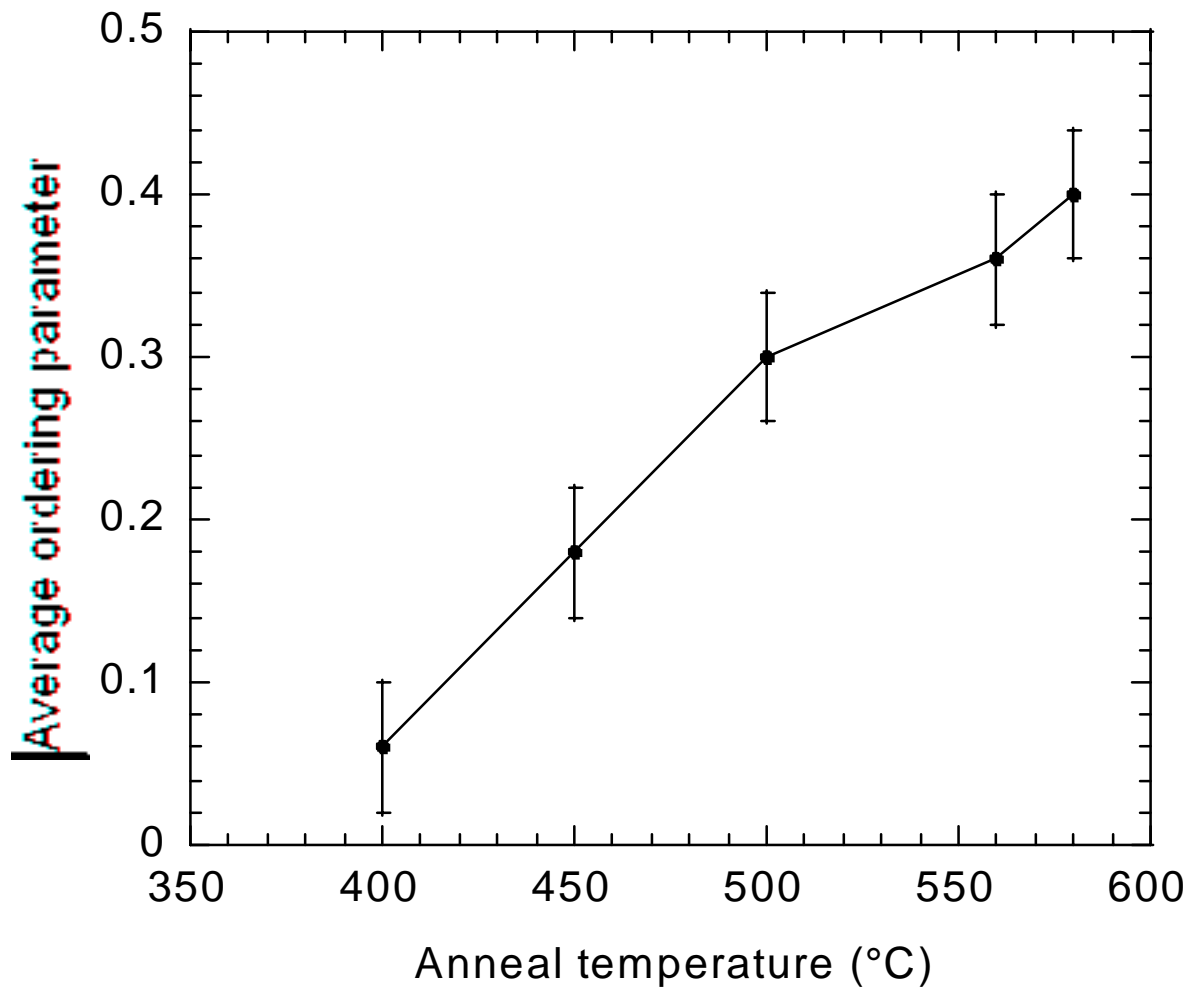


030902-E 560C Hc=2.7 kOe Ms=319 emu/cm³

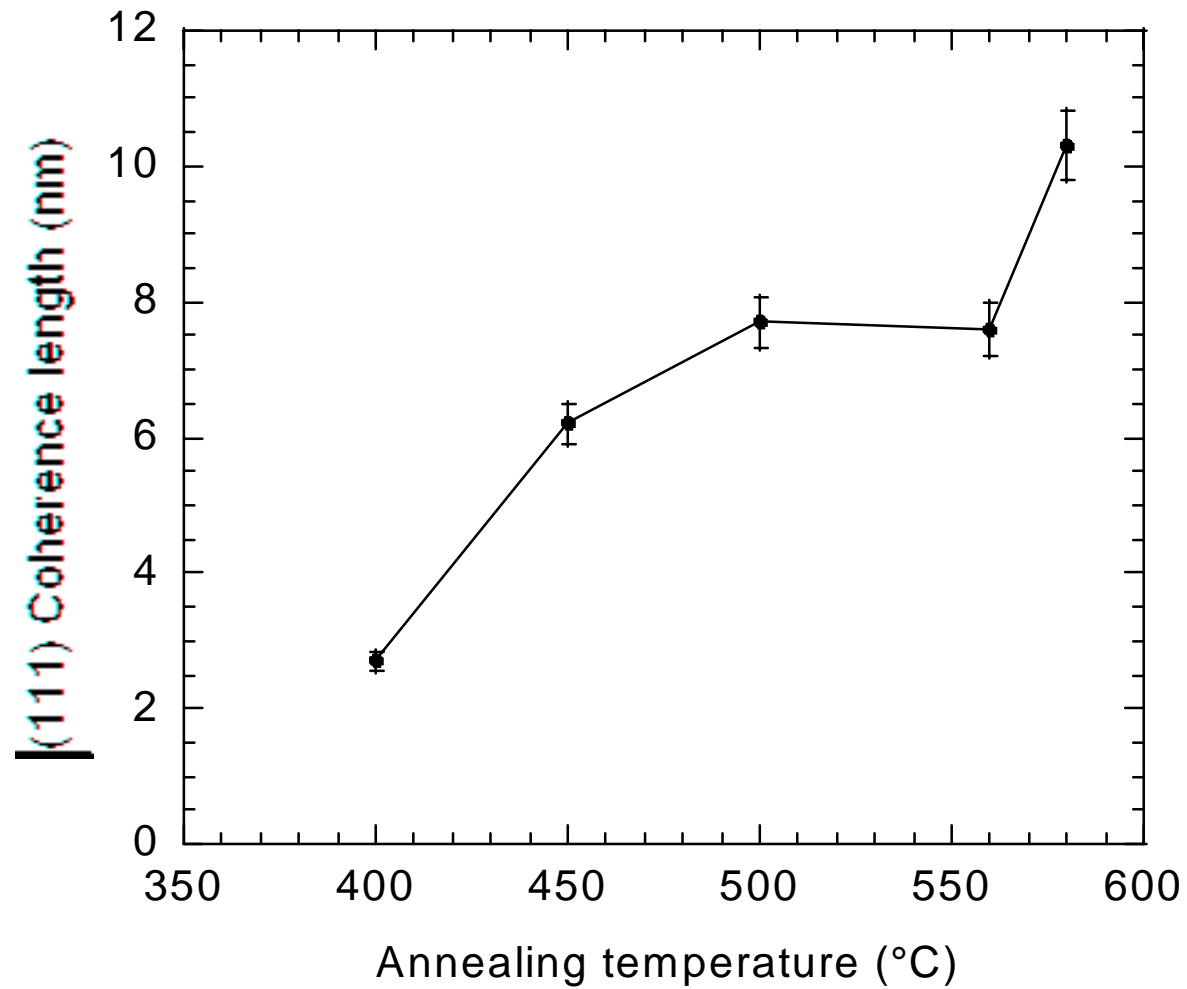


030902-F 580C Hc=4.8 kOe Ms=316 emu/cm³

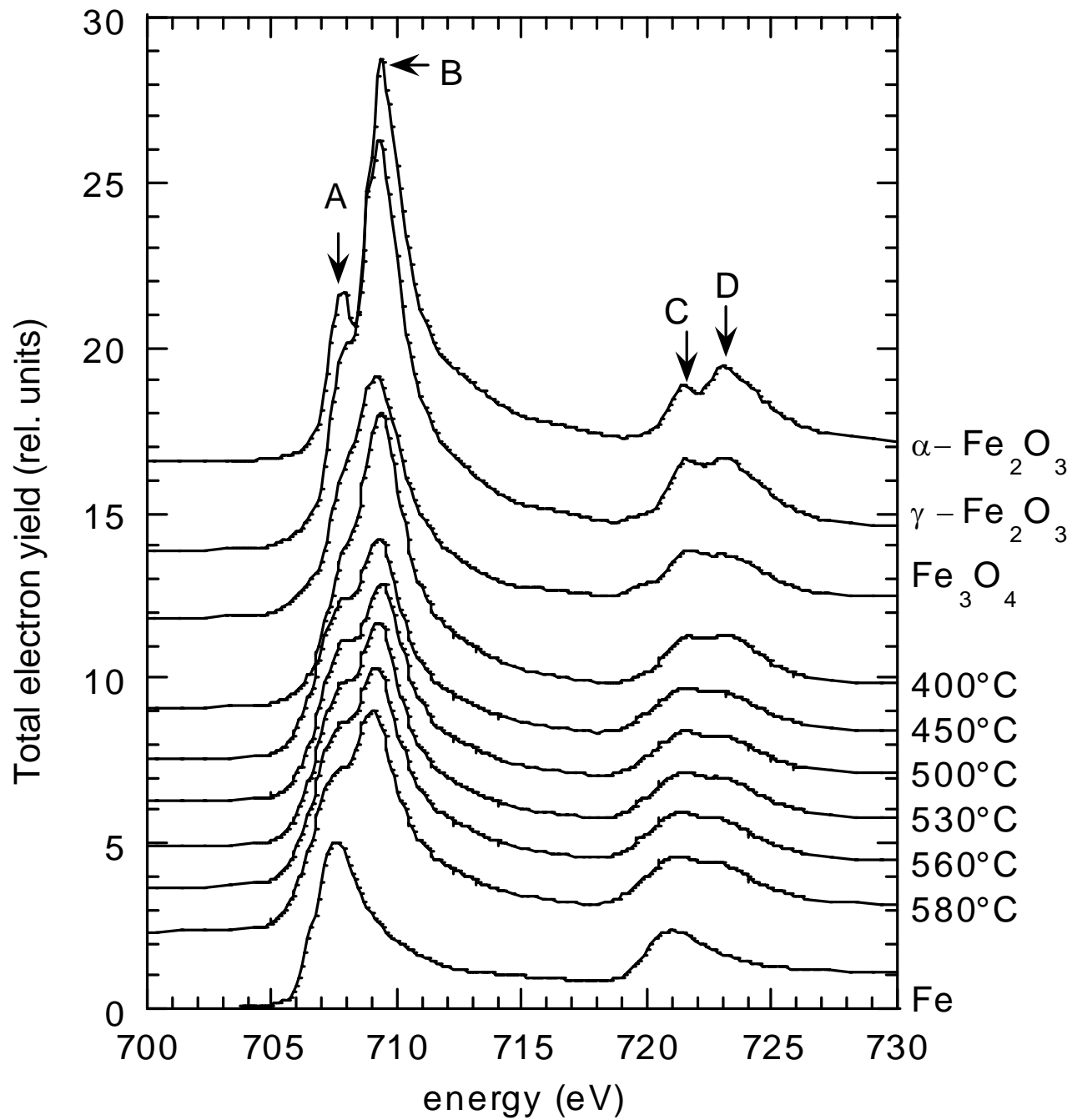




From Mike Toney, XRD



From Mike Toney, XRD

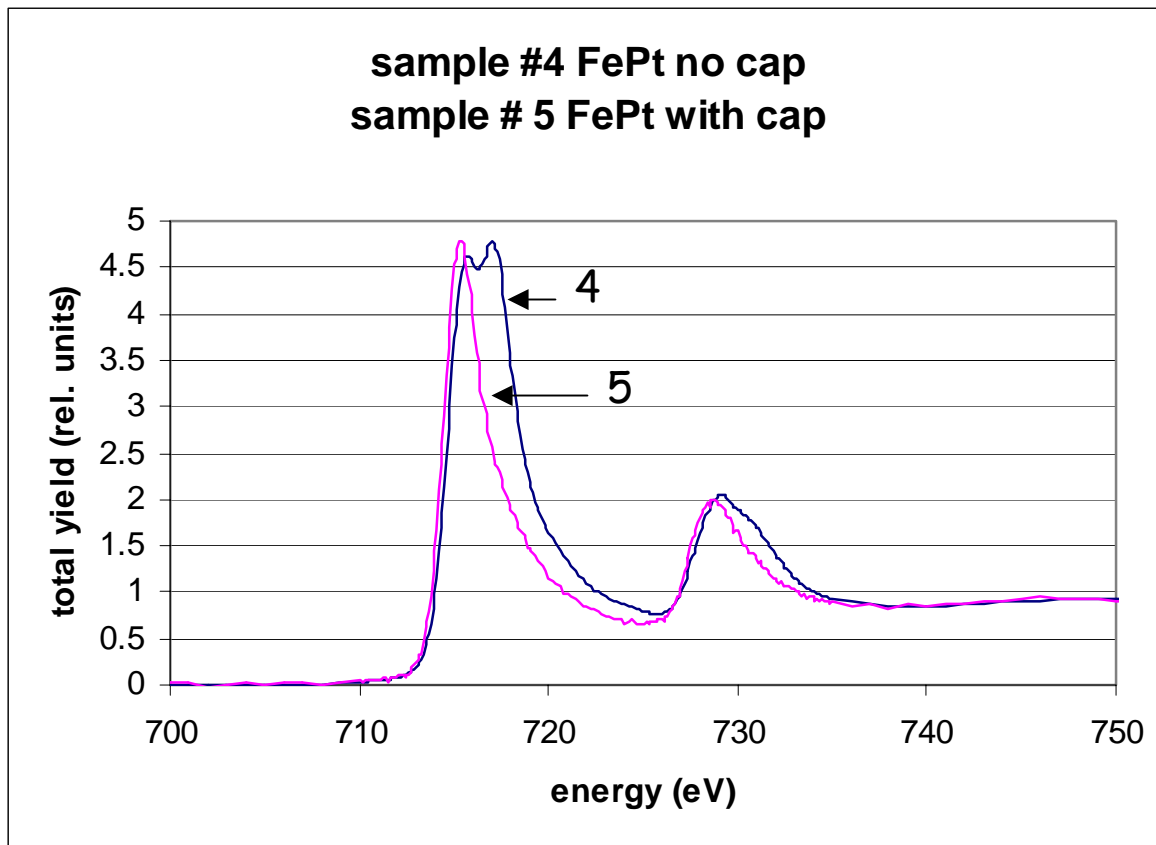


Hello,

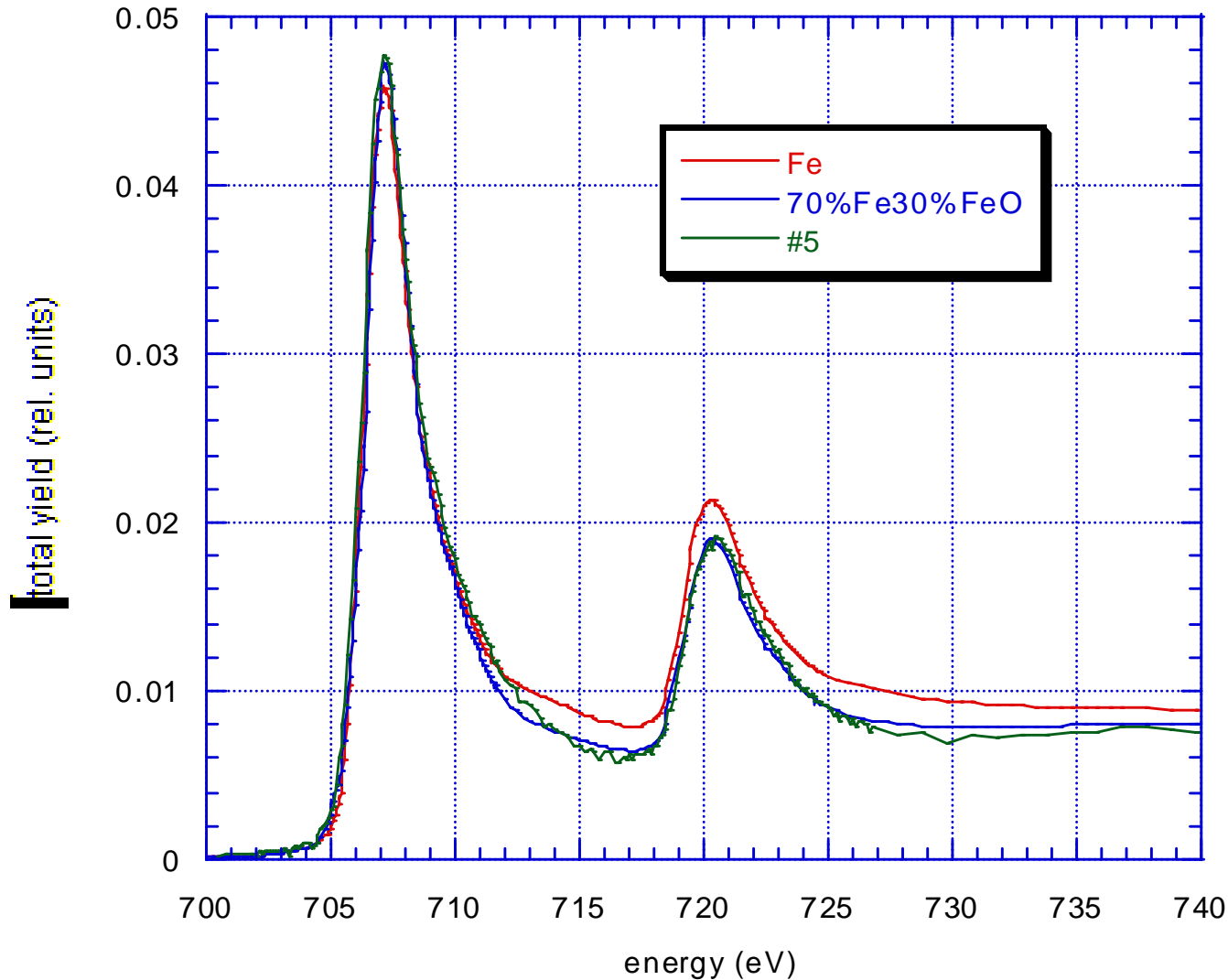
Here the data from the latest ALS run. Jan made two samples for comparison, sample #4 is 50 nm Fe₅₅Pt₄₅ without cap layer

sample #5 is 50 nm Fe₅₅Pt₄₅ with 2 nm Pt cap layer

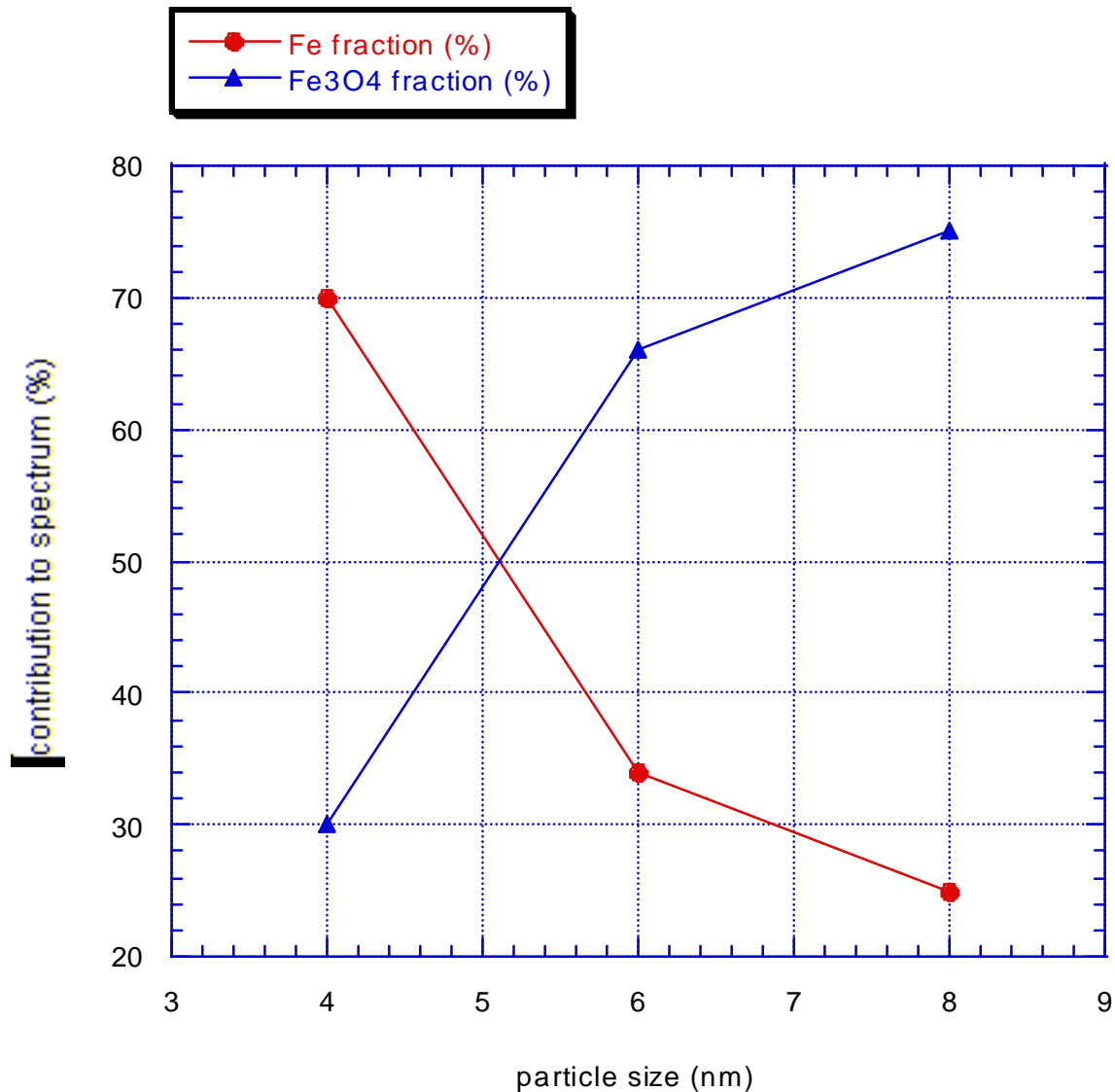
Here the Fe spectra for comparison. The one without cap layer is much more oxidized as expected.

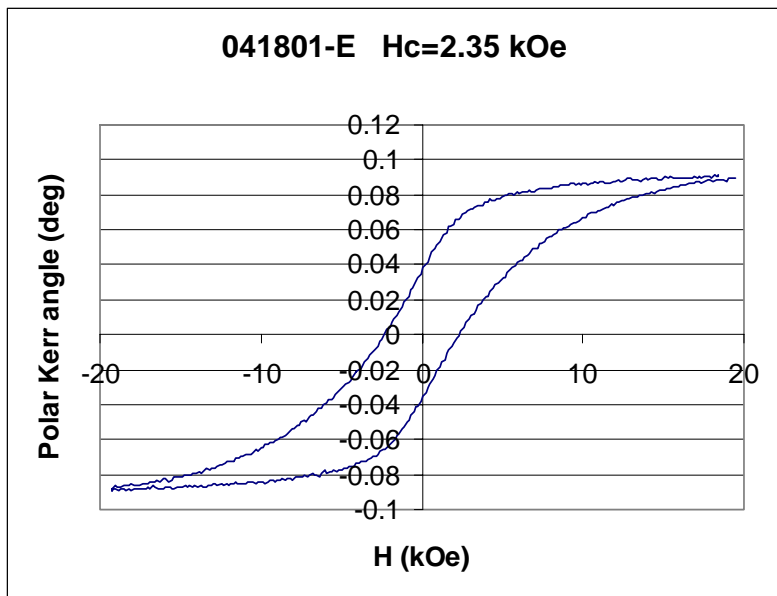


This graph shows sample #5 with respect to a clean Fe reference, and the best fit to the spectrum I got with assuming 70% Fe and 30% FeO.

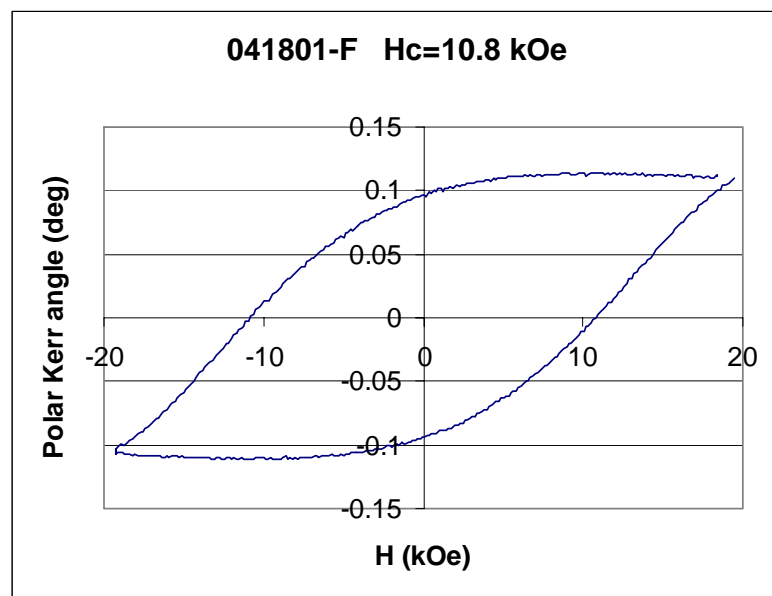


And the contribution to the spectra of Fe and Fe₃O₄ for 8nm, 6nm, and 4nm. If I put this into the model the oxide layer for the 6 and 8 nm particles seems to be thinner (2A) than for the 4 nm particles (4A).





6nm

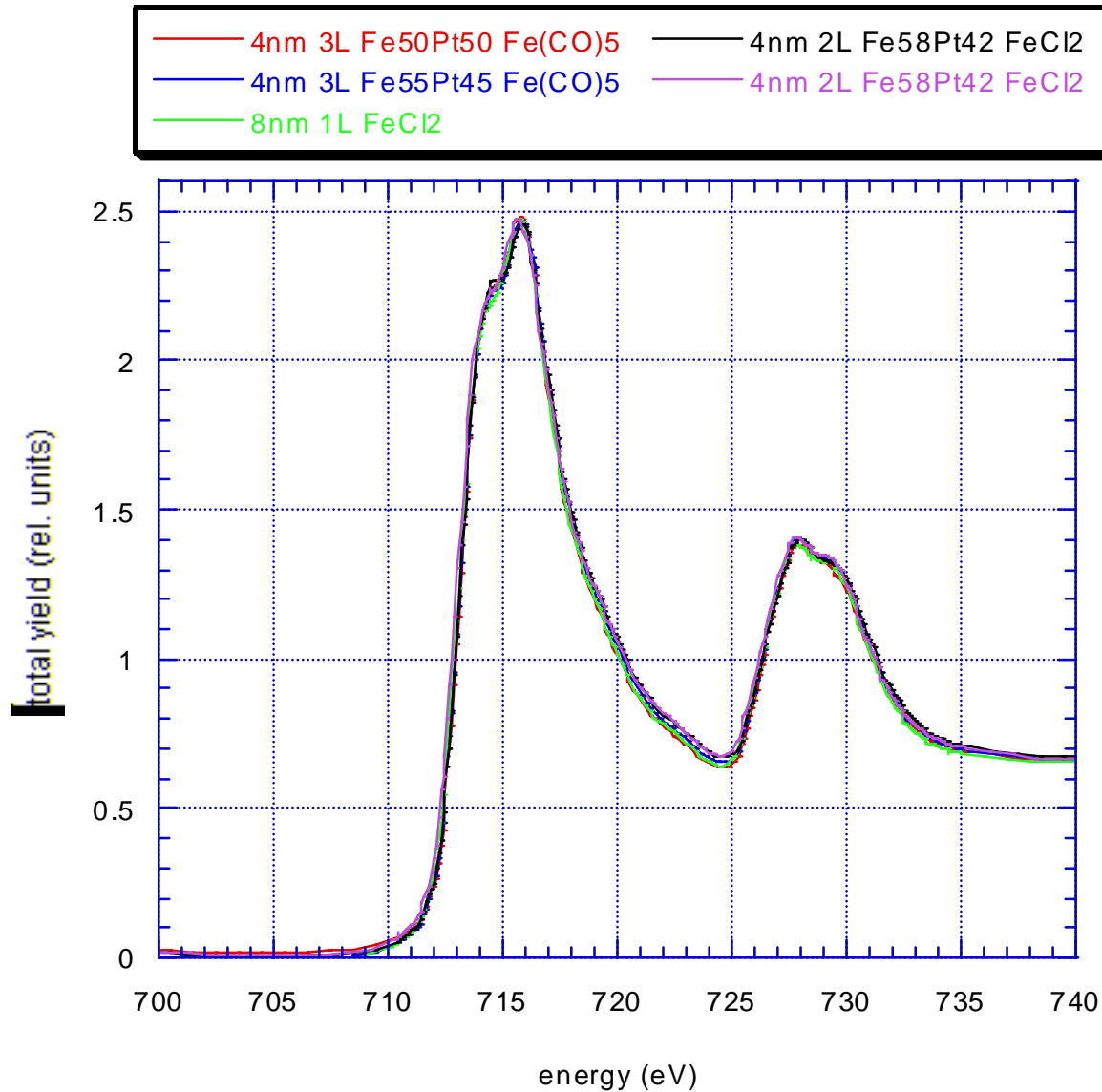


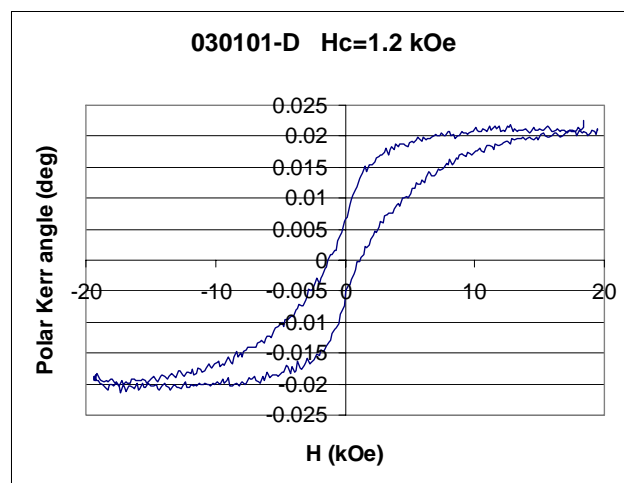
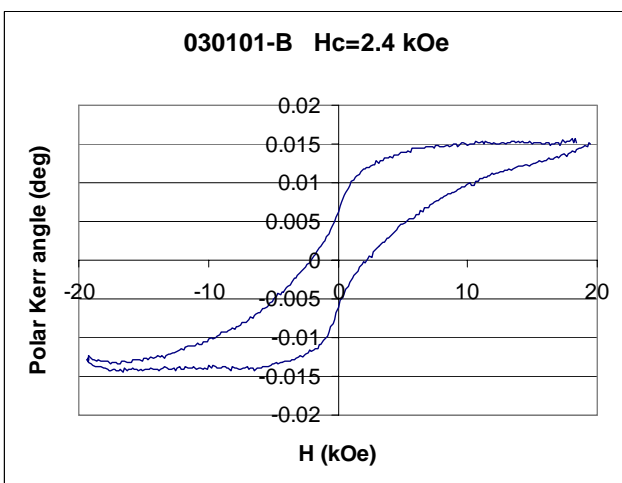
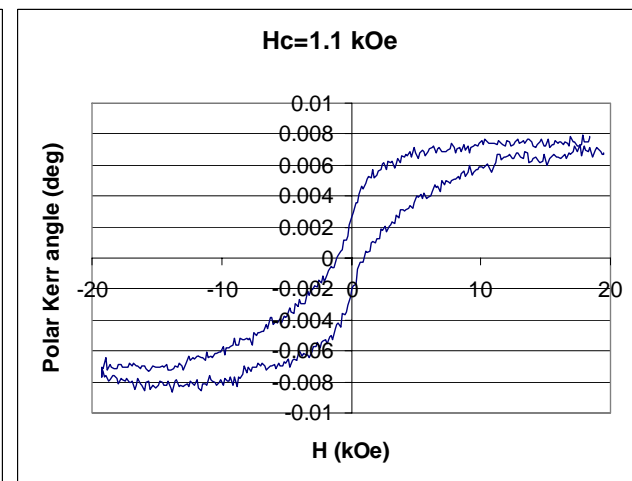
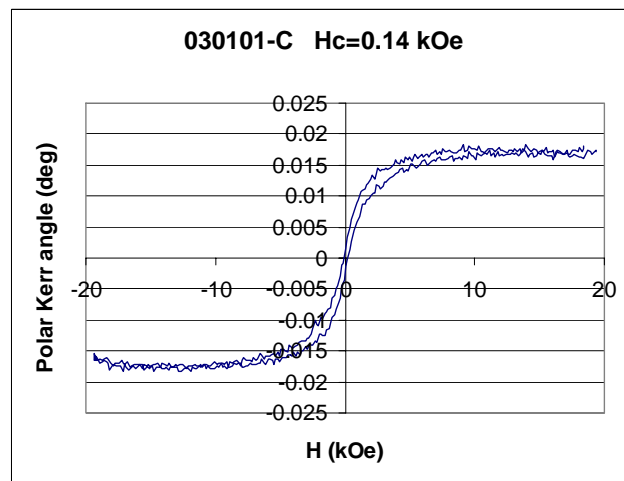
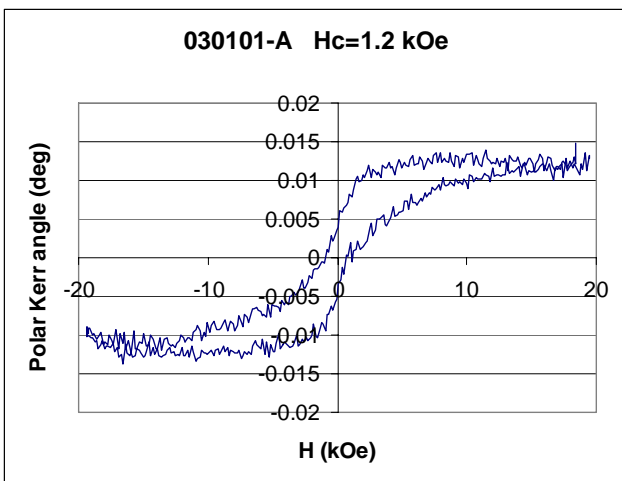
8nm

The 8nm sample has very high coercivity.

041801-E	E098, 6nm Fe ₅₂ Pt ₄₈	SiO ₂ /Si	PEI-E098, 7Layers	N ₂ , 580C, 30 min
041801-F	E095, 8 nm ~Fe ₅₂ Pt ₄₈	SiO ₂ /Si	PEI-E095, 7Layers	N ₂ , 580C, 30 min

This is a comparison of the films made 030101. They are all just after the onset of being ferromagnetic, the spectra are all very similar.



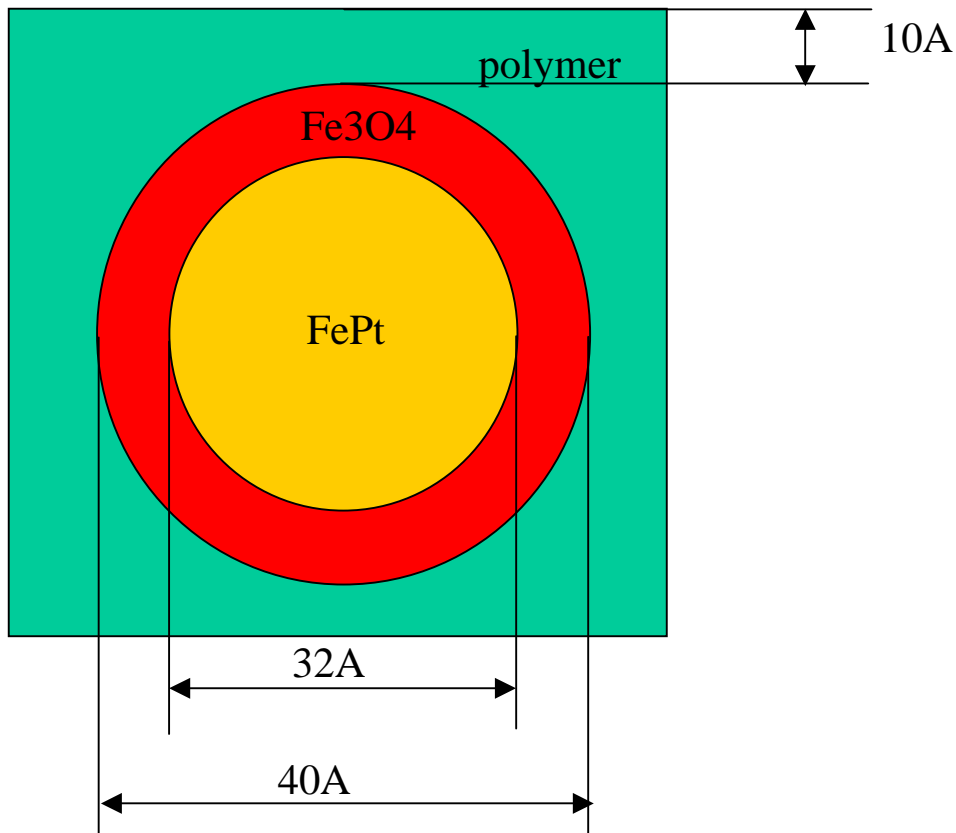


030101-A	E066, Fe ₅₈ Pt ₄₂	SiO ₂ /Si	PEI-Fe ₅₈ Pt ₄₂ , 2 layer	N ₂ , 580C, 30 min
030101-B	E066, Fe ₅₈ Pt ₄₂	SiO ₂ /Si	PEI-Fe ₅₈ Pt ₄₂ , 2 layer	N ₂ , 580C, 30 min
030101-C	F062, Fe ₅₀ Pt ₅₀	SiO ₂ /Si	PEI-Fe ₅₀ Pt ₅₀ , 3 layers	N ₂ , 580C, 30 min
030101-D	F070, Fe ₅₅ Pt ₄₅	SiO ₂ /Si	PEI-Fe ₅₅ Pt ₄₅ , 3 layers	N ₂ , 580C, 30 min
030101-E	E068, ~8nm FePt	SiO ₂ /Si	PEI-FePt, 1 layer	N ₂ , 580C, 30 min

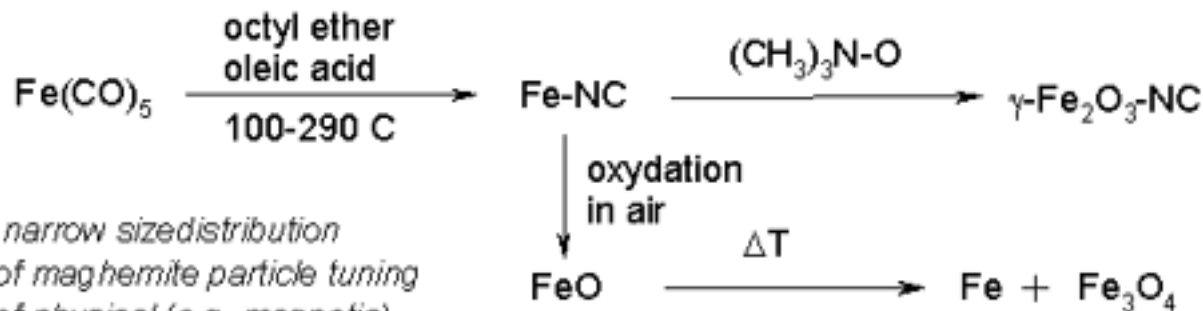
Hi all,

I did a calculation of the signal one would expect in total yield detection for the following geometry:

This is basically a particle of 40Å diameter with 32Å FePt core surrounded by one monolayer Fe₃O₄. It is embedded in the polymer (for the calculation I assumed just carbon) with 60Å particle distance, that gives about 10Å carbon on top.

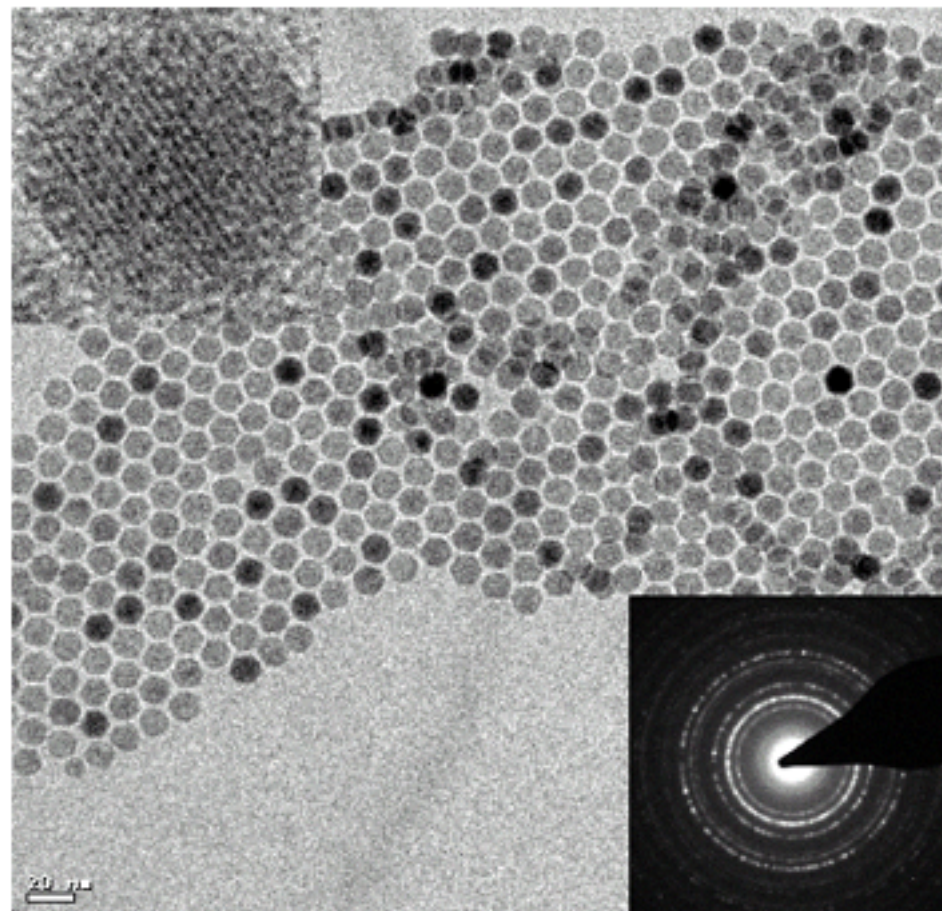
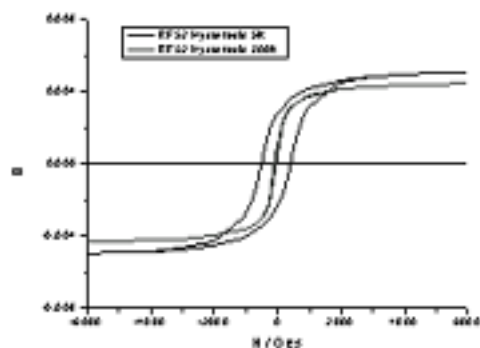
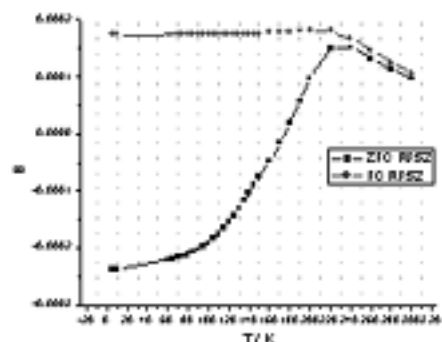


Synthesis and Characterization of Iron Oxide Nanoparticle



*narrow sizedistribution
of maghemite particle tuning
of physical (e.g. magnetic)
properties.*

*RF & Microwave
Bio applications.*



Fe₃O₄ Nanocrystals

(Sun and Zeng)

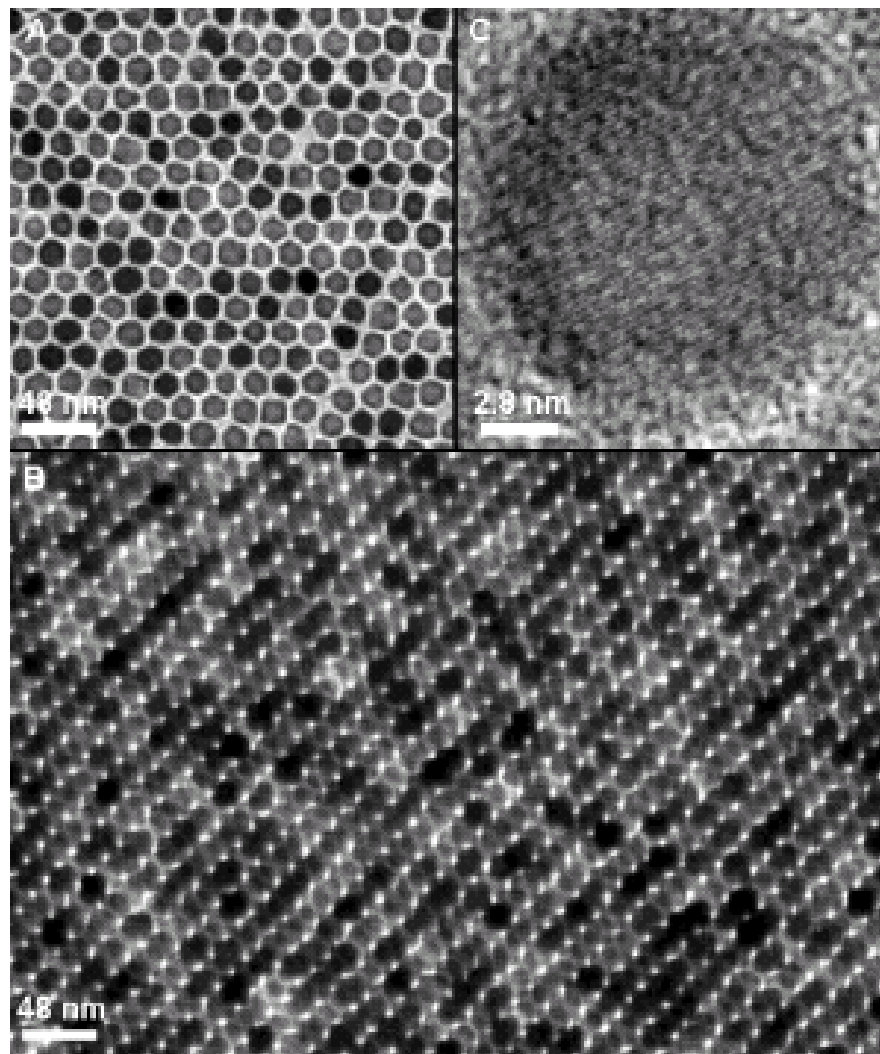
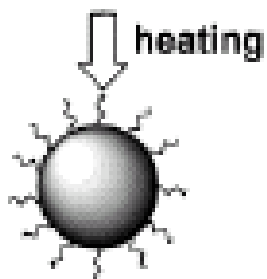
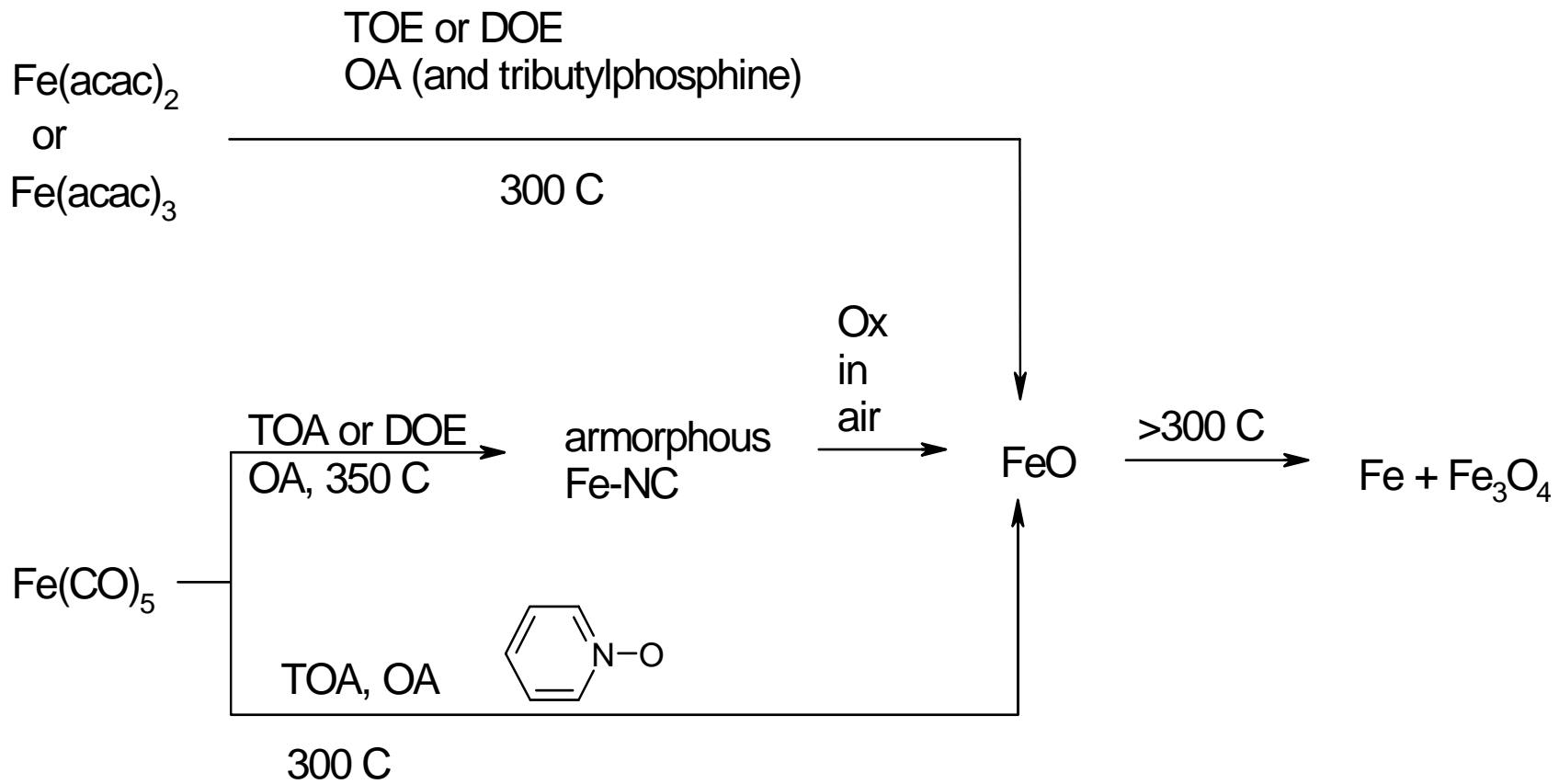
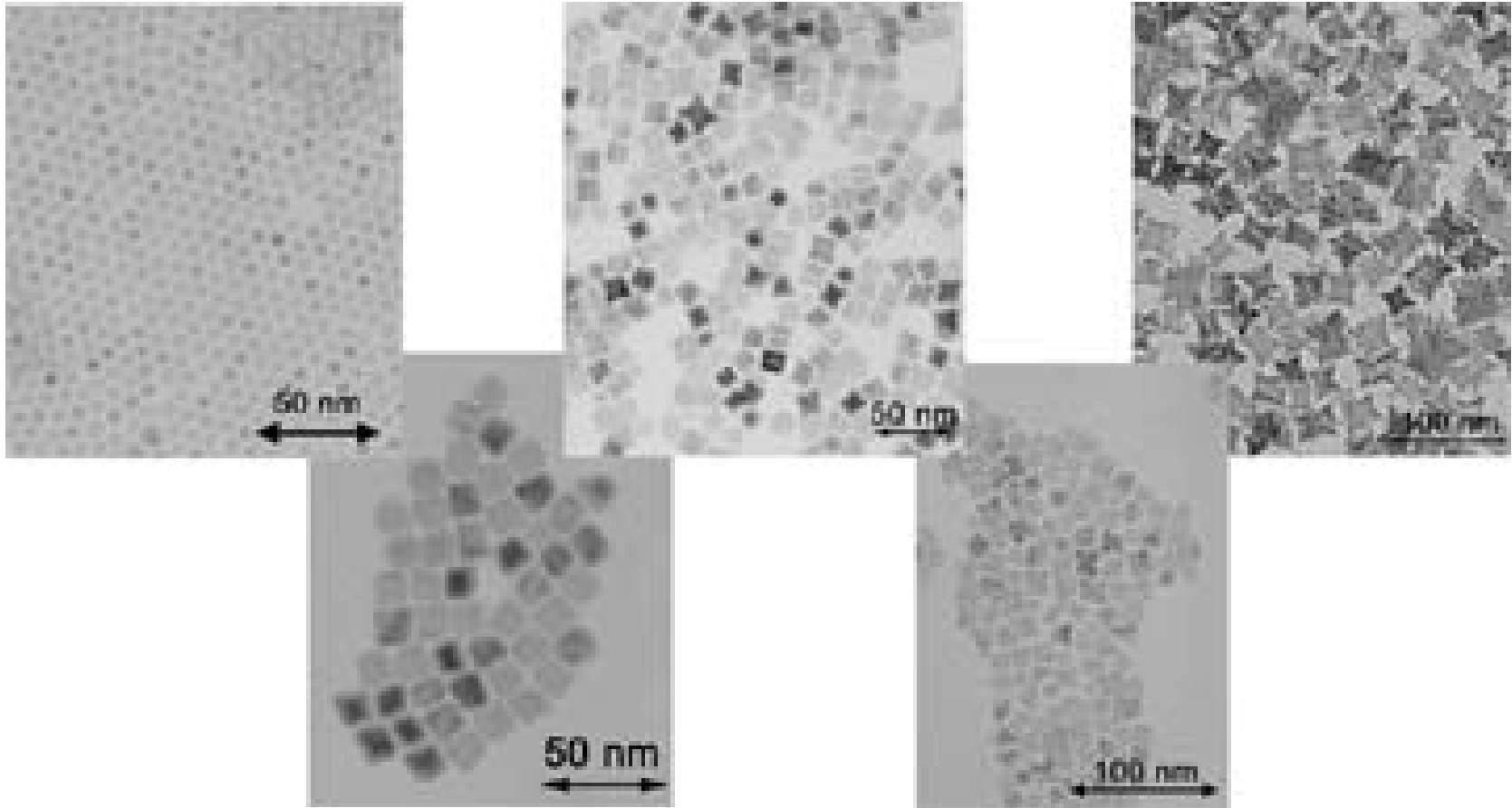
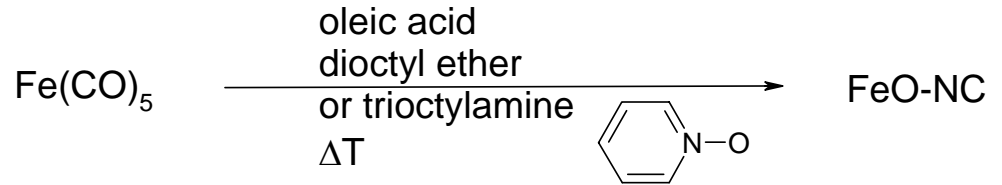


Figure 1. TEM bright field image of 16-nm Fe₃O₄ nanoparticles deposited from their dodecane dispersion on amorphous carbon surface and dried at 60 °C for 30 min: (A) a monolayer assembly, (B) a multilayer assembly, (C) HRTEM image of a single Fe₃O₄ nanoparticle. The images were acquired from a Philips EM 430 at 300 KV.

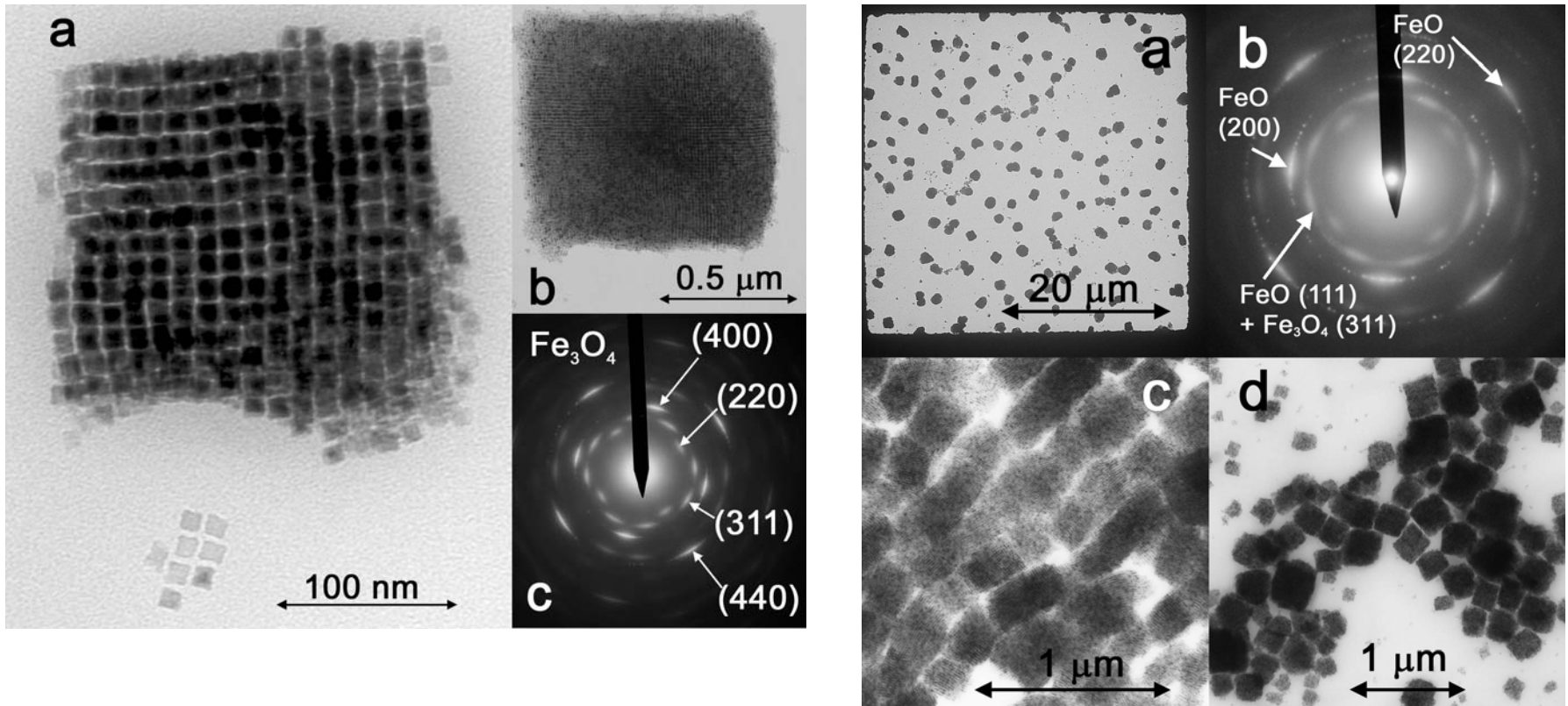


Shape selective synthesis of wuestite

Substitute
trimethylamine N-oxide
with pyridin N-oxide



FeO Nanoparticles



Right a) TEM image of a single cubic superlattice built of cubic FeO nanocrystals with 11 nm edge length. b) TEM image of a larger superlattice oxidized or decomposed after storage. c) SAED of the cubic superlattice in b) showing reflections for magnetite and orientational ordering in the superlattice.

Right: a) LRTEM image of a quadratic subunit of a TEM grid showing nearly cubic superlattice built up of cubic wuestite nanocrystals. b) SAED of a selected superlattice with uneven but symmetric intensity distribution caused by preferred alignment of the particles (orientational ordering). c) TEM image of aligned superlattices arising during deposition of cubic FeO nanocrystals in a magnetic field parallel to the substrate. d) TEM image of aggregated superlattices deposited without external magnetic field.

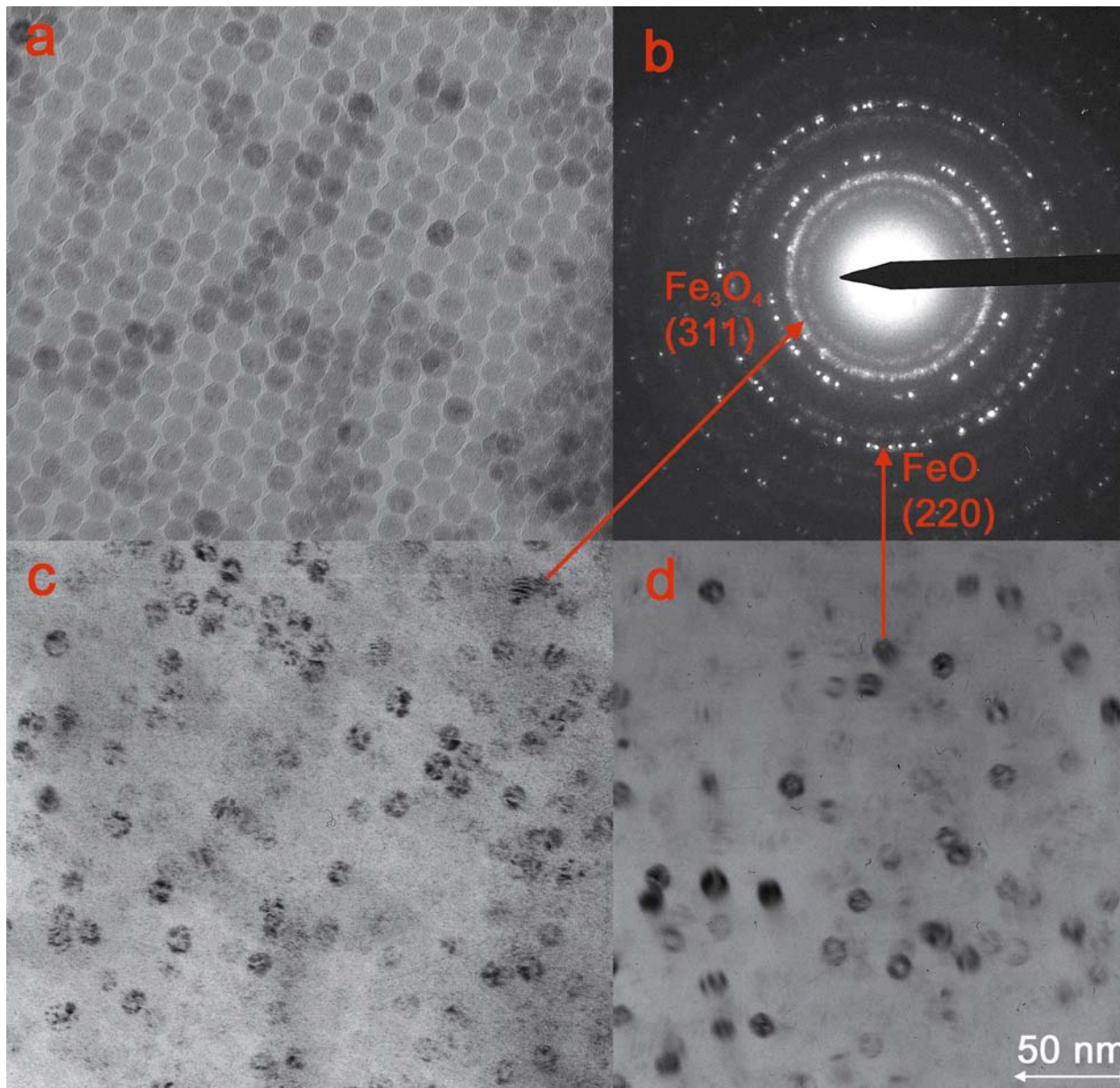
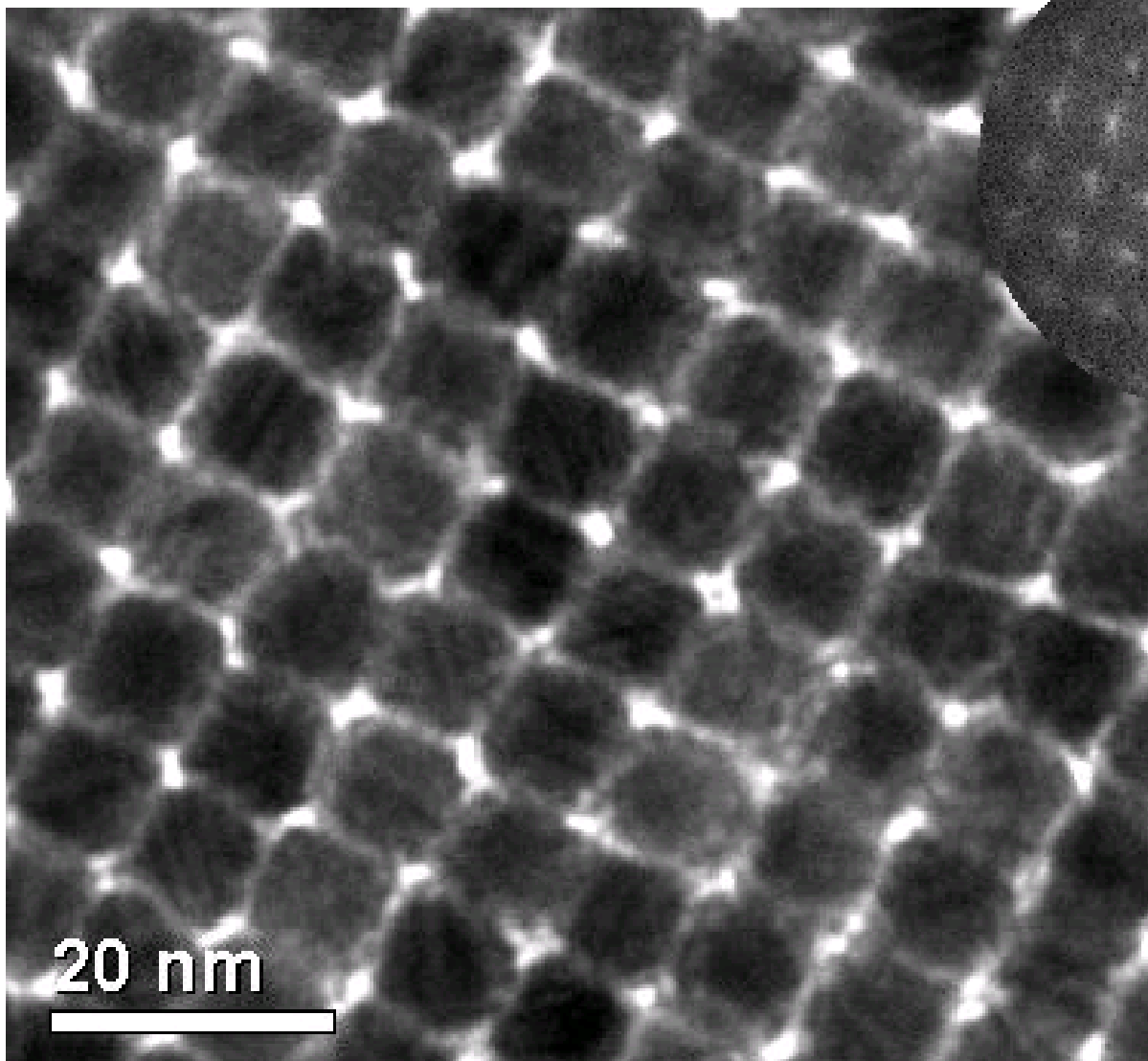


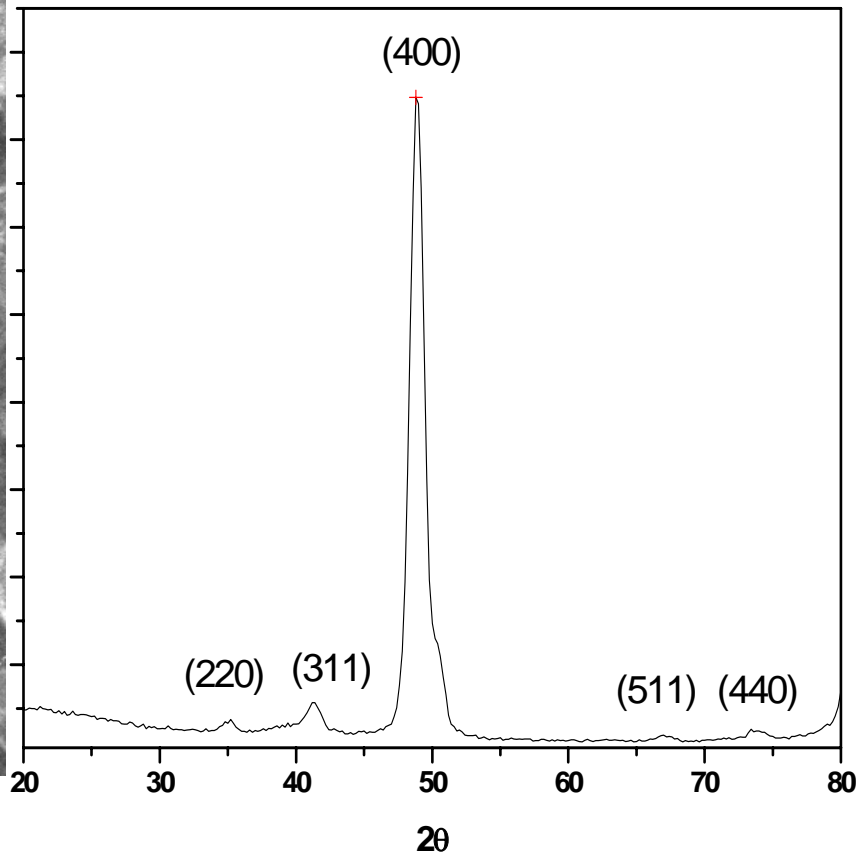
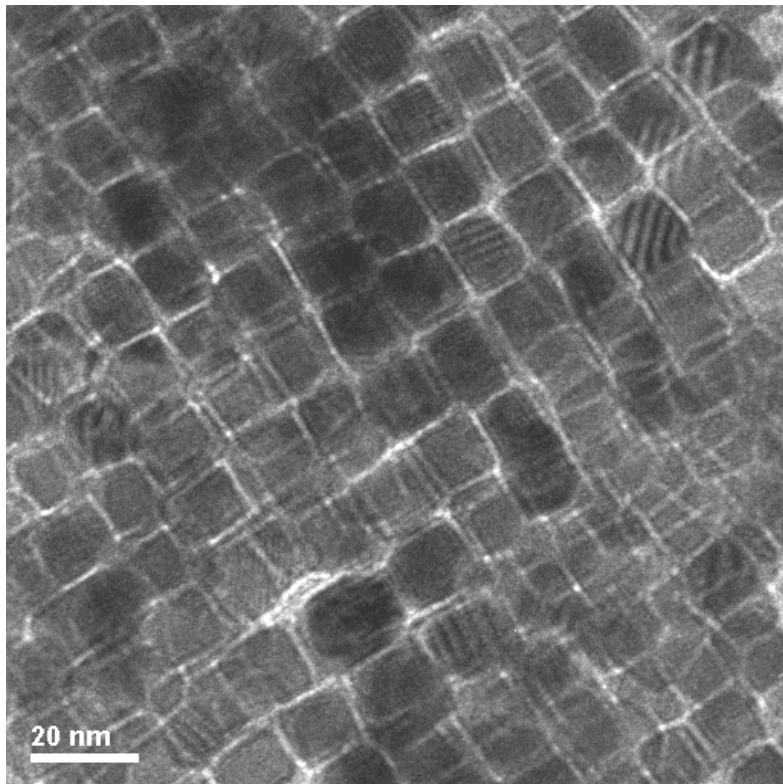
Figure 6: a) TEM image of wuestite nanocrystals with seeds of magnetite inside. b) SAED of the material showing a speckled pattern for FeO reflections and diffuse rings for magnetite reflections. c) Dark-field image of the region in Figure 5a (shown as negative); a part of the magnetite reflections were selected with the objective aperture. d) Dark-field image of the region in Figure 5a (shown as negative); a part of the wuestite reflections were selected with the objective aperture.

Fe₃O₄ nanoparticles



Shape induce crystal alignment (14 nm MnFe_2O_4 nanoparticles)

(100) texture



Dark Field Imaging of the Fe₃O₄ and FeO in TEM.

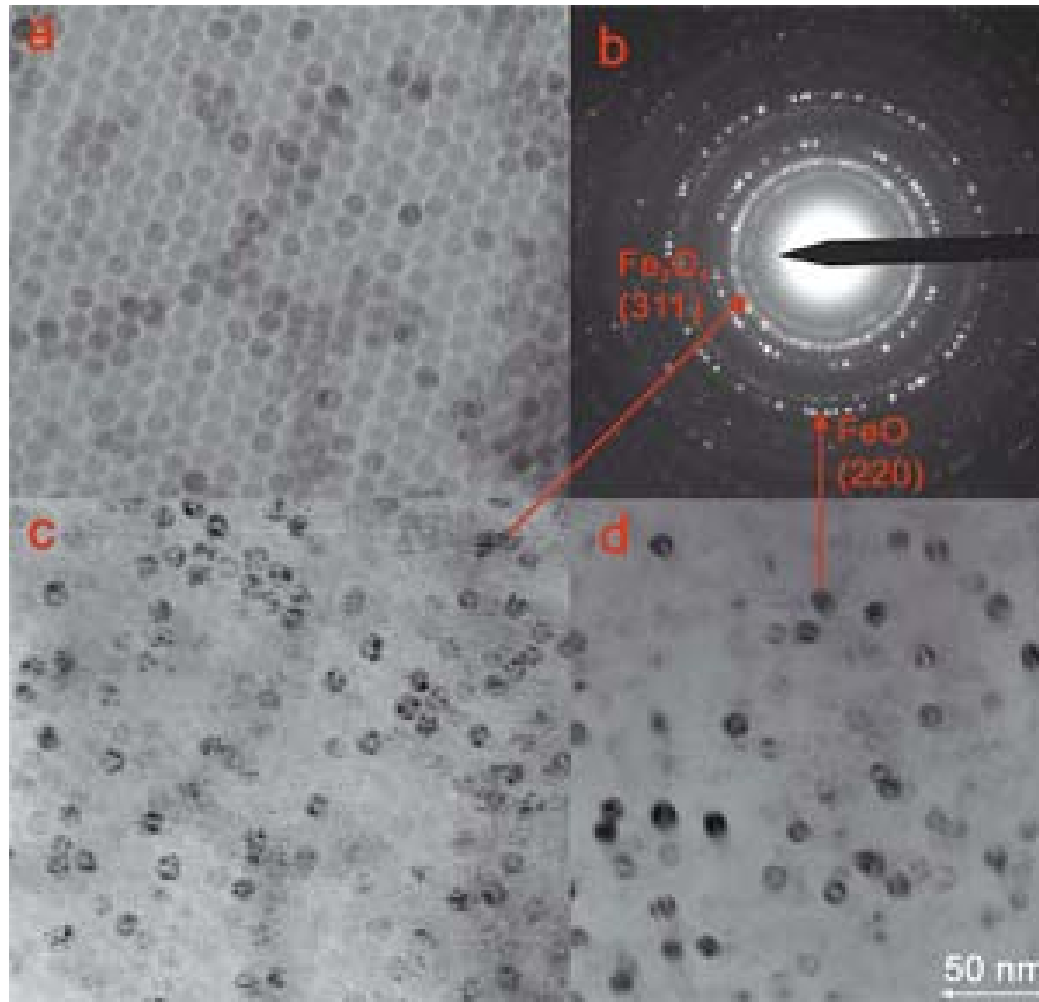


Figure 6: a) TEM image of wuestite nanocrystals with seeds of magnetite inside. b) SAED of the material showing a speckled pattern for FeO reflections and diffuse rings for magnetite reflections. c) Dark-field image of the region in Figure 5a (shown as negative); a part of the magnetite reflections were selected with the objective aperture. d) Dark-field image of the region in Figure 5a (shown as negative); a part of the wuestite reflections were selected with the objective aperture.

Bimagnetic Core/Shell Nanoparticles

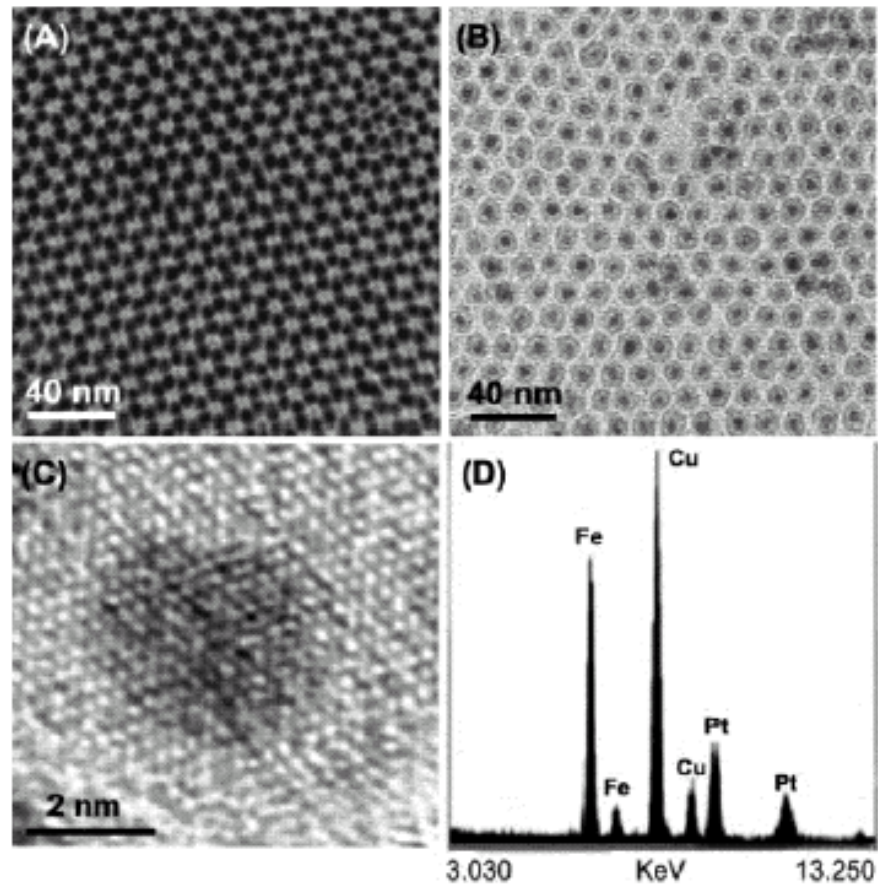
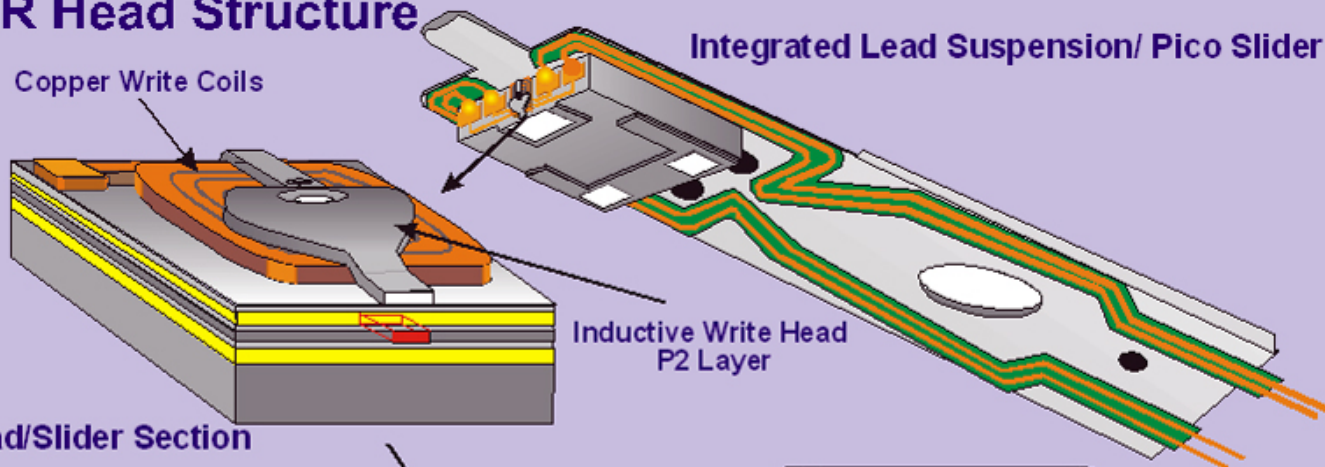


Figure 1. TEM bright field images of core/shell $\text{Fe}_{58}\text{Pt}_{42}/\text{Fe}_3\text{O}_4$ nanoparticles with core/shell being (A) 4 nm/0.5 nm and (B) 4 nm/2 nm; (C) HRTEM of a single $\text{Fe}_{58}\text{Pt}_{42}/\text{Fe}_3\text{O}_4$ particle with 4 nm core and 2 nm shell; and (D) EDX spectrum of a group of $\text{Fe}_{58}\text{Pt}_{42}/\text{Fe}_3\text{O}_4$ nanoparticles with 4 nm core and 1 nm shell. The shell thickness is measured statistically with standard deviation at around 11%.

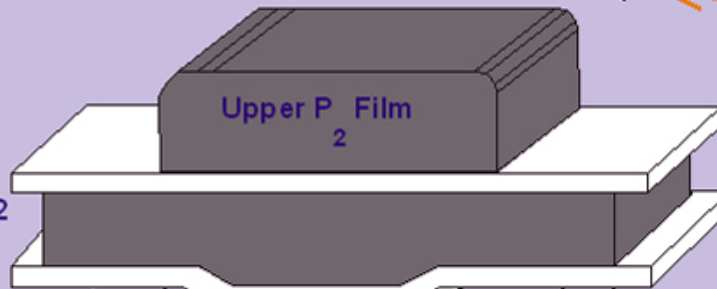
GMR Head Structure



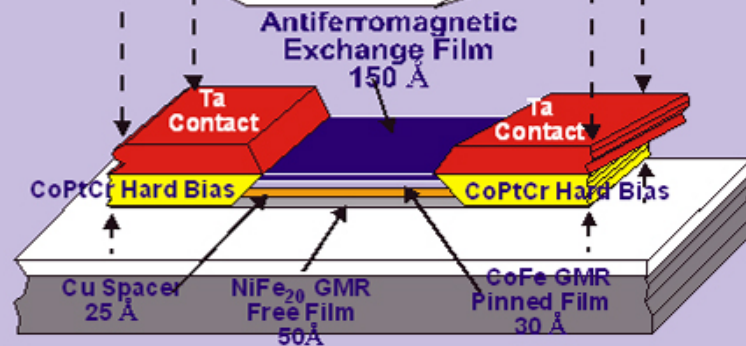
Head/Slider Section

Inductive Write

Lower P1-Shield 2



Spin Valve/GMR Read

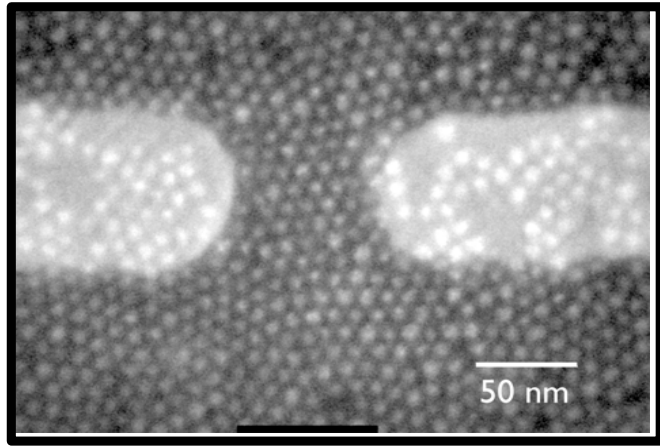


INSITE4e.CDR

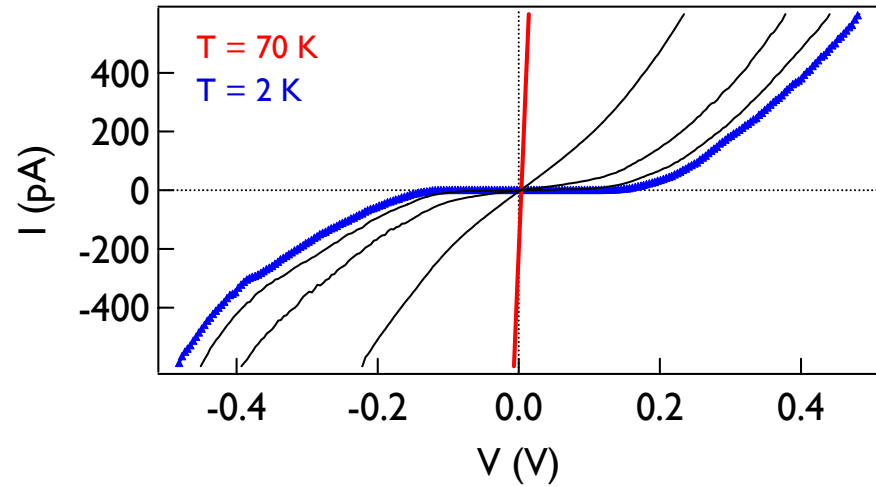


Spin-dependent tunneling in Nanocrystal arrays

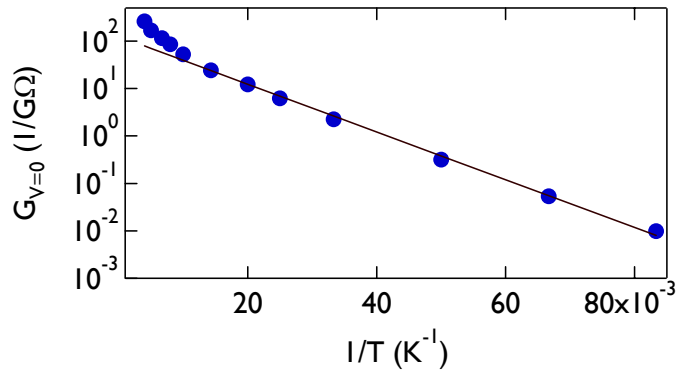
Chuck Black, Bob Sandstrom, Chris Murray, Shouheng Sun



▶ shortest current path \sim 8 nanocrystals



$G_{V=0}$ follows simple thermal-activation

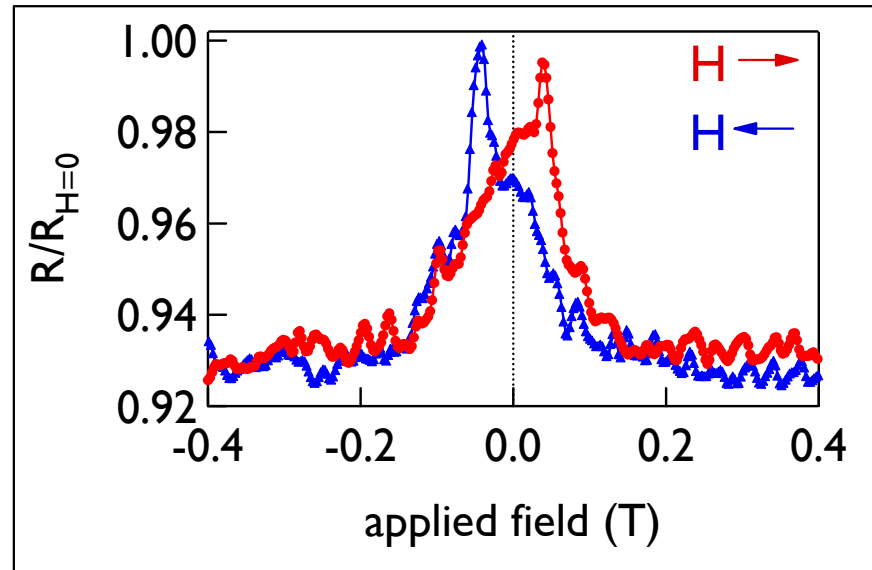


data fit by:

$$\ln(G_{V=0}) = \text{const.} - E_c/k_B T$$

▶ from fit to data, measure $E_c \sim 10$ meV

▶ for all devices measured, $10 \text{ meV} < E_c < 14 \text{ meV}$



Fe₃O₄ Nanocrystals

(Sun and Zeng)

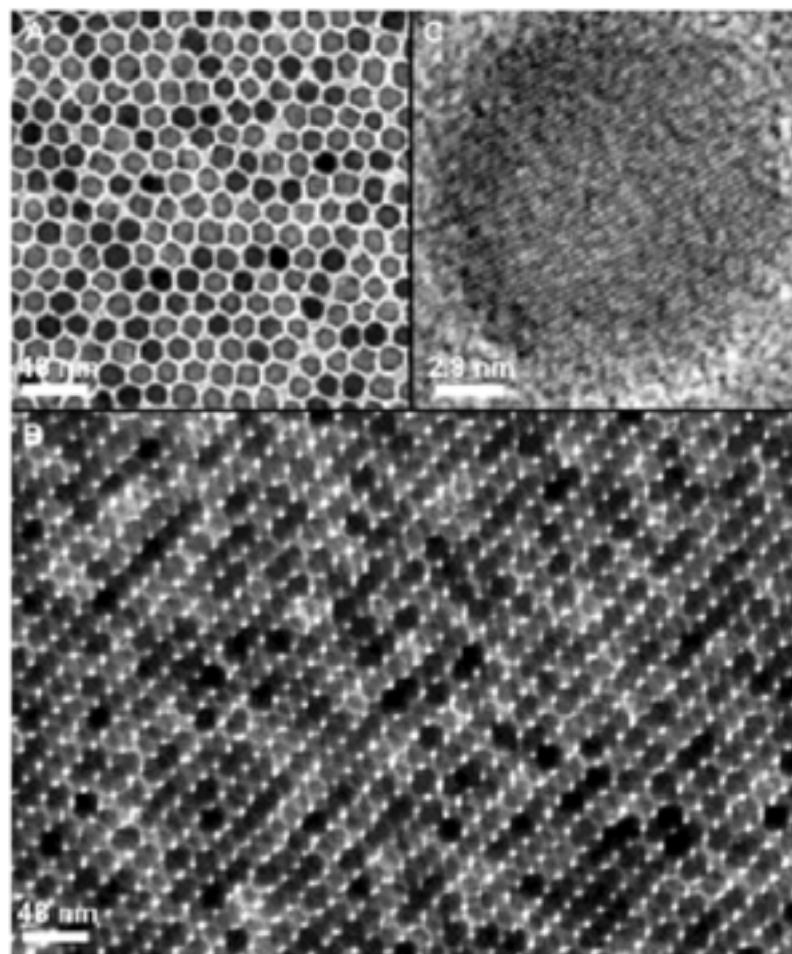
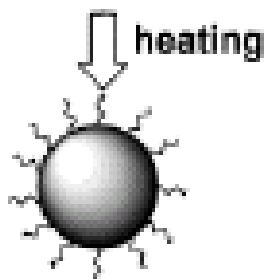
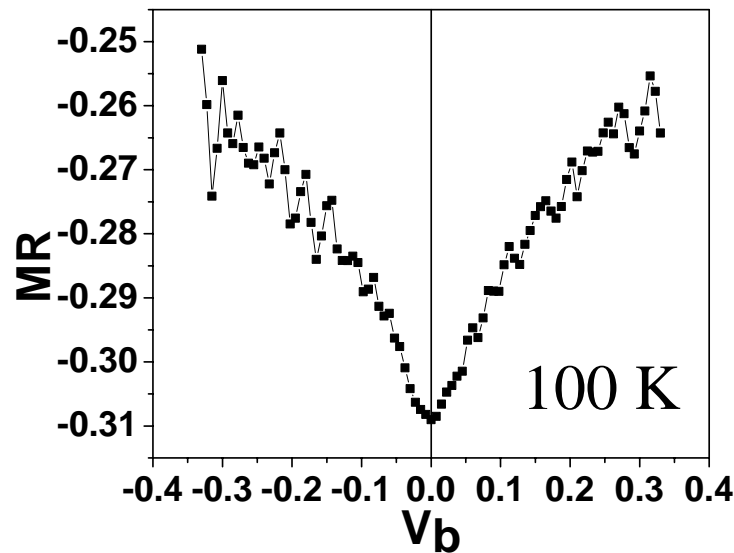
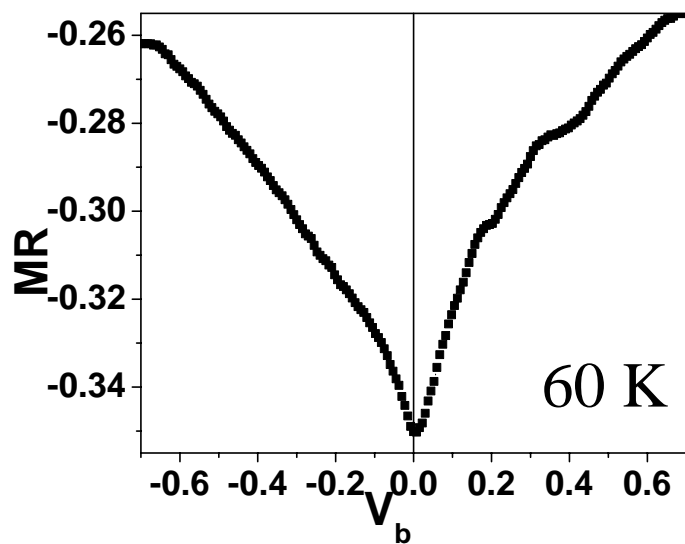
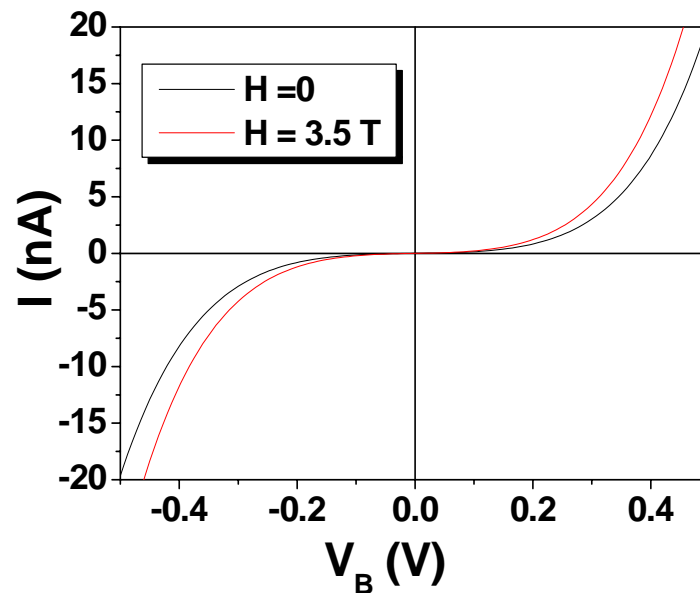
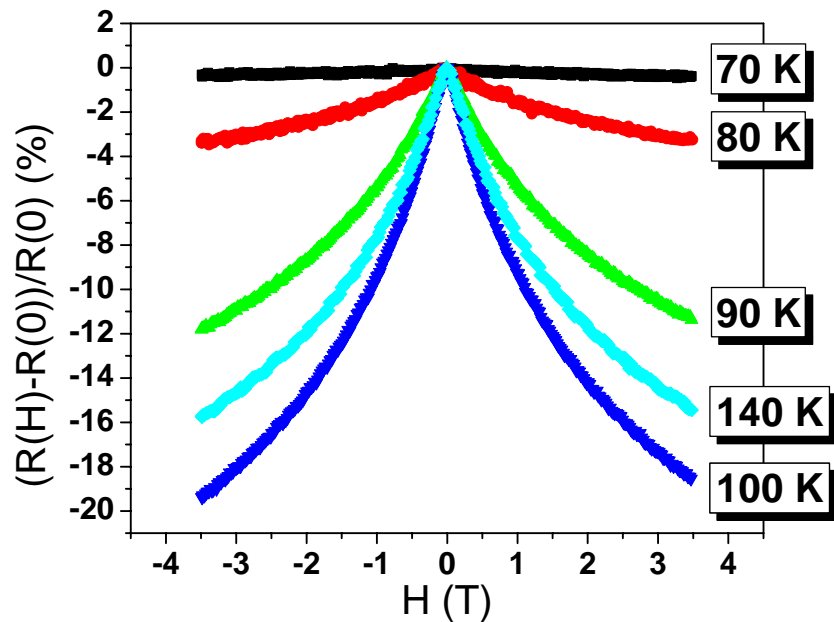
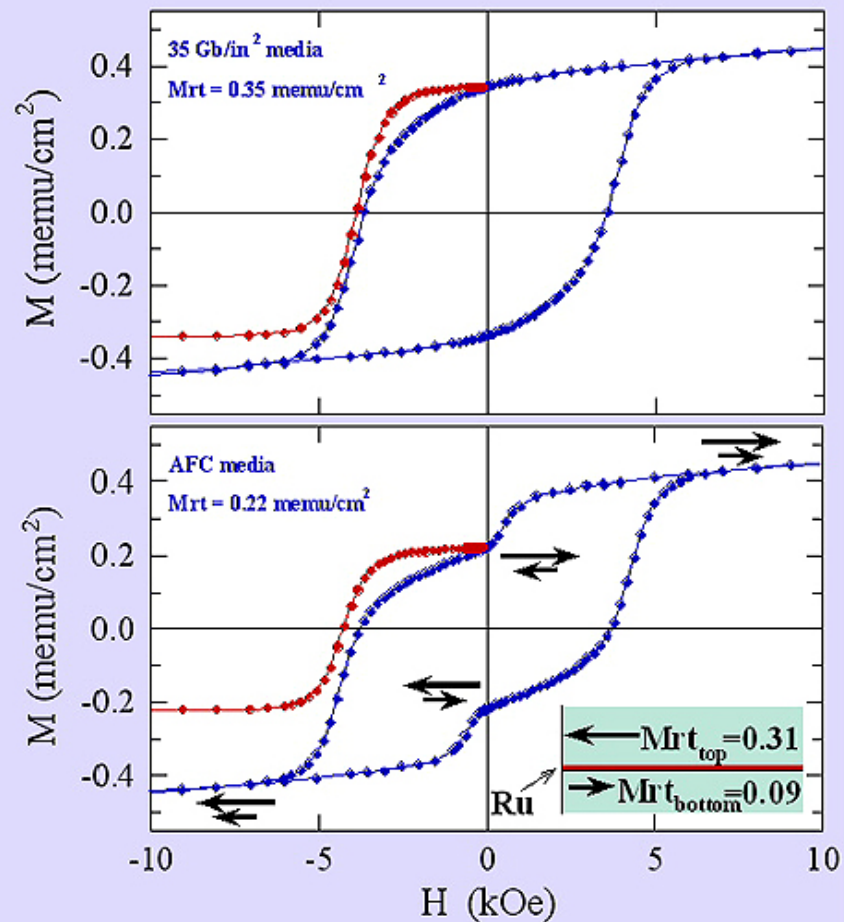
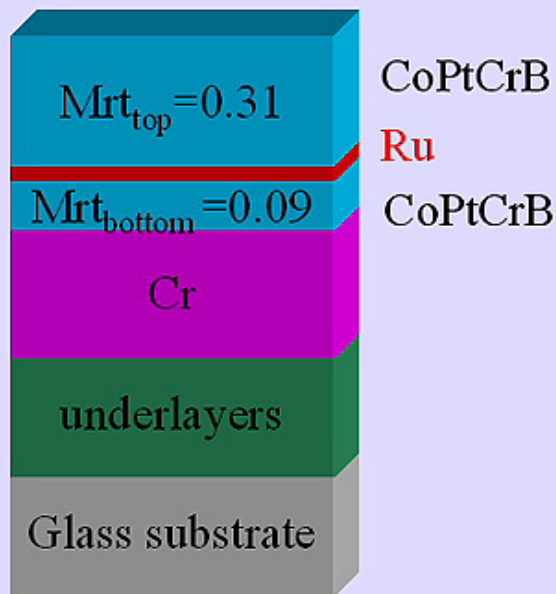


Figure 1. TEM bright field image of 16-nm Fe₃O₄ nanoparticles deposited from their dodecane dispersion on amorphous carbon surface and dried at 60 °C for 30 min: (A) a monolayer assembly, (B) a multilayer assembly, (C) HRTEM image of a single Fe₃O₄ nanoparticle. The images were acquired from a Philips EM 430 at 300 KV.



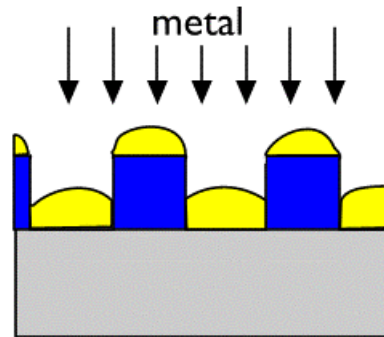
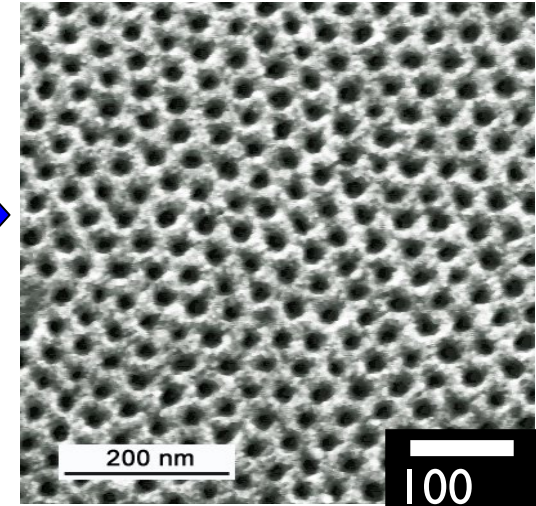
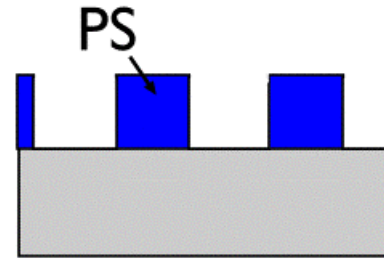
Potential for spintronic device applications

AFC media magnetization response to magnetic field

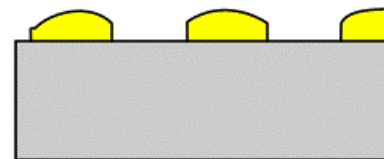


Nanoparticle synthesis from self-assembled polymer templates

- Diblock copolymer system PS/PMMA
- Self-assembly promoted by heating
- Removal of PMMA



metallization



remove polymer

